LIMBURGS
UNIVERSITAIR
CENTRUM

Instituut voor Materiaalonderzoek

Faculteit Wetenschappen

PHYSICAL PROPERTIES OF POLY(ARYLENE VINYLENE) POLYMERS.

Electro-optical properties and ageing behaviour of polymer light-emitting diodes (PLED's)

Proefschrift voorgelegd tot het behalen van de graad van

Doctor in de Wetenschappen

aan het Limburgs Universitair Centrum, te verdedigen door

Wim Bijnens

Promotoren :

Prof. Dr. L. De Schepper

Prof. Dr. D. Vanderzande

1998

Instituut voor Materiaalonderzoek

LIMBURGS
UNIVERSITAIR
CENTRUM

Faculteit Wetenschappen

PHYSICAL PROPERTIES OF POLY(ARYLENE VINYLENE) POLYMERS.

Electro-optical properties and ageing behaviour of polymer light-emitting diodes (PLED's)

Proefschrift voorgelegd tot het behalen van de graad van

Doctor in de Wetenschappen

aan het Limburgs Universitair Centrum, te verdedigen door

Wim Bijnens

Promotoren :

Prof. Dr. L. De Schepper

Prof. Dr. D. Vanderzande

1998

Promotoren : Prof. Dr. L. De Schepper
Prof. Dr. D. Vanderzande (Secretaris)

Juryleden : Prof. Dr. F. Dumortier, LUC (Voorzitter)
Prof. Dr. L. Stals, LUC
Prof. Dr. J. Gelan, LUC
Dr. W. De Ceunick, LUC
Dr. R.-J. Visser, Philips/NATLAB
Prof. Dr. G. Maes, KULeuven
Prof. Dr. H. Geise, UIA
Prof. Dr. R. Mertens, IMEC/KULeuven

"A clear desk is a sign of sick mind." Dit las ik ergens op een bureau, toen ik aankwam in Diepenbeek. Ik hoop dat dit een waarheid is, anders gaat het met mij degelijk mislopen. Lezers, geen paniek, dit schrijfsel is veruit het meest gestructureerde werk dat ik ooit neergeschreven heb. Het ligt misschien aan het feit dat het niet in mijn handschrift geschreven is of omdat er een inhoudsopgave bij is. Alleszins vat dit werk alle rommel rond mijn meetopstelling, mijn bureau en mijn legendarische kast samen. Een hele prestatie, niet?

In de afgelopen vier jaar hebben heel wat mensen interesse getoond in dit werk en hebben zo actief of passief een zeer grote bijdrage geleverd bij het tot stand komen van dit werk.

Niet in het minst, de man op wiens bureau ik deze spreuk vond, Prof. D. Vanderzande (één van de promotoren van deze thesis). Dirk, blijkbaar besefte je van het begin al dat om deze uitdaging tot een goed einde te brengen, we hulp nodig hadden van een fysicus, met meer orde en structuur. Vandaar dat dit werk een tweede promotor heeft: Prof. L. De Schepper. Dirk en Luc, ik hoop dat ik de kansen die jullie mij gegeven hebben ten volle benut heb. En dat het niet blijft bij deze eerste poging tot samenwerking tussen de fysica en scheikunde, maar dat het "geleidend polymeer project" een meerwaarde geeft aan het interdisciplinair Instituut voor Materiaal Onderzoek. Ik ben jullie enorm dankbaar voor de manier waarop ik dit project heb mogen uitvoeren.

Verder dank ik ook Prof. J. Gelan en Prof. L. Stals voor de stimulerende discussies en de interesse die ze vertoonden in dit werk.

Jean, eigenlijk moet dit werk misschien wel twee auteurs hebben, immers heb je niet alleen vier jaar lang een enorme interesse vertoond. Je hebt ook zeer veel tijd gestoken in de LEDjes. Zelfs toen we het licht nog moesten uitdoen om ze te zien branden, gaf je het niet op. Ook voor de laatste maanden ben ik u zeer dankbaar, want zonder uw correcties was deze tekst nooit geworden wat hij nu is.

Mark, Jan en Ting-Di, ik denk dat de hoeveelheid analyse in deze thesis voor zich spreekt. Ook jullie hulp was onmisbaar, zonder jullie werk waren we nooit zoveel te weten gekomen over wat er allemaal misloopt bij deze PLED's.

JC, Eric en Danny zonder jullie had ik nooit één meting kunnen uitvoeren, mijn dank daarvoor.

Mik en Anne I, ik dank u voor het geduld dat jullie aan de dag gelegd hebben om mij polymeren te leren maken.

Voor mijn meest wilde experimenten, ben ik langs geweest op IMEC. Ingrid en Guido ik ben jullie zeer erkentelijk voor de tijd die jullie gespendeerd hebben aan mijn ideeën en ik dank jullie voor de experimenten die we samen hebben gedaan.

Zoals hoofdstuk drie en vier laten vermoeden ben ik voor zeer veel resultaten gaan shoppen bij Philips. Peter, er zijn zonder enige twijfel maar weinig mensen met zo'n klare kijk op dit onderzoeksdomein. Ik dank u voor het vertrouwen en de mogelijkheden die jij mij geboden hebt in de vier maanden die ik op NATLAB heb doorgebracht. Paul, naar mijn bescheiden mening ben jij de beste wetenschapper die ik tot nu toe tegengekomen ben. Ik dank u voor uw enorm geduld en al de tijd die jij opgeofferd hebt om een scheikundige te leren modelleren. Het staat als een paal boven water dat uw model een enorme impact heeft op alles wat er in de volgende jaren gaat verteld en gedaan worden rond PLED's in de wereld.

Dit alles doet vermoeden dat ik vier jaar lang niets anders dan aan wetenschap heb gedaan. Niets is minder waar. Ik ben al mijn collega's op fysica, scheikunde (zowel onderzoek, FTO, didactiek als de technische ploeg) en op NATLAB, zeer veel verschuldigd voor alle leuke momenten. Immers zonder al dat gezwets en gezever had ik het nooit vier jaar volgehouden. Ook diegenen, die de bittere teleurstelling ervaren hier niet genoemd te worden, wil ik danken voor hun bijdrage. Sommigen horen hier toch expliciet vernoemd te worden : Steven, Ben, Dirk, Koen, Marlies, Anne P, Jo en Kristien dank u voor uw vriendschap. Tom, ik hoop dat je veel plezier zult beleven aan de voortzetting van dit werk.

Mama en Papa, jullie hebben het geweldig gedaan. Als Katrien en ik het nog maar half zo goed doen, is de opvoeding van onze zonen al meer dan geslaagd.

Bram en Thomas, zonder de mama, was mij dit alles nooit gelukt. Katrien, voor uw bijdrag zijn er dan ook geen woorden. Immers de afgelopen maanden waren buitengewoon zwaar maar, tegelijkertijd enorm boeiend. En dit is nog maar het begin ...

Wim Bijnens, november '98

Introduction

1 Chapter 1

The physics of conducting polymers.

1.1. General introduction

In spite of the fact that Electroluminescence (EL) in organic materials dates from 1963 when Pope et al⁽¹⁾. detected blue light emission at high fields in an anthracene single-crystal, most of the attention in the field has gone to the inorganic materials⁽²⁾. The interest in the use of organic materials for EL applications was triggered by the approach of Tang and Van Slyke⁽³⁾. They presented a new device configuration, where an organic dye (small evaporated molecule) is combined with a hole and electron-transporting layer, sandwiched between two electrodes. Like this they obtained devices with high external efficiencies (about 1%) and high brightness 1000 cd/m^2 operating at voltages lower than 10 volts. An important discovery in the domain of organic EL came in 1990 with the finding that not only dyes but also polymer can be used for EL applications⁽⁴⁾.

At the institute of material research (IMO), we are working since the beginning of the nineties on the synthesis of precursor routes towards conducting polymers⁽⁵⁻⁶⁾. This method of approach supplies a non-ionic, in organic media soluble precursor polymer. Without exception, the colourless precursor polymers are easy to handle and environmentally stable powders. They can be stored in the solid state during several months at ambient conditions with no or minor occurrence of elimination. The thermal elimination and the degradation temperature are sufficiently separated to avoid degradation during thermal conversion. The solubility of the precursor is established by the sulphoxy-group. By changing the aliphatic tail, these materials can be made soluble in almost every solvent.

One of the main problems in this field of research is the stability of the devices. In this thesis an effort is made to point out the shortcomings in lifetime and operation of a polymer light emitting diode PLED based on precursor poly (p-phenylene vinylene) (PPV). The models for the description of the basic properties of a PLED are used to understand the origin of catastrophic failure in these devices.

In the following parts of this chapter, the basic physics of conducting polymers are discussed. The models for the description of the bulk structure and its properties are presented. The spectroscopic properties are used to introduce the concepts for understanding the physics of conducting polymers. Charge transport is treated in the framework of disordered molecular solids.

Chapter 2 deals with the chemistry behind the PLED's. The choice to use a precursor material for the synthesis and the advantages and disadvantages resulting from this option are discussed. The concept of tailoring the emission wavelength in the various polymers to encompass a large range in the visible spectrum is presented. All the steps in the device preparation and their problems are pointed out in the last part of this chapter.

The electrical properties of the single-layer devices based on PPV are the central focus of chapter 3. It has been suggested that charge carrier injection is the dominant factor in these devices. The most important argument to reject these models is the fact that they cannot adequately account for the temperature and field dependent transport in these type of materials. Based on experimental results, Blom et al. developed a device model describing the bulk properties of the polymer. There experimental results show that the devices contacts are ohmic resulting in a current that is bulk limited. Before using this model to explain the experimental results a complete description of the model is given in the first part of the chapter. In the second part the experimental results for the hole-only devices are presented. The field and temperature behaviour of these PEDOT/PPV/Ag-devices is discussed. These results are then used to interpret the behaviour of an actual PLED. Going along this chapter the problem of leakage current becomes obvious. The danger of modelling the leakage current and using these results to explain the device properties is pointed out.

The ageing of PLED's is the main subject of chapter 4. A great deal of effort is made to study the stability of these devices. We did not attempt to optimise the devices, but we focused on the analytical techniques to study the degradation. Analytical techniques like Scanning Electron Microscopy (SEM), Secondary Ion Mass Spectroscopy (SIMS), infra-red monitoring (IR) and Emission Microscopy (EMMI) are discussed in the framework of the reliability study of PLED's. The combination of these analytical techniques together with electrical measurements has shown to be very useful in the progress of understanding the failure mechanisms in PLED's. This study provides evidence for electric field induced ageing at defects already present in the as-produced device. These pre-existing imperfections are the cause for the formation of leakage current, meaning that the leakage current is the electrical fingerprint of the device imperfections.

Chapter 5 deals with a problem (negative resistance) one runs across when studying the electrical properties of metal-insulator-metal devices. Also here it is shown that pre-existing defects in the device play a crucial role. It will be concluded that without any doubt the leakage current resulting from these defects is the main cause for the anomalies in the electrical behaviour of the devices.

By studying the experimental results and reading the discussions in the other chapters it becomes clear that leakage current, and everything that goes with it, must be the biggest concern when making polymer devices. In this last chapter 6 conclusions are drawn and in chapter 7 some suggestions are made for a continuation of this research.

1.2. Polymers in LED's.

It is not surprising that for the kind of devices studied in this work (metal-semiconductor-metal, MSM) the electrode-semiconductor interfaces, the bulk material and the geometry have a great influence on the device properties. To visualise the properties and to make a discussion possible, band-like picture are used to describe the PLED. Here we present a schematic structure of a PLED at an applied voltage bias (eg. 5V).

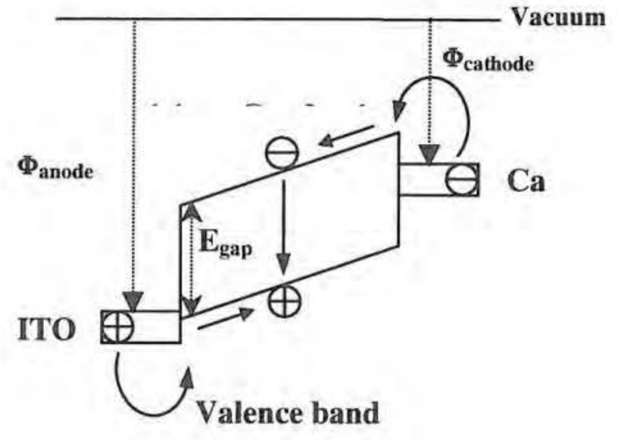

Figure 1 : Schematic structure of a PLED at an applied voltage bias (right), e.g. anode = ITO and cathode = Ca.

In [Figure 1] one can see that to get recombination of holes and electrons, the charge carriers have to overcome a barrier at the metal/polymer interface (eg. difference between the work function of the Ca ($\Phi_{cathode}$) and the onset of the conduction band). When the carriers are injected into the bulk, they have to be transported to each other.

This means that the interesting phenomena to study in these devices are: charge injection, charge transport, electron-hole interaction (exciton binding energy) and radiative recombination(7). The limiting factor for carrier injection is the formation of a barrier at the interface. Here one has to question the nature of the electrode contact. Transport in the bulk is discussed in detail in this chapter. The question rises whether the nature of the lowest energy elementary excitations is mobile charge carriers (charge polarons) or bound neutral excitons(8). Is charge transport in these materials band like(9) or hopping transport(10)? The electron-hole coupling is still the subject of a fundamental controversy; the theoretical maximum efficiency for electroluminescence is 25% in the bound excitons picture, wherein the band model the theoretical maximum efficiency can approach unity.

The urge for the understanding of the physics of conducting polymers makes a basic model for the description of the bulk structure and its properties of obvious importance. A model is also important for the applications based on these materials. Within the domain, there lives a fundamental controversy over how to explain, understand and describe these materials.

1.3. Molecular exciton or semiconductor band model.

Organic solids differ from inorganic ones in many essential aspects. Firstly, the charge carrier mobility in polymers is low (eg. PPV: 10^{-13} m^2/Vs, poly(thiophene)s (PT): 10^{-4} m^2/Vs) compared to silicon 10^{-1} m^2/Vs. Secondly, the electronic interaction between the molecules constituting the lattice is weak, and thirdly the relative dielectric constant (ε_r) is low. Typical values for an organic solid are 3 to 4 compared, for instance, with $\varepsilon_r = 11$ for silicon. The second difference implies that the valence and conduction bands as well as exciton bands are narrow(11).

If we accept the simplification that in carbon compounds hydrogen atoms just have the purpose of saturating dangling bonds (bonds without a partner) and that otherwise they do not contribute to the physical properties of the material, conducting polymers consist of single- and double-bonded carbon atoms. From organic chemistry it is well-know that double bonds can be "isolated" (separated by many single bonds), "conjugated" (in strict alternation with single bonds), or "cumulated" (adjacent). In a conjugated polymer each carbon-atom has a total of 4 valence electrons, 3 of which take place in sp^2-hybrid orbitals which form covalent σ-bonds with neighbour C or H atoms. The geometry of those σ-bonds is a cylindrically symmetric electron-cloud joining the two involving nuclei. The fourth unpaired electron associated which each C-atom takes position in the π-electron cloud, formed upon overlap of the p_z-orbitals perpendicular to the backbone. These π-bonding orbitals in which electrons are decollated give rise to the interesting electronic properties, such as its conductivity.

[Figure 1.1] shows polyacetylene, the prototype polyene, the simplest polymer with conjugated double bonds. The structure is simplified since by convention carbon atoms do not have to be drawn explicitly at the ends of the bonds and protons at the chain ends are neglected.

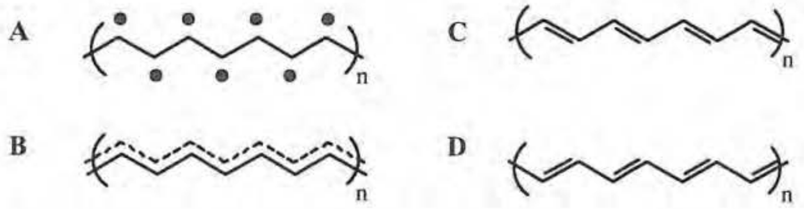

Figure 1.1 Trans poly(acetylene) A : the electrons are localised on the p-orbitals of the carbon atoms, B : the electrons are fully delocalised over the lattice. The degenerated lattices C and D.

In a simplified picture an infinite polyacetylene chain can be seen as a one-dimensional system. Real systems however are only quasi and not strictly one-dimensional. Real systems differ from ideal systems by having chains of finite rather than infinite length. In addition the chains show imperfections such as kinks, bends, twists or impurities. They are contained in an environment other than perfect vacuum, with neighbouring chains at a finite distance and thus a non-zero interaction between them. A trivial aspect of one-dimensional systems is the low conductivity. Each atom is connected to two other atoms only: one to the left-hand side and one to the right-hand side. In three-dimensional solids there are connections to neighbours in the back and front as well as to neighbours above and below.

At this point we have come to the issue where the discussion in the literature starts, about how to describe these polymer systems. If bonds are completely broken, an one-dimensional system separates into two pieces. Usually complete breaking of bonds does not happen, however. Often bonds are only partially cleaved. In chemical terms, this means that a bonding state is excited, to form an anti-bonding state. In semiconductor physics it would be described as an electron being lifted from the valence band into the conducton band. Such a manipulation of valence electrons is quite common in semiconductors and it is the first step for photoconductivity and photoluminescence. In a three-dimensional semiconductor like silicon the transfer of an electron from the valence to the conduction band creates mobile charge carriers (an electron in the conduction band and a hole in the valence band), but it does not change the arrangement of the atoms in the crystal. The question is if in a conjugated polymer each change in bond strength (e.g. photoexcitation) leads to a large distortion of the lattice, resulting in a strong electron-lattice coupling. Or that the first step for photoconductivity can be explained by disorder.

The low dielectric constant causes coulombic effects to be important. Depending on the strength of coupling among the structural elements, optical transitions in insulating solids are appropriately described in terms of either the exciton or the semiconductor band model. Weak intersite coupling in conjugation with a low dielectric constant favours the generation of strongly correlated electron-hole pairs (excitons) upon photon absorption, while strong coupling leads to the formation of uncorrelated electron hole pairs. Conjugated polymers, could in principle fall into either category. This discussion is best released in the book(12) edited by N. S. Sariciftci: Primary photoexitations in conjugated polymers: molecular exciton versus semiconductor band model. Here the photophysics/photochemistry of these materials is explained in terms of (I) a semiconductor band model(13-18) and (II) localised excitations on conjugated segments in disordered organic semiconductors(19-24).

- (I) The question is whether we can describe these materials as a system where lattice bonding is strong, implying strong intersite coupling and, as a result broad transport bands while the coulombic interaction between electron and holes is weak. Within this formalism, the existence of a gap in the absorption spectrum of the polymer is solely due to electron-phonon interactions, that will distort the lattice, leading to bond alternation (Peierls distortion). This means that these materials can be described as one-dimensional metals where the electrons are fully delocalised and free to move within the lattice of the polymer backbone.

- (II) In the second model, the material is described as a polymer with conjugated segments leading to a Gaussian distribution of localised states. In this way, a generated exciton at a specified site will execute a random walk while relaxing within this density of states. Eventually the exciton will reach the energy site with a longer conjugation length where the jump to lower energy is less preferably than the decay rate of the exciton.

1.4. Electrical conduction in conjugated polymers

1.4.1. The semiconductor band model.

In the previous section have pointed out the ongoing discussion about how to describe these conjugated polymers. In this section we shall focus on the concepts that are important to discuss the electrical properties of polymer LED's. The highly insulating nature of most of the organic solids, coupled with low charge carrier mobility's resulting from weak intermolecular interactions and the disorder, favours the use of a hopping model for rationalising their electrical properties. Nevertheless the basic concepts of the band model help to clarify the phenomena that take place in PLED's. From a fundamental point of view, if one wants to study the properties of one perfect conjugated polymer chain, the band model can adequately describe the properties of the chain (in reality chain segment). For this reason a brief description of the model is provided below. One can find a detailed description, of the properties of one-dimensional synthetic metals, in the book by S. Roth(27). Real systems however are fare from perfect, they are not infinitely long and conjugation is often broken, which rises the question of the applicability of the band model for a real system.

Most of the conducting polymers do not have good electrical properties when they are chemically pure. They are insulators, or at best, semiconductors. Only after treatment with oxidising or reducing agents they become conducting. This procedure is called doping. The term doping in this context is somewhat controversial, like a lot of terms used in this field of conductive polymers. A lot of terms are taken from the field of solid state physics but have a slightly different meaning when interpreted in the context of conducting polymers. One should be aware of this problem.

The preparation methods of thin films and the synthetic polymerisation routes to form these materials however cause unintentional doping of the polymers. This strong relation between thin film conductivity's and preparation methods of the materials makes it difficult to compare experimental results of different synthesis batches of even the same basic material. This variation in uncontrolled structural properties hampers the visualisation in terms of a well-defined lattice.

Lets start from poly(acetylene) as discussed before. Ideally poly(acetylene) can be represented as a long chain of CH-groups each possessing an unpaired electron [Figure 1.1]. According to solid state physics this structure can be considered as a one-dimensional lattice with one unbound electron per lattice-site. This corresponds with a half-filled band. In this situation metallic conductivity could be possible. However, the Peierls theorem states that a one-dimensional metal with a half-filled band is unstable. So in reality, the electrons in poly(acetylene) are not completely delocalised. Electron phonon interactions will distort the lattice, leading to pairing of the successive sites along the chain (dimerization) and to an alternation of short (double) bonds and long (single) bonds. This results in a splitting of the band into a completely filled valence band and an empty conduction band separated by a forbidden zone, the bandgap. Since the structures of the two alternative lattices of poly(acetylene) are degenerate, the energies of the two binding structures (structure C and D in [Figure 1.1] are equal. The conduction properties of these types of semiconductors are theoretically derived in terms of a semiconductor band picture using a single-chain one-electron model based upon the Su-Schieffer-Heeger (SSH) hamiltonian.(25,26)

1.4.2. *Conjugational defects*

It has already been discussed that when a chemical bond is broken, the system separates into two pieces. This means that defects can only be generated in pairs leaving two dangling bonds on the polymer chain. There are three methods to generate defects in the system: (I) by chemical doping (chemical redox reaction), (II) photogeneration, and (III) charge injection.

Polymer systems are chemically doped up to several percents, whereas typical doping concentrations of conventional semiconductors are in the ppm range. Saturation doping of polymers leads to a new material with another chemical formula (e.g. $[(CH)_7I_3]_n$ for iodine-doped polyacetylene instead of $(CH)_n$). In the case of doped silicon we do not describe it as a new material. This chemical doping will change the conductivity of conjugated polymers by many orders of magnitude.

Photogeneration of defects is accomplished by lifting an electron from the valence (π) band to the conduction (π^*) band by absorption of a photon. The lattice will relax around this electron-hole pair, the bond lengths readjust and negative and positive (or anti) defects are formed.

Charge injection is also known from semiconductor physics and is the main focus of chapter 3.

1.4.2.1. Degenerate ground state polymers : solitons

In polyacetylene there is strict bond alternation. For a chemist this is trivial since dimers (pairs) were polymerised. For a physicist dimerisation is a phase transition from a metallic to a semiconducting state. One can imagine that the phase transition nucleates at several points of the chain with domains growing around these nucleation centres. Finally misfits are created at touching domains.

Figure 1.2 Interruption of the regular bond alternation pattern at the position of a misfit (soliton), resulting in a dangling bond (a radical).

These misfits are very interesting. The bond alternation is interrupted by two adjacent single bonds, and the charge density wave has a 180° phase slip [Figure 1.2]. To keep the carbon atom in the misfit tetravalent, a dangling bond must exist (two bonds join neighbouring carbons, one the hydrogen atom; the fourth bond has no partner, meaning that it is a non-bonding state). Organic chemists know this type of defect as a radical. Over the years several synonyms for this defect are used: conformational defect, conjugational defect, misfit, domain wall, phase slip centre, kink, dangling bond, radical, soliton, etc.

From a physicists point of view, it is acceptable to call this type of conjugational defects (interruption in the double single bond alternation) a soliton(27). These excitations only exist in materials with a degenerate ground state, like polyacetylene, in which two possible patterns of alternating single and double bonds exist. If the gap is explained as the separation of bonding and anti-bonding states, a soliton, which is neither bonding nor anti-bonding but non-bonding, must be in the gap, at exactly the mid-gap posistion because of the symmetry of the structure. The non-bonding states have spin $s=1/2$ and charge neutrality, but upon doping the state can become a positively or a negatively charged soliton with zero spin. Chemist call the neutral soliton a radical, the positive soliton a carbocation and the negative soliton a carbanion. These solitons are able to move in a non-degenerate polymer since the variation of the systems energy is small as the soliton moves.

1.4.2.2. Non-degenerate ground-state polymers : polarons

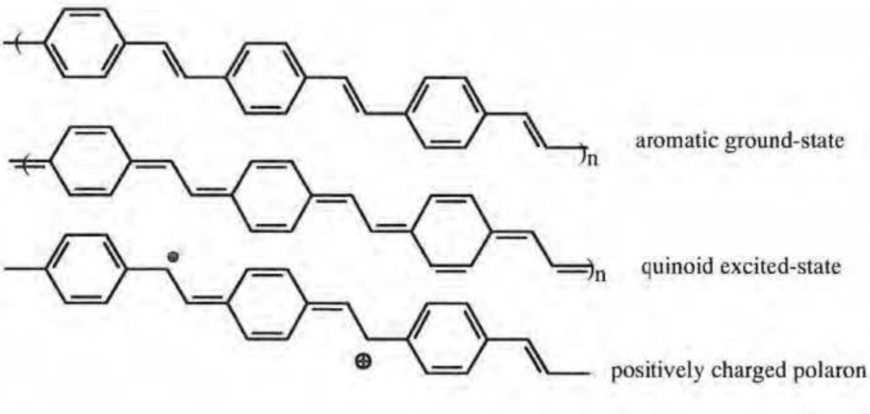

Figure 1.3 Chemical representation of the two non-degenerated lattices (aromatic and quinoid) in PPV. To stabilise conjugational defects in a non-degenerated polymer we have to create bound double-defects (polarons).

In contrast to degenerate ground state polymers, most conjugated polymers will have a non-degenerate ground state. PPV is an example of such a polymer [Figure 1.3]. Degenerated means that the energy does not change when single and double bonds are interchanged. In PPV, however, interchange of single and double bonds leads from the ground- aromatic state (three double bonds within the ring) to the excited- quinoid state with only two double bonds within the ring. A conjugational defect in non-degenerated ground-state polymer separates a low energy (aromatic) region from a high-energy (quinoid) region. As a result a single defect is unstable and the system will always tend to return to an aromatic configuration. Therefore the soliton will be driven to the chain ends. The stabilisation of these defects needs the creation of bound double defects. These double defects are called polarons.

In this picture the lowest excited state in PPV is a polaron. As discussed above, the optical signature of a soliton is the midgap state; a polaron is characterised by two states in the gap. The two-gap states of the polarons can be occupied by zero, one or two electrons each [Figure 1.4]. In the band model polarons and solitons are principally localised states. This means that addition of an electron or a hole to the conducting polymer results in a self-localised excitation, which deforms the semiconductor lattice.

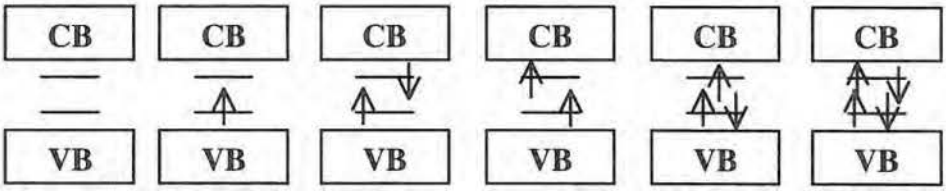

Positive bipolaron

positive polaron

Singlet polaron-exciton

Triplet polaron-exciton

Negative polaron

Negative bipolaron

Figure 1.4 Polarons in polymers, VB = valence band, CB = conduction band

1.4.3. *Hopping in a structural disordered material : the exciton model.*

A lot of people are critical of the concepts of the SSH-model. This criticism is based on the fact that the self-localisation of the defects in conjugated polymers and their disorder make that these segments behave as individual molecules. Individual molecules means that the have different lengths, a different environment and as a result, different energy levels. This is described by Bässler(10) with a Gaussian distribution of localised states. Here conjugated polymer chains consist of conjugated parts separated by non-conducting parts (with an effective conjugation length of about 8) [Figure 1.5]. Since there is a weak coupling between the conjugated parts in these materials the conjugated segments behave as individual molecules. These perfectly conjugated chain segments, separated by defects from other segments, should be identified as energetically different transport sites.

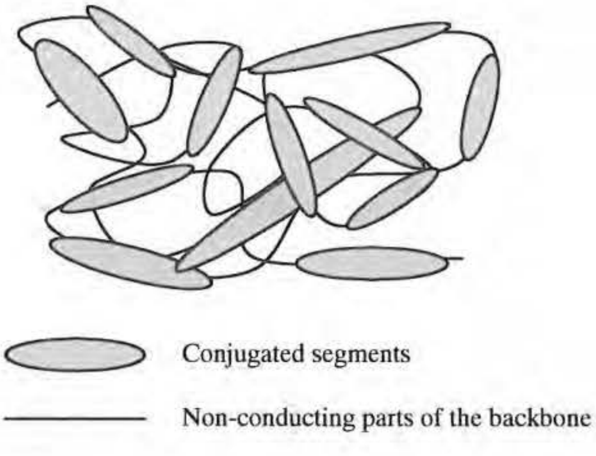

Figure 1.5 Schematic drawing of a conjugated polymer showing the aspect of self-localisation. Meaning that an excited-state only sees a short effective conjugation lenght.

The low charge carrier mobility, which reflects their localisation on the conjugated segments, will thus be described in terms of hopping transport in disordered semiconductors.

1.4.3.1. Spectroscopic properties of conducting polymers.

In this part, the optical spectra are used to introduce the concept of structural disorder, which is important for the understanding of the physics of conducting polymers. There will be no details given and the description will be of a semiquantitative nature. The only purpose of this part is to visualise the concept of disorder, which will be very useful to explain the experiments on PLED's. For more details about the different models see the references(12-24).

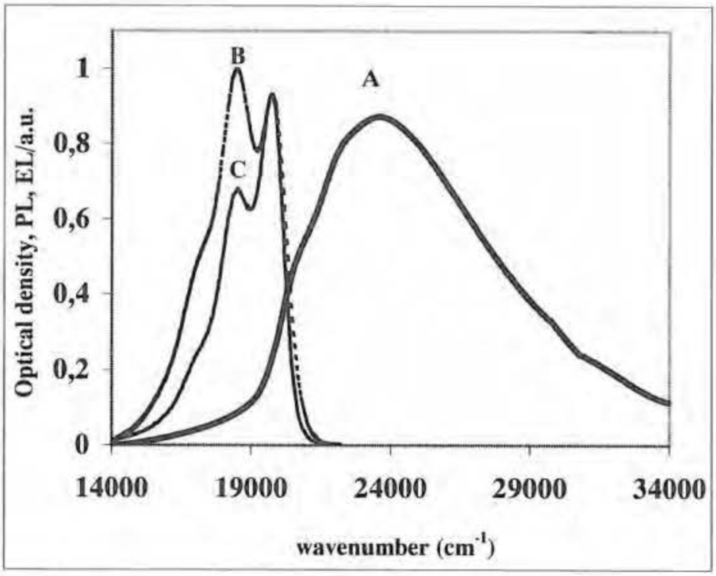

Figure 1.6 Optical absorption (optical density, A), photoluminescence (PL, B) and electroluminescence (EL, C) spectra at room temperature for PPV obtained via the non-ionic precursor rout

Of particular importance for the understanding of the spectroscopy of non-crystalline conjugated polymers and oligomers (small organic molecules build out of a few monomers) are disorder effects. Disorder can be of inter- or intra-molecular origin. The conjugated polymer is visualised as an array of chromophores (small conjugated organic molecules), identified as segments of the polymer backbone over which the excitation is delocalised. Each segment has an effective conjugation length much smaller than the total chain length(28,29). The chain segments may be delineated by chemical defects, conformational imperfections and disorder, including dynamic motion of the polymer chain. Meaning, that this average length reflects the perfection of the locale structure of the polymer chains. This statistical distribution results into a variation of excitation energies of the segments. Hence, it contributes to the inhomogeneous broadening of the optical spectra (absorption and emission) [Figure 1.6].

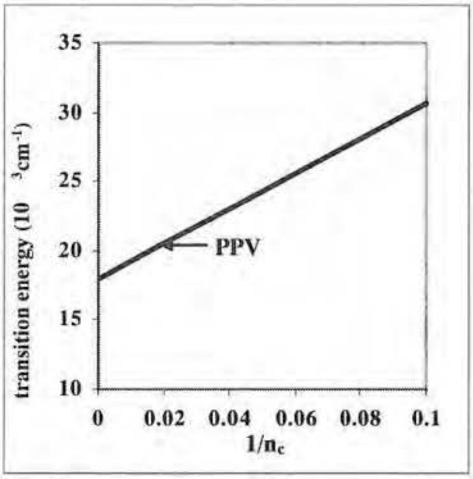

Figure 1.7 Peak energies of the S_0-S_1 (0-0) absorption band in oligophenylenevinylenes as a function of the inverse number of carbon atoms (n_c) in the shortest path between the ends of the molecules (n_c=6n-2), n being the number op phenylrings in the molecule. (Data and figure taken from Mahrt et al. 1990(27)) The transition energies of ordinary PPV indicated for comparison.

Starting from this idea, we end up with the concept, where the dominant electronic excitation created by photoexcitation across the π–π^* energy gap is a singlet excitation. The exciton can move, by an energy transfer, to another segment of the same chain or a neighbour chain whose excitation energy is lower. At the end of its random walk, the excitation will arrive at an acceptor site at which it decays radiatively or non-radiatively because there are no other sites with still lower energy available as acceptor.

One can make a rough estimation of the segment length(30,31) by plotting the S_0-S_1 (0-0)-transition energy, $E_{S1\text{-}S0}$, of the polymer versus the reciprocal segment length, L^{-1}. Given the limitations of this model and the corresponding uncertainty of the extrapolation of the transition energy towards the average effective conjugation length we need to be hesitant to derive absolute numbers. Nevertheless, it is obvious that the effective conjugation length is short. Transition energy of 20200 cm^{-1} for PPV translates into an effective conjugation length of 8.5 [Figure 1.7]. The random walk model offers a simple and intuitively obvious way of relating the width and position of the spectra to the degree of disorder. The more perfect the structure becomes the more elongated the emitting segments will be and the more red-shifted the emission. At the same time the inhomogeneous widths of the emission bands decreases because (I) the relative variation of effective conjugation lengths decreases and (II) with increasing motion of the excitation along a chain segment the effect of random variations in the van der Waals interaction energies with neighbouring chains becomes smeared out (motional narrowing).

S. Heun et al.(24) calculated the σ-value of the Gaussian width of inhomogeneously broadened bands out of the absorption spectra of PPV. A transition energy of 20200 cm^{-1} translate into a σ-value of 650 cm^{-1}.

1.4.3.2. Charge transport in disordered molecular solids

Charge transport phenomena in disordered molecular solids are of interest because of their practical importance in, e.g. electrophotography(32) and PLED's(33,34).

Unfortunately, there is no direct way to link optical data in terms of disorder (σ_{abs}) to the transport properties (σ_{tranp}). In both cases the width of the disorder-broadened DOS is indirectly measured, this hampers a direct comparison. In the optical measurements, we have to consider exciton binding energy (0.3-0.4 eV).

Although there is no direct physical parameter that links optics with transport properties, Bässler(10,35) proposed that the width of the DOS for charge carriers is about 1.5 times as big as that for a singlet excitation. Measuring the DOS for singlet excitations thus permits concluding on the width of the DOS for charge carriers as well.

Experiments have indicated similarities in the observed features in disordered molecular solids, despite the wide diversity in chemical and physical structures(36-37). The most striking features are:

- A carrier mobility yielding an activation energy of about 0.4 to 0.6 eV independent of chemical constitution and synthesis if analysed in terms of the Arrhenius equation.
- A field dependence of mobility resembling the Pool-Frenkel law, $ln\mu \sim SE^{1/2}$, over an extended range of electrical field(39).

These similarities suggest that impurity effects play a minor role and one can conclude that the features above reflect an intrinsic transport property of the various systems.

This field and temperature dependence is first incorporated into an empirical relation for hole and electron mobility by Gill(43). He fitted his experimental results by eq. 1.1.

$$\mu = \mu_0 e^{-\beta\Delta + B(\beta - \beta_0)\sqrt{E}} \qquad 1.1$$

With $\beta = 1/(kT)$ and $\beta_0 = 1/(kT_0)$ and B is a constant.

No physical understanding of the parameters is given by Gill. Nevertheless there are numerous experiments on moleculary doped polymers, pendant group polymers, amorphous molecular glasses and conjugated polymers which have revealed a similar behaviour, with typical parameter values of $\Delta \sim 0.5$ eV, $B \sim 3\ 10^{-5}$ eV(m/V)$^{1/2}$ and $T_0 \sim 600$ K(36-38).

Bässler(10) used Monte Carlo simulations to calculate the mobility in polymers. He based his simulations on the idea that a conjugated polymer can be described as individual molecules with different lengths, a different environment and as a result, different energy levels (using a Gaussian form of the DOS). He was able to fit his calculated data with the Gill equation and by doing so, he gave a physical explanation for this empirical low.

These Monte Carlo simulations of hopping between sites that are subject to both positional and energetic disorder only agree with equation 1.1 over a limited field range. This range may be increased by taking into account spatial correlation in the energetic disorder(44,47).

It is straightforward to assume that in a non-crystalline organic solid with severe disorder the main free path of a carrier between subsequent phonon scattering events is short. The elementary transport step in such systems is then the transfer of a charge carrier among adjacent transporting molecules (transport sites). In chemical terms, this thermally activated tunnelling (hopping) is a redox process involving identical species(40) [Figure 1.8].

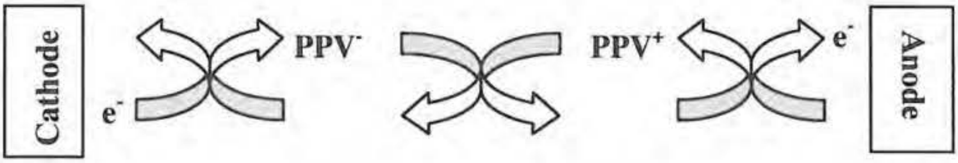

Figure 1.8 Redox chemistry in polymer LED's, thermally activated tunnelling (hopping) is a redox process involving identical species

1.4.3.2.1. Temperature dependence

The activation energy for carrier mobility in a conjugated polymer is the result of the energy difference of the chemically identical hopping sites due to local disorder. This local statistical variation(41) subjects the lattice contribution to the energy of the neutral and charged molecule. This contribution is due to the change in molecular conformation upon removal or addition of charge (oxidation/reduction)

The essential difference between the different models describing transport in these materials is related to the relative importance of the electron-electron and the electron-phonon interaction. The hopping model assumes that the coupling of the charge to inter (or intra)-molecular modes is weak. The activation energy reflecting basically the static energy disorder of the hopping sites. The polaron model, on the other hand, considers the disorder energy to be unimportant compared to the intramolecular deformation energy.

A σ of 0.1eV at 295 K seems to be a representative value of the energetic disorder parameter for many experimental systems. Bässler predicted that many random systems follow a temperature dependence for the mobility as first reported by Ferry et al.(42)

$$\mu(T) = \mu_0 \exp\left(-\left(\frac{2\sigma}{3kT}\right)^2\right) \qquad 1.2$$

In this way one can calculate the Arrhenius activation energy Δ_0 if one plots $\mu(T)$ in an Arrhenius fashion and determines the Δ_0 from the slope at a given T:

$$\Delta_0 = -k\frac{\partial \ln \mu}{\partial \frac{1}{T}} = -\frac{8\sigma^2}{9kT} \qquad 1.3$$

An apparent activation energy of 0.4 eV at 300 K is then consistent with a hopping system characterised by a DOS of width σ of 0.108 eV as expected on the basis of the optical bands.

1.4.3.2.2. Field dependence

The theory of Bässler(10) predicts that the slopes of the lnμ versus $E^{1/2}$ becomes negative for $T>T_0$ in eq 1.1. This is explained by energy disorder. Energetic and geometric disorder must give rise to a field dependence of the hopping mobility, however in an opposite way. Since tilting the DOS by an electrostatic potential reduces the average barrier height for energetic uphill jumps in the field direction, therefore μ must increase with E. Geometric disorder, on the other hand, can generate dead ends for the diffusing carriers. Since the emptying of these dead ends may involve jumps against the field direction, μ will decrease with E.

1.5. References

(1) Pope, M., Kallman, H. and Magnante, P., *J. Chem. Phys.*, **38**, 2042 (1963)

(2) Kobayashi, H., In *Electroluminescent Materials, Devices and Large-Screen Displays*, Edited by Conwell, E.M., Stolka, M. and Miller R. Proc. SPIE **1910**, 15 (1993), Bellingham (U.S.A) : SPIE

(3) Tang, C.W. and Van Slyke, S.A., *Appl. Phys. Let.*, **51**, 913 (1987)

(4) Burroughes, J.H., Bradley, D.D.C., Brown, A.R., Marks, R.N., Mackay, K., Friend, R.H., Burns, P.L. and Holmes, A.B., *Nature*, **347**, 539 (1990)

(5) Gelan, J., Vanderzande, D. and Louwet, F., *European Patent* (1994), 0 644 217 A1.

(6) Louwet, F., Vanderzande D., Gelan, J. and Mulens, J., *Macromolecules*, **28**, 1330 (1995)

(7) Bradley, D.D.C., *Synth. Met.*, **54**, 401 (1993)

(8) Pakbaz, K., Lee, C.H., Heeger, A.J., Hagler, T.W. and McBranch, D., *Synth. Met.*, **64**, 295 (1994)

(9) Heeger, A.J., Kivelson, S., Schrieffer, R.J. and Su, W.P., *Rev. Mod. Phys.*, **60**, 782 (1988)

(10) Bässler, H., *Phys, Status Solidi B*, **175**, 15 (1993)

(11) Silinsh, E.A., *Organic Molecular Crystals*, Springer, Berlin (1980)

(12) edited by Sariciftci, N. S., *Primary photoexitations in conjugated polymers : molecular exciton versus semiconcuctor band model*, World Scientific Singapore (1997)

(13) Lauchlan, L., Etemad, S., Chung, T.C., Heeger, A.J. and MacDiarmid,A.G., *Phys. Rev. B*, **24**, 3701 (1981)

(14) Schacklette, L.W., Chance, R.R., Ivory, D.M., Miller, G.G. and Baughman, R.H., *Synth. Met*, **1**, 307 (1979)

(15) Taliani, C., Danielli, R., Zambioni, R., Ostaja, P. and Porzio, W., *Synth. Met.*, **18**, 177 (1987)

(16) Su, W.P., Schrieffer, J.R. and Heeger, A.J., *Phys. Rev. Lett.*, **42**, 1698 (1979)

(17) Rice, M.J., *Phys. Rev. Let.*, **17A**, 152 (1979)

(18) J. Orenstien, *Handbook of Conduction Polymers*, edited by T. Skotheim, Marcel Dekker, New York (1986)

(19) Sebastian, L. and Weiser, G., *Phys. Rev. Let.*, **46**, 1156 (1981)

(20) Lochner, K., Bässler, H., Tieke, B. and Wegner, G., *Phys. Status Solidi B*, **88**, 653 (1978)

(21) Rughooputh, D.D.V., Bloor, D., Phillips, D., Jankowiak, J., Schütz, L. and Bässler, H., *Chem. Phys.*, **125**, 355 (1988)

(22) Pautmeier, L., Rauscher, U. and Bässler, H., *Chem Phys.*, **146**, 291 (1990)

(23) Rauscher, U., Bässler, H., Bradley, D.D.C. and Hennecke, M., *Phys. Rev. B*, **42 (16)**, 9830 (1990)

(24) Heun, S., Mahrt, R.F., Greiner, A., Lemmer U., Bässler, H., Halliday, D.A., Bradley, D.D.C., Burn, P.L. and Holmes, A.B., *J. Phys. Condens. Matter*, **5**, 247 (1993)

(25) Heeger, A.J., Kivelson, S., Schrieffer, R.J. and Su, W.P., *Rev. Mod. Phys.*, **60**, 782 (1988)

(26) Su, W.P., Schrieffer, J.R. and Heeger, A.J., *Phys. Rev. Lett.*, **42**, 1698 (1979)

(27) Roth, S., *One-dimensional meals*, CVH Verlagsgesellschaft mbH Weinheim (1995)

(28) Kohler, B.E. and Woehl, J.C., *J. Chem. Phys.*, **103**, 6253 (1995)

(29) Woo, H.S., Graham, S.C., Braldley, D.D.C., Friend, R.H., Burn, P.L. and Holmes, A.B., *Phys. Rev. B*, **46**, 7379 (1992)

(30) Mahrt, R.F., Yang, J., Griener, A., Bässler, H. and Bradley, D.D.C., *Makromol. Chem. Rapid. Commun.*, **11**, 415 (1990)

(31) Schmidt, A. Anderson, M.C., Dunphy, D., Wehrmeister, T., Müllen, K. and Armstrong, N.R., *Adv. Mat.*, **7**, 722 (1995)

(32) Pai, D.M. and Springett, B.E., *Rev. Mod. Phys*, **65**, 163 (1993)

(33) Blom, P.W.M., de Jong, M.J.M., Vleggaar, J.J.M., *Appl. Phys. Lett*, **68**, 3308 (1996)

(34) Blom, P.W.M. and Vissenberg, M.C.J.M., *Phys. Rev. Lett.*, **80**, 3819 (1998)

(35) Mahrt, R.F., Yang, J and Bässler, H., *Chem. Phys. Lett.*, **192**, 576 (1992)

(36) Pai, D.M., *J. Chem. Phys.*, **52**, 2285 (1970)

(37) Santos Lemus, S.J. and Hirsch, J., *Phil. Mag. B*, **53(1)**, 25 (1986)

(38) Blom, P.W.M., de Jong, M.J.M. and Munster, M.G., *Phys. Rev. B*, **55**, R656 (1997)

(39) Borsenberger, P.M., *J. Appl. Phys.*, **68**, 6263 (1990)

(40) edited by Lyons, M.E.G., *Electroactive polymer electrochemistry*, Plenum Press, New York (1994)

(41) Bässler, H., *Phys. Stat. Sol. B*, **107**, 9 (1981)

(42) Ferry, J.D., *J. Appl. Phys.*, **24**, 912 (1953)

(43) Gill, W.D., *J. Appl. Phys.*, **43**, 5033 (1972)

(44) Vissenberg, M.C.J.M. and Matters, M., to be published

(45) Vissenberg, M.C.J.M., to be published

(46) Gartstein, N.Y. and Conwell, E.M., *Chem. Phys. Lett.*, **245**, 351 (1995)

(47) Dunlap, D.H., Parris, P.E. and Kenkre, V.M., *Phys. Rev. Lett.*, **77**, 542 (1996)

Chapter 2

Synthesis and device preparation

For a number of reasons organic semiconductor materials form attractive candidates to serve as active layers in LED's. The specific advantages of polymer materials offer the possibility to produce large-area thin film devices at low cost, in which the emission colour can be tuned by proper chemical modification of the material at the molecular level. PPV and aspecially the PPV synthesised by the precursor route used in this work, offer the possibility of tuning as well the colour as the film properties of the emissive layer. In this chapter we will deal with the chemistry and engineering behind the PLED's.

2.1. Synthesis of PPV related polymers.

A variety of new conjugated PPV-related polymers have been synthesised using a synthetic approach that allows the tailoring of the chemical structure of the polymer backbone. In this way we have been able to prepare not only poly (p-phenylene vinylene) (PPV) **(1)**, but also some electron rich PPV derivatives such as poly (2,5-dimethyl-1, 4-phenylene vinylene) (PDMetPV) **(2)**, poly (2,5-dimethoxy-1, 4-phenylene vinylene) (PDMeoPV) **(3)** -and its soluble derivative OC_1C_{10} **(6)**- , PPV derivatives with an enlarged aromatic system, poly (4,4'-bisphenylene vinylene) (PBPV) **(4)** and poly (2,6-naphthalene vinylene) (PNV) **(5)** [Figure 2.1]. These materials were characterised in terms of molecular weight (GPC), elimination temperature (TGA, FT-IR), optical properties (UV-VIS) and photoluminescence (PL).

Precursor routes for conjugated materials, used in devices for opto-electrical applications, are of great importance. The processible precursor polymers facilitate the incorporation of these materials into devices. One precursor route that has shown to be very versatile, is the route introduced by Wessling and Zimmerman in the late 60's(1-3) and investigated thoroughly for this purpose by Lenz and Karasz in the beginning of the 80's(4). Based on Wessling's method poly (p-phenylene vinylene) (PPV) is obtained after thermal conversion. PPV possesses very good mechanical properties, high thermal stability and large electrical conductivities after doping. This polymer currently shows great promise for the development of PLED's(5,6). However the Wessling method still has some drawbacks, such as the instability of the precursor polymer and gel formation (7). These problems have been circumvented by Yamada et al(8) by substitution of the sulphonium groups in the precursor by alkoxy ether groups. Another limitation documented in the literature is the observation that monomers possessing enlarged aromatic systems, e.g. 4,4'-biphenylene or 2,6-naphthalene, show no tendency to polymerise in the circumstances used in general for the Wessling precursor(7) route. Solutions may be found by understanding the involved chemistry in detail. The Wessling precursor route is a typical example of the polymerisation behaviour of p-quinodimethane systems. In our work(9) we have tried to define the prerequisites of such polymerisation routes.

We have introduced a generalised scheme in which a clear distinction is made in the three steps of the process. Firstly, the in situ formation of the actual monomer, the p-quinodimethane system. Secondly, the polymerisation reaction, which in our view can be described as a self-initiating radical chain polymerisation(9,10) and finally the conversion into the fully conjugated system. The monomer used in this route possesses a leaving group and a polariser. The polariser stabilises the anion formed in the acid-base equilibrium and ensures head to tail polymerisation. The leaving group is necessary for the 1,6-elimination, forming the quinoid structure. The so formed quinodimethane system will then polymerise. This route has the advantage that the polariser, leaving group, base and solvent can be chosen in function of the monomer that must be polymerised.

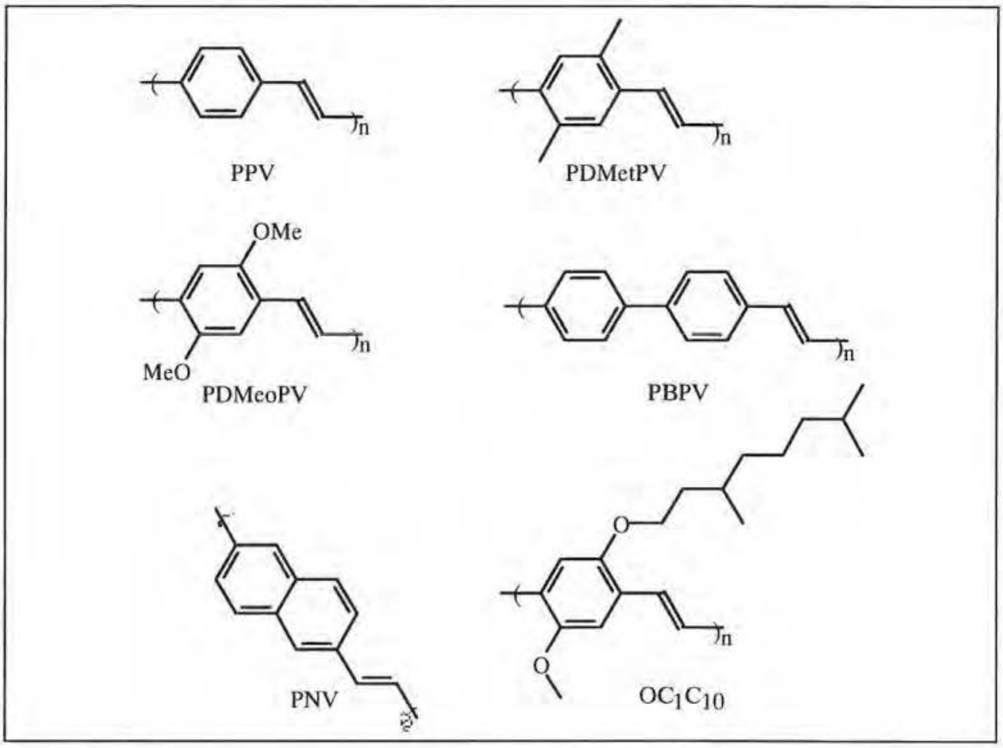

Figure 2.1: The chemical structure of the PPV derivatives.

Without exception the colourless precursor polymers are easy to handle and environmentally stable powders. They can be stored in the solid state during several months at ambient conditions with no or minor occurrence of elimination. All ^{1}H-NMR and ^{13}C-NMR data are consistent with the proposed highly purified precursor polymer structures. The thermal elimination of the sulphoxy groups and the degradation of the conjugated polymers are examined with thermal gravimetric analyses (TGA). Elimination and degradation temperatures are sufficiently separated to avoid degradation during thermal conversion. These results are summarised in [Table 2.1](13). The difference between the theoretical and experimental weight after the elimination in the TGA-experiments is explained by FT-IR spectra. These spectra show a complete elimination of the sulphoxy group, but some of the reaction products remain in the conjugated polymer matrix. This means that an elevated temperature or high vacuum conditions are necessary to evaporate the residual elimination products and is of importance in device preparation. Photoluminescence measurements are shown in [Figure 2.2]. These results show that we can deliver blue and red shifted materials according to classical PPV by tuning the synthesis.

The solubility of the precursors is established by the sulphoxy-group, by changing the aliphatic tail, these materials can be made soluble in almost every solvent. An overview of the general properties of the materials is given in [Table 2.1]. Issaris(14) describes these PPV-precursor and the polymerisation mechanism in detail.

	GPC		Thermal analyses		UV-Vis
	Molecular weight $\overline{M}_w(.10^4)$	*Distribution* *D*	*Elimination temperature (°C)*	*Degradation temperature (°C)*	*Bandgap* *Eg (eV)*
PPV	60 - 100	2.2 – 3.4	150	565	2.35
PDMetPV	19 - 39	1.9 – 2.9	155	490	2.48
PDMeoPV	10 - 27	1.7 – 1.8	160	440	2.27
PBPV	4.9 - 5.6	1.8 – 2.1	150	580	2.68
PNV	16.5 - 24.5	1.9 – 5.2	165	570	2.51

Table 2.1: Overview of the general properties of the polymers: Molecular Weight and Distribution; Elimination and Degradation Temperature; Bandgap (derived from the optical absorption data).

In conclusion we have synthesised a series of PPV-related polymers using a new synthetic approach allowing the tailoring of the chemical structure of the polymer backbone(11-13). The materials exhibit high molecular weights. Elimination and degradation temperatures are sufficiently separated to avoid degradation during thermal conversion. The sulphoxy group allows tuning the solubility. Both maximum absorption and emission can be tailored in the various polymers to encompass a large range in the visible spectrum.

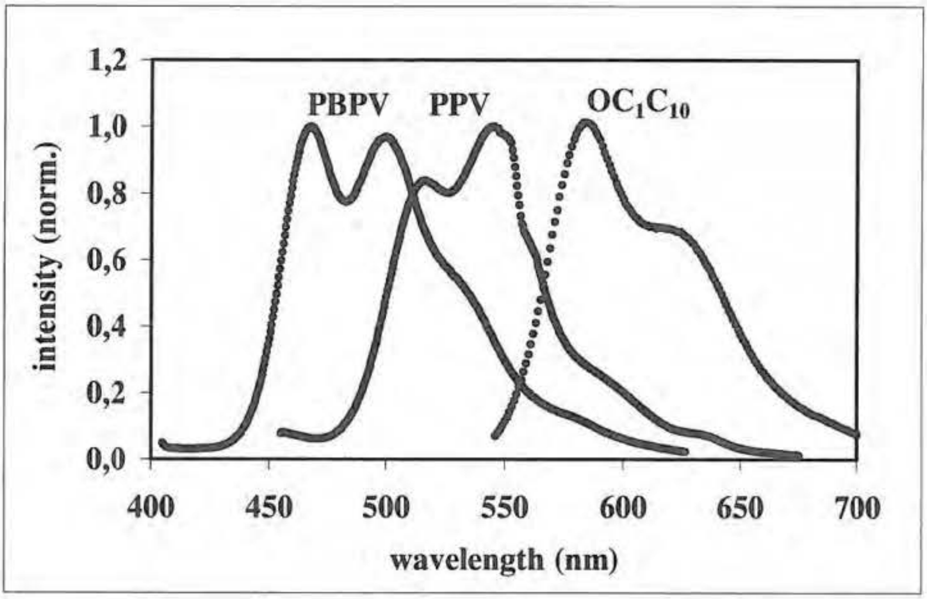

Figure 2.2 Photoluminescence spectra of poly(p-phenyle vinylene) (PPV), poly(2,5-dialkoxy-1,4-phenylene vinylene) (OC_1C_{10}) and poly(4,4'-bisphenylene vinylene) (PBPV)

2.2. Device preparation

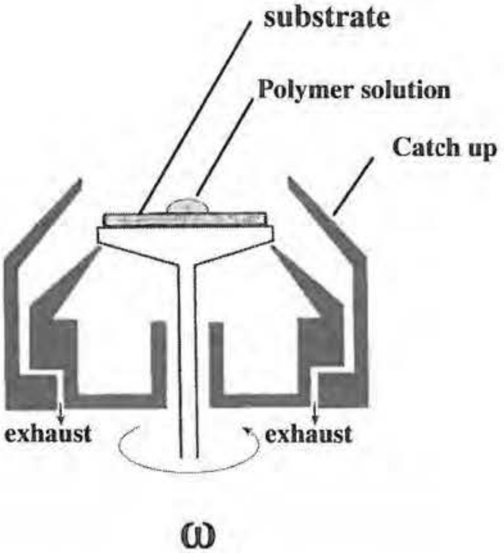

Figure 2.3 Schematic diagram of a typical spin coating system

Spincoating has been accepted as one of the best coating methods for obtaining suitable films over a wide range of thickness, typically 50 to 1000 nm. [Figure 2.3] shows a schematic diagram of a typical spin coating system. The thickness is accomplished by covering the substrate with a polymer solution and rotating it at a constant spinning velocity until the solvent evaporates. In particular, spin coated films are uniform in thickness and smooth over large areas when all parameters are well defined. The spin coating process is extensively used in microelectronics for coating planar surfaces. Here it is used for preparing single polymer films sandwiched between two electrodes. Knowledge of the parameters affecting the film thickness is of crucial importance for controling the device properties and modelling of the electrical behaviour. The significant parameters affecting the film thickness are the solvent boiling point, the concentration of the solution - molecular weight of the polymer (viscosity), the spin velocity and the substrate quality. These parameters will be discussed in more detail.

2.2.1. *Substrate quality*

The bottom substrate consists of a glass substrate coated with a transparent electrode (e.g. indium-tin-oxide, ITO). The most important aspect here, is the fact that the substrate should be dust particle free. By doing so, the film is free of comet-tail like defects. Another aspect improving device quality is the UV/O_3-or an O_2-plasma cleaning treatment. This treatment removes all organic impurities that are left on the substrate. The oxidation of the ITO is responsible for the observed work function increase(15) by up to 0.8-0.9 eV and hence an improved device performance(16). This results in bulk limited transport instead of contact limited behaviour. A supplementary gain is given by the extra oxygen at the surface, improving the affinity for the polymer solution, and by doing so, improving the structure at the interface. The use of an additional conducting polymer layer (PEDOT) [Figure 2.4] between the ITO and the emissive polymer layer results in a large improvement of device lifetime(17).

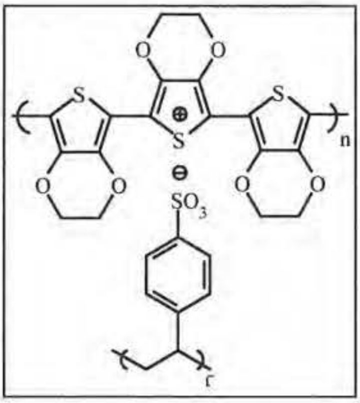

Figure 2.4 Chemical structure of the conducting polymer PEDOT, which is used as an anode coating.

2.2.2. Solution properties

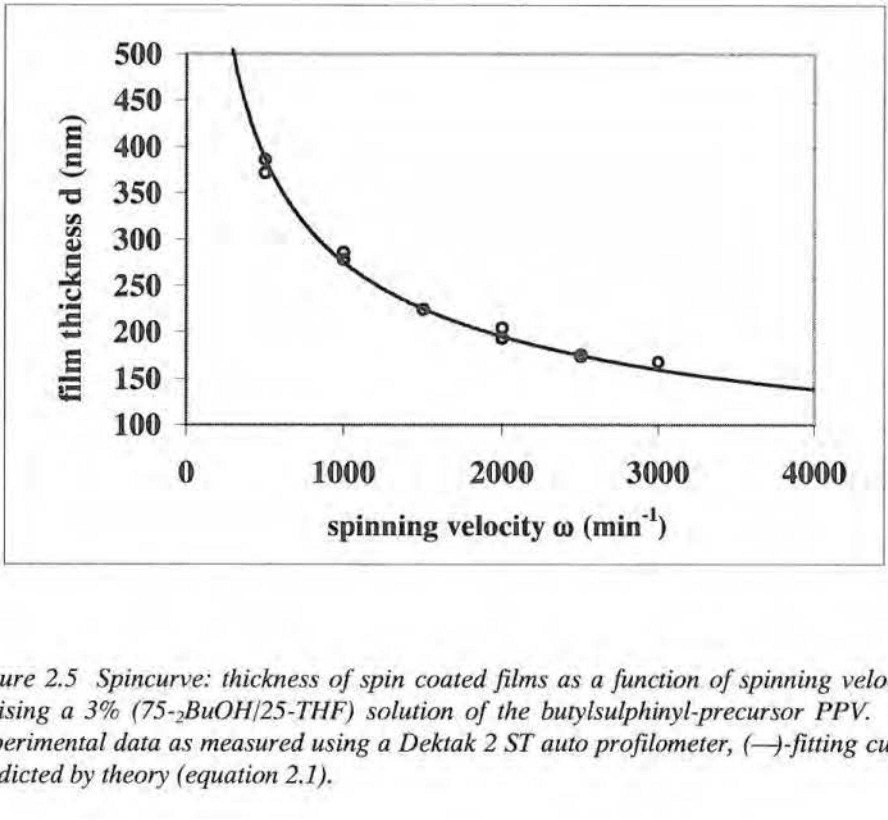

Figure 2.5 Spincurve: thickness of spin coated films as a function of spinning velocity utilising a 3% (75-$_2$BuOH/25-THF) solution of the butylsulphinyl-precursor PPV. (0) Experimental data as measured using a Dektak 2 ST auto profilometer, (—)-fitting curve predicted by theory (equation 2.1).

First of all, all solutions should be filtered in order to prevent comet-tail like defects. The concentration of the solution is important. Here one has to distinguish between precursor materials that have to be eliminated after spin coating and directly soluble derivatives like OC_1C_{10} (a dialkoxy substituted PPV). For the n-butylsulphinyl-precursor, we obtained the best results by using a 3% (75-$_2$BuOH/25-THF) solution [Figure 2.5] at room temperature. THF is added to prevent a concentric stripe-pattern, as observed in a pure alcohol solution. For soluble derivative (OC_1C_{10}) we used 0.5% (75-toluene/25-THF) at 50°C. Here THF is used to prevent gelation during spinning. In most cases the problem of inhomogenious films can be overcome by using a 3-step-spinning program: (1) first applying the solution at low spinning speed (15 sec); (2) than spinning at a higher speed with a closed cover during 45 sec, to form the thickness; (3) followed by dry spinning of the film with an open cover during 30 sec.

Theoretical approaches(18,19) predict a relation connecting film thickness (d) with spinning velocity (ω) :

$$d \sim \frac{1}{\sqrt{\omega}} \qquad 2.1$$

2.2.3. Thermal conversion

The conversion of the precursor into the conducting form is done by heating under vacuum (10^{-3}mbar, 180-240°C, 1-4 hours). There is a severe influence of temperature, pressure and chemical structure of the leaving group. More details about these parameters can be found in the work of De Kok(20). As a result of the chemical properties of our polymers we do not have an $InCl_3$-doping of the film during elimination as compared with the classical Wessling materials, where HCl is formed during the thermal conversion step. As a consequence, our films do not posses mobile (ions) charge carriers at sufficient concentration, so that a depletion layer and bandbendig-effects necessary for a Schottky-type of device behaviour, are excluded. The influence of the heating treatment on the ITO/polymer interface is not completely understood. After thermal treatment the PPV film is 3 times thinner than its precursor.

2.2.4. *Evaporation of the cathode*

The last step in the preparation of a metal/polymer/metal structure is the formation of the top electrode. The manner in which the electrical contact is made to the polymer is crucial. Contacts between metals and inorganic semiconductors are extensively described and understood within the framework of the band model. However, it is difficult to extrapolate these properties for band-type materials to the case of disordered materials, where carriers are localised and transport involves hopping between localised states. Since metal contacts are deposited by vacuum evaporation, parameters like evaporating speed, temperature and pressure are of obvious importance. A mechanism known to occur during vapour deposition of various metal contacts on organic thin films is diffusion of the metal atoms into the film(21). An additional difficulty is that some metals like Ca and Al chemically interact with the polymer during evaporation(22,23). In addition one has to account for the possibility of reorganisation of polymer molecules at the interface(24). Such phenomena could affect the injection properties at the interface. So, one has to be careful: slow evaporation speeds, high vacuum and control of the substrate temperature are recommended. Therefore it is advisable to leave the device to stabilise for several hours in an inert atmosphere before measuring the electrical properties. An inert atmosphere is of great importance to avoid an additional oxide layer at the interface.

If all distinguished steps in the device preparation are properly performed one end up with a perfect planar structure: glass/ITO/Polymer/Metal [Figure 2.6].

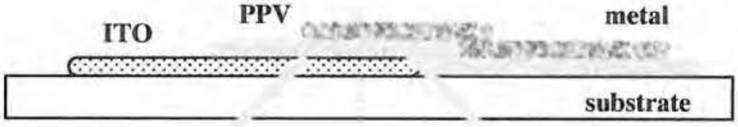

Figure 2.6 Schematic cross-section of the basic concept of a polymer LED, showing the metal cathode, the ITO anode and the emissive polymer layer (eg. PPV).

2.3. References

(48) Wessling, R.A. and. Zimmerman, R.G.,US Pat. 3,401,152 (1968)

(49) Wessling, R.A. and. Zimmerman, R.G.,US Pat. 3,706,677 (1972)

(50) Wessling, R.A., *Journal of Polymer Science: Polymer Symposium*, **72**, 55 (1986)

(51) Lenz, R.W., Han, C.H., Stenger-Smith, J. and Karasz, F.E., *Journal of Polymer Science:Part A: Polymer Chemistry*, **26** 3241 (1988)

(52) Burroughes, H., Bradley, D.D.C., Brown, A.R., Marks, R.N., MacKay, K., Friend, R.H. Burns P.L. and Holmes A.B., *Nature*, **347**,539 (1990)

(53) Greenham, N.C., Moratti, S.C., Bradley, D.D.C., Friend R.H. and Holmes, A.B. *Nature*, **365**, 628 (1993)

(54) Garay R.G. and Lenz, R.W., *Makromolekulare Chemie: Supplements*, **15**, 1 (1989)

(55) Yamada, S., Tokito, S., Tsutui T., and Saito, S., *J. Chem. Soc. Chem. Commun.*, 1448 (1987)

(56) Issaris, A., Vanderzande D. and Gelan, J., *Polymer*, **38** 2571 (1997)

(57) Louwet, F., Vanderzande, D., Gelan J., and Mullens, J., *Macromolecules*, **28** 1330 (1995)

(58) Van Der Borght, M., Vanderzande D., and Gelan, J., *Synthetic Metals*, **84** 399 (1997)

(59) Van Der Borght, M., Vanderzande D., and Gelan, J., *Polymer*, submitted for publication.

(60) Bijnens, W., Van Der Borght, M., Manca, J., De Ceuninck, W., De Schepper, L., Vanderzande, D., Gelan, J. and Stals, L., *Optical Materials*, **9**, 150 (1998)

(61) Issaris, A., *PPV-precursoren en hun polymerisatiemechanisme : Anionisch of toch radicalair?*, PhD. Thesis , L.U.C. (1997)

(62) Berntsen, A., Croonen, Y., Cuijpers, R., Habets, B., Liedenbaum, C.T.H.F., Schoo, H., Visser, R.J., Vleggaar, J.J.M. and van de Weijer, P., *proceedings of the Int. Symp. On Optical Science, Engineering and Instrumentation (SPIE)*, San Diego (1997)

(63) Blom, P.W.M., de Jong, M.J.M. and Munster, M.G., *Phys. Rev. B*, **55**, R656 (1997)

(64) Liedenbaum, C., Croonen, Y., van de Weijer, P., Vleggaar, J. and Schoo, H., *Synth. Met.*, **91**, 109 (1997)

(65) Meyerhofer, D., *J. Appl. Phys.*, **49**, 3993 (1978)

(66) Bornside, D.E., Brown, R.A., Ackmann, P.W., Frank, J.R., Tryba, A.A., Geyling, F.T., *J. Appl. Phys.*, **73**, 585

(67) De Kok, M., PhD. Thesis (1998)

(68) Wool, R.P., *Polymer Interfaces*, (Hanser-Verslag, Munich, 1995)

(69) Löglund, M., Dannetun, P., Stafström, S., Salaneck, W.R., Lazzaroni, R., Frederiksson, C. and Brédas, J.L., *Phys. Rev. Lett.*, **70**, 970 (1993)

(70) Löglund, M and Brédas, J.L., *J. Cheml. Phys.*, **101**, 4357 (1994)

(71) Ioannidis, A., Facci, J.S. and Abkowitz, M.A., *J. Appl. Phys*, in Press

Chapter 3

Electrical conduction mechanisms in Polymer LED's.

Electroluminescence in PLED's involves the processes of charge injection, recombination of charge carriers, creation of excited states, their quenching and finally their radiative decay producing light. The study of standard DC and EL techniques applied on as well hole only as double injection devices with different electrode materials, makes an evaluation of these properties possible.

3.1. Experimental

The substrates used for this study have four different active areas (ITO-coating). Most of the time the smaller areas (10 mm^2 or 20 mm^2) are used due to the better reproducibility. A selection of evaporated cathode materials is made to obtain single (eg. Al, Ag) and double (eg. Ca) carrier devices. On the anode side, ITO is coated with PEDOT to get a better reproducibility. The thickness of the active polymer layer is varied between 50 nm and 300 nm.

Hole-only devices are used to determine the transport properties of the holes. These experiments will give the hole mobility μ and its field and temperature dependence. The double injection devices are used to determine the recombination.

All low temperature current-voltage measurements are performed, at NATLAB Philips research centre in Eindhoven, in a glove box under nitrogen atmosphere, if it is not stated otherwise. The sample is placed in a special sample holder which has contact strips for each contact of the device, a nitrogen gas flow is used to cool the sample. The temperature of the nitrogen gas can be accurately controlled by altering the flow of gas through a heat exchanger cooled with liquid nitrogen. By doing so the temperature can be altered within the temperature range from 170 K to 300 K. The temperature can be kept constant within 1 K and is measured just below the sample with a thermo-couple.

A dedicated computer program controls the measurement of both the current and the light output as a function of applied voltage. The program controls a Keithley 2400 combined voltage source-electrometer measuring unit to measure the J-V characteristics and a Keithley 487 pico-amperemeter to read out the current of the photodiode.

For the optical detection a Minolta luminance LS-100-meter is used, this device makes it possible to measure the brightness of the PLED in Cd/m^2.

To be able to fit the experimental data presented we used a simulation program developed by Philips. This program makes it possible to simulate the *J-V* curves of hole-only, electron-only and two-carrier devices as function of temperature (between 200K and 300K). All parameters characterising the device can be changed in order to fit the experimentally observed *J-V* curves

3.2. Introduction

The structure of a PLED is presented in chapter 1, and discussed below (section 3.3). We have pointed out that as well the barrier at the metal/polymer interface as the carrier transport in the bulk are important. The first thing one has to do is to give a decisive answer whether the device is contact or bulk limited.

To answer this question one has to build up a strategy. First, one has to make hole- and electron-only devices with different metal contacts. Secondly, one has to measure their temperature, field and thickness dependent properties. By doing so, one obtains information about the injection and transport properties of the holes and electrons. In this way one can distinguish between contact or bulk limited behaviour.

In doped inorganic semiconductors the compensating positive charge, to establish equilibrium at the interface, is delivered via impurity ionisation. It gives rise to the formation of a Schottky-type depletion layer(1). In PLED's, where the PPV-film is prepared via the Wessling polymerisation route, sufficient dopant sites ($InCl_3$-doping) are present that act as electron donors or acceptors(2), so that a Schottky-type of behaviour can explain the properties of these type of devices.

In our materials however, donor/acceptor concentrations are too low for formation of a depletion layer. Band bending at the contacts is therefore negligible. This means that the energy barriers that control the hole and electron injection are $\Delta_h = IP\text{-}\Phi_{anode}$ and $\Delta_e = \Phi_{cathode} - EA$(3) [Figure 3.3] Depending on the magnitude of Δ the current is either injection or bulk (space charge limited, SCLC) controlled. The latter case requires the electrode contact to be ohmic, meaning that the electrode is able to supply more charge carriers per unit time than the bulk can transport (in this concept the metal is an infinite charge reservoir). Otherwise charge carrier injection will be the rate-limiting step(2).

Two models for carrier injection are extensively studied in the context of PLED's: the Fowler Nordheim (FN) model for tunnelling injection(4) ,and the Richardson-Schottky (RS) model for thermionic emission(1,5). This interpretation in terms of contact limited currents is based on the experimental observation by Parker(8) that the current scales with the field.

Both models have there shortcomings$^{(6,7)}$. At an electrical field of about 10^6V/cm (customary in PLED) the barrier lowering is comparable to the barrier height itself and its neglect in the FN-tunnelling model is problematic as is the implication of a triangular barrier and temperature independence. The application of the RS model suffers from the neglect of inelastic carrier scattering inside the potential well which is of crucial importance in organic solids in which transport is an incoherent process and the main free path is comparable to the intermolecular distance. Despite these shortcomings, both models have extensively been applied to PLED's. The motivation for the FN model is the reasonable values for the barrier height (25% less than the actual barriers) and the fact that at high fields one obtains a linear shape when plotting the data in a $\ln(J/E^2)$ versus *1/E plots*, as predicted by the theory$^{(8)}$. However this functional agreement is accidental. The absolute currents are orders of magnitude lower than expected on the basis of the theory$^{(9)}$.

Blom et al.$^{(10-16)}$ first performed experiments on OC_1C_{10} based hole-only devices. They found that the current was space charge limited (SCLC). They based a model on their field and temperature dependent measurement and concluded that the mobility can be described by the Gill equations. There experiments are consisted with the idea of disorder as proposed by Bäsller et al$^{(6)}$. In the model of Blom, the experimental result, concerning the current-voltage measurements, are interpreted in terms of hopping (oxidation/reduction) in a structural disordered material, where the hopping sites are short conjugated segments randomly distributed throughout the bulk.

Our experimental results are best explained by the model of Blom. The option for this disorder model has its implication on the description of the electrical properties like the mobility of the material. In this model the mobility will have a field and temperature dependence as described in chapter 1 (section 1.4.3). We will start with Ohm's law and than fill-in the field- and temperature dependent mobility. It will be shown that this idea of disorder in the bulk material, results in a straightforward description of the current-voltage curves of a PLED. And by doing so, we are able to describe the J-V curves over a large voltage range, much larger than when using the standard models for injection.

In a first part of the experimental results we will use hole-only devices to study the field and temperature behaviour of the J-V curves. By doing so, we are able to calculate the hole-mobility in our PPV material. In a second part, this hole-mobility will be used to describe double injection devices (actual PLED's), their transport properties and conversion efficiency.

However before going to the experimental results we will first present the different models discussed in the literature: (I) the standard model of charge injection and (II) the bulk model based on disorder. Since we will use the bulk-model, a detailed description of this model will be given.

Before we are able to discus the properties of a PLED, we need to visualise its electronic energy structure. In the literature it is always done by using pictures based on the semiconductor band model. To visualise the results we use the simplified representation of conduction and valence band, with electrons and holes. However, the charge carriers have a very low mobility, due to their localisation on the conjugated segments. Mobility will thus be described in terms of hopping transport in disordered semiconductors.

3.3. Schematic electronic energy structures of PLED's.

With the knowledge that a polymer is a disordered medium, resulting in a Gaussian distribution of the DOS. one can see the top of the valence band (HOMO, highest occupied molecular orbital, IP, ionisation potential) or the bottom of the conduction band (LUMO, lowest unoccupied molecular orbital, EA, electron affinity) as the maximum of the DOS.

As discussed in chapter 2, a PLED consists of a polymer film sandwiched between two different metal contacts. The bottom contact is ITO or ITO coated with a polymer (PEDOT) with a high work function (Φ_{anode}) close to the valence band. The top contact is typically evaporated Ca with a low work function ($\Phi_{cathode}$) close to the conduction band of PPV. ITO is the hole injection contact and Ca is the electron injection contact. Upon contacting the polymer with the metal electrodes the Fermi levels on both sides of either contact have to equilibrate. This is among other things accomplished by charge exchange across the interface [Figure 3.2].

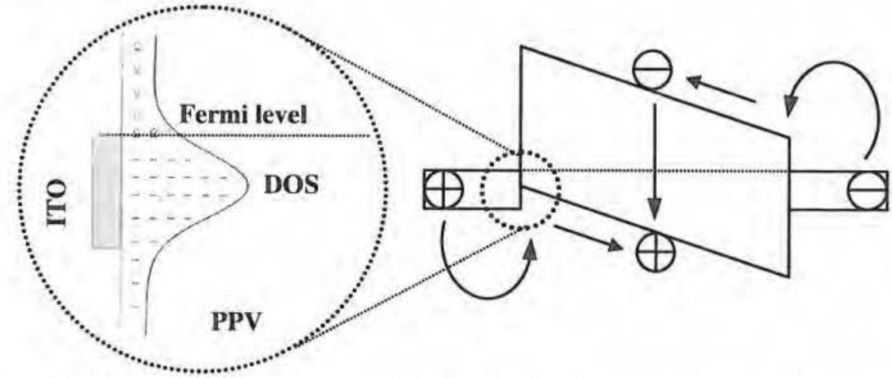

Figure 3.2 Schematic energy diagram for a disordered semiconductor with a distribution of localised states (DOS), in two-carrier devices at zero bias. The insert shows the detailed picture at the ITO-PPV interface. To establish equilibrium at the PPV-ITO contact electrons will flow from the PPV into the ITO until the Fermi-levels of the two materials are lined up. (o) represent the localised states occupied by holes in order to line up the Fermi level at the interface.

When two metals with a different work function are contacted to an insulator (or a semiconductor with a large bandgap) the equilibrium is accomplished by a charge build-up in the metal at the interface. This results in a built-in voltage (V_B) as can be seen in [Figure 3.2]. The difference in work function causes an internal electrical field. Further, if an external forward bias is applied, the Fermi level of the cathode is lifted upwards. By doing so the internal field is lowered until this field is totally compensated by the built in voltage (V_B) [Figure 3.3]. At this point there is only diffusion current due to the difference in Fermi levels. At higher voltages carriers can flow and the device works.

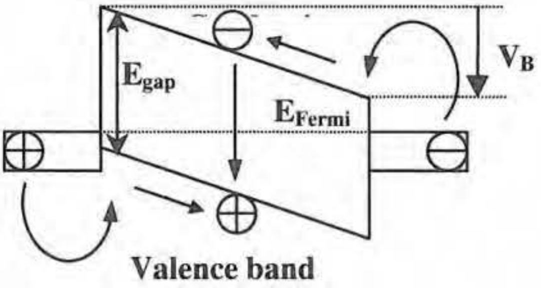

Figure 32. Schematic view of a PLED with electron and hole injection contacts at zero bias. E_{gap} = energy difference between the HOMO and LUMU, in the semiconductor band-picture, the bandgap. E_F = the Fermi level. V_B = the build-in voltage.

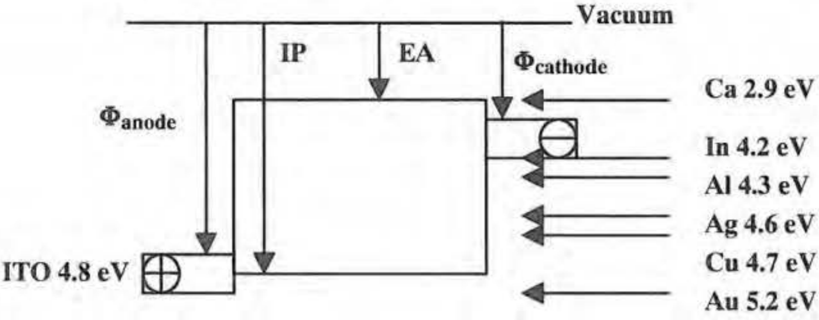

Figure 3.3 Schematic flat-band representation of a PLED under a forward external bias equal to the build in voltage, with a range of metallic electrodes as cathodes. Parker et al.(11). IP = ionisation potential, EA = electron affinity, F = work function of the metal.

3.4. Charge carrier injection

3.4.1. Field-assisted thermionic injection over an image force barrier.

The RS model assumes that carriers entering the sample are thermalised at a discrete distance, or are distributed exponentially from the geometrical interface with an average penetration depth. Only a fraction of this emitter-base current can enter the medium because there is an image force barrier located, at a certain distance of the interface, which reflects part of the carriers. When neglecting tunnelling through the barrier, thermal activation over the barrier is the process determining the fraction of the carrier, which contribute to the collected current. The barrier height decreases with the applied field (Schottky effect), so the collected current (J) is an increasing function of E and ($J(E)$) will follow$^{(1,5)}$:

$$J(E) = A_{RS} T^2 \exp - \left(\Delta /_{kT} \right) \exp\left(\beta \sqrt{E} \right) \qquad 3.1$$

With $\beta = (e/kT)(e/\pi\varepsilon_r\varepsilon_0)^{1/2}$, ε_0 is the permittivity of free space and ε_r the relative dielectric constant of the material, A_{RS} is a constant.

3.4.2. *Tunnelling through a triangular barrier (FN model)*

Tunnelling is described by the classic FN model of electron injection, ignoring the image force barrier. The current (*j(E)*) is predicted by$^{(4)}$:

$$j(E) = A_{FN} E \exp- \left(\frac{8\pi \sqrt{2m^* \Delta\Phi^{3/2}}}{3ehE} \right) \qquad 3.2$$

Where E is the electrical-field, $\Delta\Phi$ is the barrier height and m^* is the effective mass of the charge carriers, A_{FN} is a constant. Here charge tunnels from the metal through a triangular barrier into unbound continuum states independent of temperature.

3.5. The device model of Blom et al.

The conventional models of carrier injection, suggesting that the charge injection is the dominant step in the device properties cannot adequately account for the temperature and field dependence transport in polymer devices. Recently Blom, de Jong and Vissenberg developed a device model based on their experiments(10-18). In this model the device contacts are ohmic resulting in a current that is bulk limited (space charge limited current , SCLC).

Before going to our experimental results on precursor polymers, in this last part of the theory, we will give a comprehensive description of the theory by Blom et al. The device model is based on the theory of conventional double-injection semiconductor devices(19). Meaning that in steady state, the carrier flow is defined by the drift equation (Ohm's law)(20) and the Poisson equation:

$$J = ep(x)\mu E(x)^{1} \qquad 3.3$$

$$\frac{\varepsilon}{e}\frac{\partial E(x)}{\partial x} = p(x) \qquad 3.4$$

With J the current density, e the elementary charge, $p(x)$ the carrier density at position x, μ the carrier mobility, $E(x)$ the electrical field and ε the dielectric constant.

---

[1] Ohm's law : $I = \frac{V}{R}$ and $R = \frac{\rho l}{A}$ and $\rho^{-1} = \sigma , \sigma = p\mu e$ with I the current, V the voltage, R the resistance, l the length of the sample, A the cross-section and σ the conductivity

3.5.1. Hole-only devices

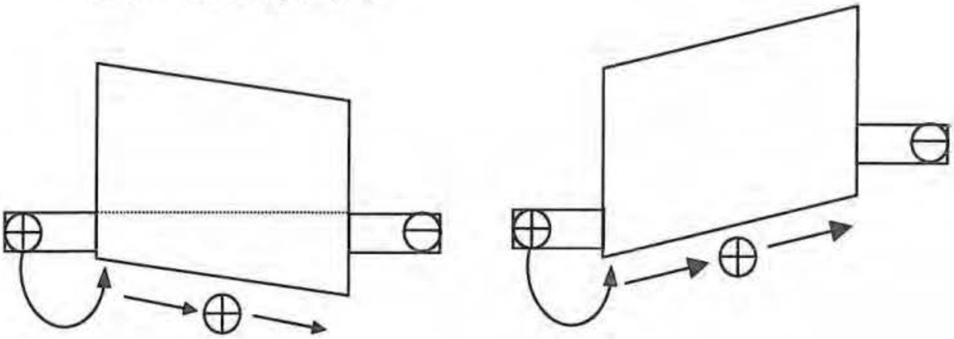

Figure 3.4: Schematic structure of a hole-only device at zero voltage (left) and at an applied voltage bias (right), e.g. anode = ITO and cathode = Ag.

A hole-only device has two metallic contacts with work functions near the valence band of the polymer, (eg. ITO, PEDOT and Al, Ag) [Figure 3.4]. In this way ohmic contacts are formed and holes can easily be injected while the barrier for electrons is too high. Charge transport is then completely dominated by holes moving around in the HOMO. And since electron injection into the LUMO is impossible a hole-only device will not emit light.

Combining equation 3.3 with 3.4 results in

$$\frac{\partial E(x)}{\partial (x)} = \frac{J}{\varepsilon \mu E(x)} \qquad 3.5$$

Integration gives:

$$E(x) = \sqrt{E^2(0) + \frac{2J}{\varepsilon \mu}} \qquad 3.6$$

With the boundary condition E(0)=0 of an ohmic contact we obtain the relation for the space charge limited current (SCLC):

$$J = \frac{9}{8}\varepsilon\mu_p\frac{V^2}{L^3} \qquad 3.7$$

with $\varepsilon=\varepsilon_0\varepsilon_r$ the permittivity of the polymer and μ_p the hole mobility. Eq. 3.7 provides a good description of the *J-V* characteristics(11) at low voltages using $\mu_p=5.10^{-11}$ m^2/Vs and $\varepsilon_r=3$.

At higher voltage the observed current density J is larger than expected by equation 3.7. Since SCLC depends only on the bulk mobility, this deviation may be explained by $\mu(E)$. As demonstrated in chapter 1 the field dependent mobility can be described by:

$$\mu_p(E) = \mu_p(0)e^{(\gamma\sqrt{E})} \qquad 3.8$$

where

$$\mu_p(0) = \mu_0 e^{(-\frac{\Delta}{k\ T})} \qquad 3.9$$

and

$$\gamma = B_\gamma(\frac{1}{kT}-\frac{1}{kT_0}) \qquad 3.10$$

where Δ is the Arrhenius activation energy and μ_0 denotes the mobility at zero field. The field dependence γ is comparable to the Poole-Frenkel effect(21). In order to describe the hole conduction at both high and low electrical field the SCLC can be combined with a field and temperature dependent mobility and the *J-V* characteristics can completely be described by equations 3.3, 3.4 and 3.8.

Equations 3.3 and 3.4 can be solved numerically for a given J. The voltage is given by:

$$V = \int_0^L E(x)dx \qquad 3.11$$

A set of experimental J-V curves as a function of temperature can now be described by equations 3.3, 3.4 and 3.8-3.10. Numerous experiments on moleculary doped polymers, pendant group polymers, amorphous molecular glasses and conjugated polymers have revealed a universal behaviour, with typical parameter values of $\Delta \sim 0.5$ eV, $B_\gamma \sim 3\ 10^{-5}$ eV(m/V)$^{1/2}$ and $T_0 \sim 600$ K. And a μ_0 (OC_1C_{10})(11)$=3.5\text{x}10^{-3}$ m^2/Vs

3.5.2. Electron-only devices

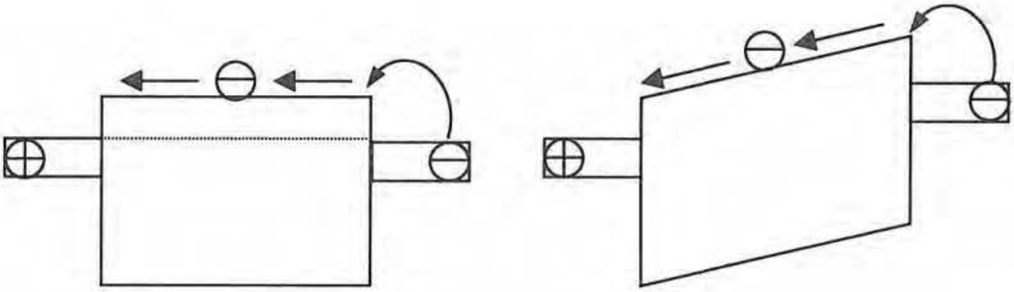

Figure 3.5: Schematic structure of an electron-only device at zero voltage and (left) at an applied voltage bias (right), e.g. anode = Ca and cathode = Ca.

An electron only device has two metallic contacts with work functions near the conduction band of the polymer, (eg. Ca). In this way ohmic contacts are formed and electrons can easily be injected while the barrier for holes is too high. Charge transport is then completely dominated by electrons moving around in the LUMO. And since hole injection into the HOMO is impossible an electron-only device will not emit light.

The electron current is smaller than the hole current and shows a very strong field dependence which is characteristic for a trap filled limited (TFL) mechanism in an insulator with traps$^{(19)}$. These traps have an exponential distribution in energy, as expected for a disordered system like PPV:

$$n_t(E_t) = \left(\frac{N_t}{kT_c}\right) e^{\left(\frac{E_t - E_c}{kT_c}\right)} \qquad 3.15$$

With $n_t(E_t)$ the trap density of states at energy E_t , N_t the total trap density, E_c the energy of the conduction band and kT_c the energy characterising the trap distribution.

In this way the TFL current is given by:

$$J = N_c e \mu_n \left(\frac{\varepsilon_0 \varepsilon_r}{e N_t} \right)^r \frac{V^{r+1}}{L^{2r+1}} C(r) \qquad 3.16$$

With $r = T_c/T$, the effective density of states in the conducting band estimated as $N_c = 2.5 \times 10^{19}$ cm^{-3} and $C(r) = r^r (2r+1)^{r+1} (r+1)^{-r-2}$. In this way Blom et al.(15) confirmed the severe trapping of electrons as observed in the time-of-flight measurements by Antoniades et al.(23)

3.5.3. *Two carrier devices : The actual LED*

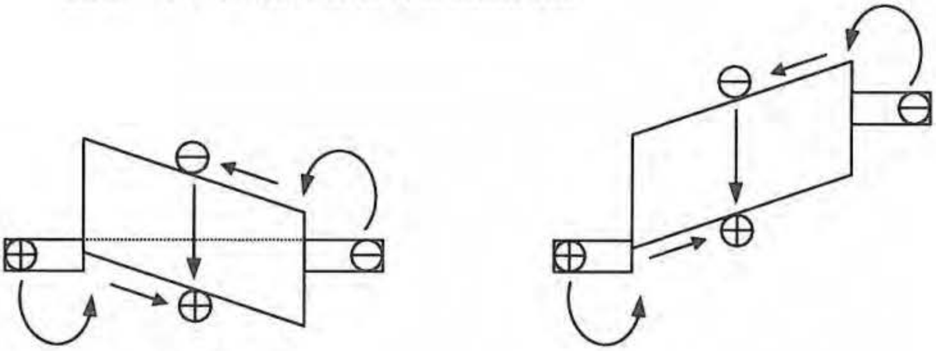

Figure 3.6: Schematic structure of a two carrier device (LED) at zero voltage (left) and at an applied voltage bias (right), e.g. anode = ITO and cathode = Ca.

A LED has one metal contact with a work function close to the valence band and the other close to the conduction band of the polymer. Both the holes and electrons are easily injected into the polymer film. Electrons in the LUMO and holes in the HOMO will determine charge transport. By recombination of electrons and holes light can be emitted by the polymer. The model takes into account the effects of both space charge (holes) and trapping (electrons). Two additional phenomena become of importance, namely *recombination* and *charge neutralisation*. In a simple case the model is based on the theory of conventional double injection semiconductor devices(19). A direct recombination between the injected electrons and holes is assumed. The difference in current between a single and a double carrier device (Eq. 3.7 and Eq. 3.11) provides direct information about the strength of the recombination process.

The device model for an LED is then characterised by the current flow equation:

$$J = J_p + J_n = e\mu_p p(x)E(x) + e\mu_e n(x)E(x) \tag{3.17}$$

The Poisson equation: this describes the neutralisation.

$$\frac{\varepsilon_0 \varepsilon_r}{e} \frac{\partial E(x)}{\partial x} = p(x) - n(x) - n_t(x) \tag{3.18}$$

And the particle conservation equation: which describes the recombination.

$$\frac{1}{e} \frac{\partial J_n}{\partial x} = -\frac{1}{e} \frac{\partial Jp}{\partial x} = Bp(x)n(x) \tag{3.19}$$

with B the bimolecular recombination constant, p(x) and n(x) the density of mobile holes and electrons, E(x) the electric field as function of position x and $n_t(x)$ the density of trapped electrons. These equations can be solved numerically.

The mobility and density of holes and electrons and the density of trapped electrons are known from the single-carrier experiments. The only unknown parameter in a double injection device is B, the recombination constant.

3.6. Experimental results

3.6.1. *Non substituted precursor PPV*

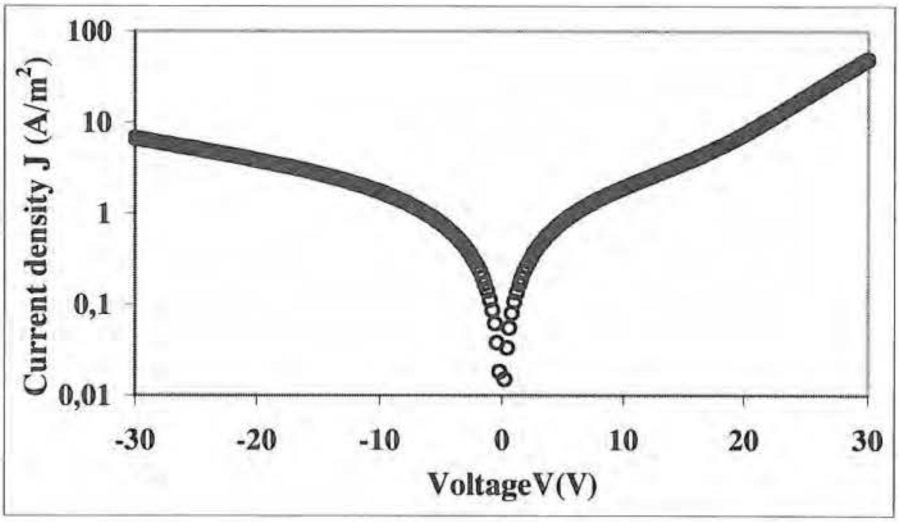

Figure 3.7 Current density J versus voltage V of a ITO/PEDOT/PPV/Ag hole only device with a polymer film thickness L= 240 nm. At room temperature.

In this part we discuss the results of the J-V experiments on LED's prepared with our precursor PPV. In [Figure 3.7] a J-V curve of a ITO/PEDOT/PPV (240 nm)/Ag hole-only device is presented.

As a result of the different work functions of PEDOT and Ag the current should be asymmetric in forward and reversed bias. The observation that the curve is almost symmetric suggest that we are measuring something else. Even if the device becomes contact limited due to the thermal treatment, the J-V curve should not by symmetric. As predicted by the theory in a contact limited sample the current is influenced by the work function of the electrode.

Nevertheless we studied the temperature dependence of the device with L=240 nm as shown in [Figure 3.8]. For this sample we observe an activation energy according to eq. 3.20 of Δ=0,054 eV and a pre-factor $C_0 = 6\times10^{-7}$ m^2/Vs [Figure 3.9].

$J = Ce^{-\Delta/kT}$, with Δ the Arrhenius activation energy. 3.20

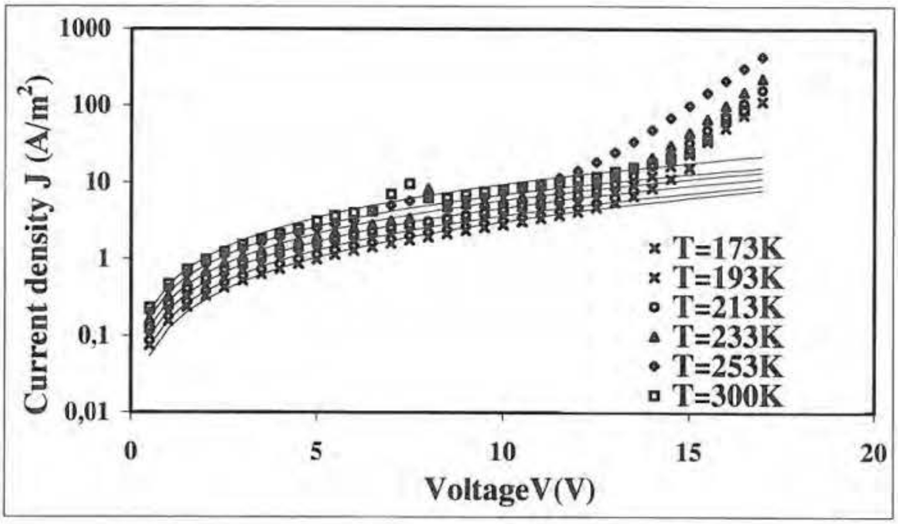

Figure 3.8 Current density J versus voltage V of a PEDOT/PPV/Al hole only devices with a polymer film thickness L= 240 nm for various temperatures. The calculated J-V is given by Eq. 3.20.

This activation energy is far off the value predicted by the theory. Especially striking is the fact the J-V curves only decrease with one order of magnitude, when going down in temperature. And this, in spite of the fact that the SCLC theory predicts a change in current of more than five orders of magnitude at low field. This low activation energy together with the fact that the curves are almost symmetric, indicates that we are measuring leakage current instead of the properties of the polymer material.

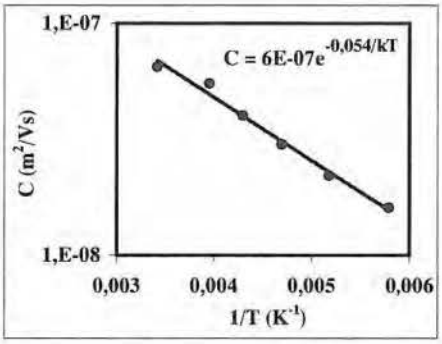

Figure 3.9 The Arrhenius plot of the pre-factor versus inverse temperature 1/T. The data are obtained using Eq. 3.20, yielding an activation energy $\Delta=0{,}054$ *eV and a* $C_0 = 6x10^{-7}$ *m*^{2}*/Vs.*

If we now make the assumption that the field dependent coefficient γ is of a universal nature, than γ should be around $5{,}6x10^{-4}$ at 300K. If we use this value with the hypothesis that the current is SCLC, we can fit the J-V curve of [Figure 3.7] and calculate the zero field hole mobility $\mu_p(E=0)$ at 300K [Figure 3.10].

As seen in [Figure 3.10] The J-V curve predicted by the SCLC theory describes the experimental curve quite well in the high field, with parameters $\gamma = 5{,}6x10^{-4}$ $(m/V)^{1/2}$ and a $\mu_p(E=0)$.= $1.0x10^{-13}$ (m^2/Vs) at 300K. These results are expected for this type of material. We now evaluate only the high field part of the J-V curves in [Figure 3.8] as being SCLC, indicated by the results of [Figure 3.10].

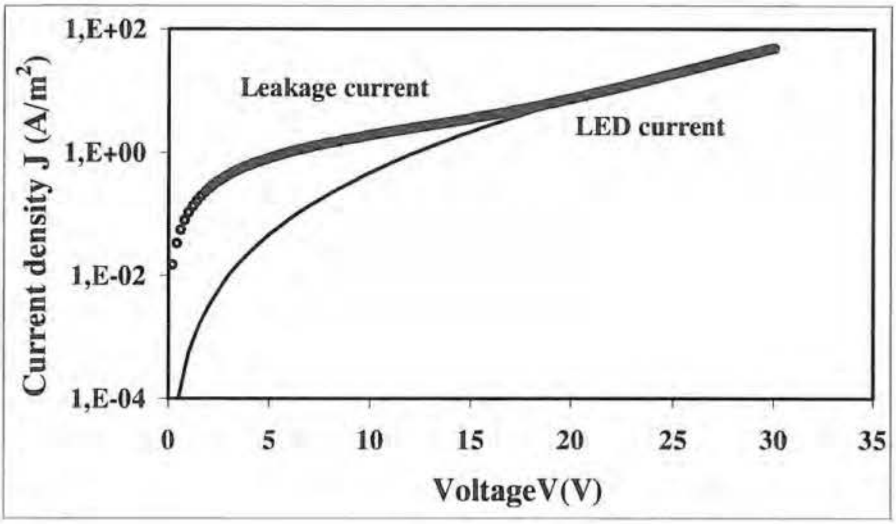

Figure 3.10 Current density J versus voltage V of a PEDOT/PPV/Al hole only devices with a polymer film thickness L= 240 nm, at room temperature. The calculated J-V characteristic is predicted by the SCLC model using a field dependent mobility. Using equations 3.8 –3.10, this gives $\gamma = 5{,}6x10^{-4}\ (m/V)^{1/2}$ *and* $\mu_p(E=0) = 1.0x10^{-13}\ (m^2/Vs)$ *at 300K.*

In this way we obtain the parameters describing the J-V curve [Figure 3.11]: Δ=0,17 eV, T_0 =828 K, B= 2,14x10^{-5}eV(m/V)$^{1/2}$and μ_0= 4x10^{-10} m^2/Vs. Keeping in mind that these results are obtained for a very small voltage range (from 12 V to 17 V in [Figure 3.8]) they are fairly good. [Figure 3.10] shows that the theory describes the experimental curve quite well in the high field and that the current is several orders of magnitude higher, at low fields, than predicted. This explains why the field dependence parameters are much better than the obtained activation energy. This is due to the fact that the mobility is obtained from the low field part using equation 3.7 and 3.9 and the γ is obtained from the high field part using equation 3.10.

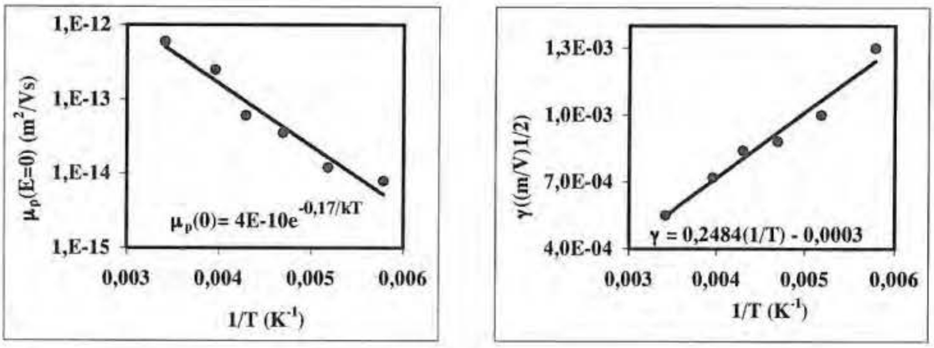

Figure 3.11 Left: The Arrhenius plot of the zero field mobility $\mu_p(0)$ versus inverse temperature 1/T. The mobility is obtained using Eq. 3.7. The solid line according to Eq. 3.9 yields an activation energy Δ=0,17 eV and a μ_0= $4x10^{-10}$ m^2/Vs. ***Right:*** *The coefficient γ (which describes the field dependence of the mobility) as a function of inverse temperature 1/T. Applying Eq. 3.10, gives T_0 =828 K and B_γ = $2,14x10^{-5} eV(m/V)^{1/2}$*

3.6.2. The leakage current of PEDOT

The current at low field is several orders of magnitude higher than predicted by theory and being symmetric means that it is independent of the electrode material. In this section it will be shown that leakage current (eg. direct contact of anode and cathode) is responsible for this behaviour. Leakage current in often used to explain deviations of the measured current from the theoreticaly expected current in the low field area$^{(2)}$. In this case leakage current could mean the presence of conductive paths between the electrodes. This implies that the leakage current should reflect the temperature and field dependence of the electrode structure. To verify this hypotheses we have measured the temperature behaviour of a PEDOT/Ag sample, prepared identically as the PEDOT/PPV/Ag, including the thermal treatment, only leaving out the precursor polymer. The J-V curve of this PEDOT sample is given in [Figure 3.12]. The characteristic is perfectly symmetric, as suspected for a metal like/metal contact.

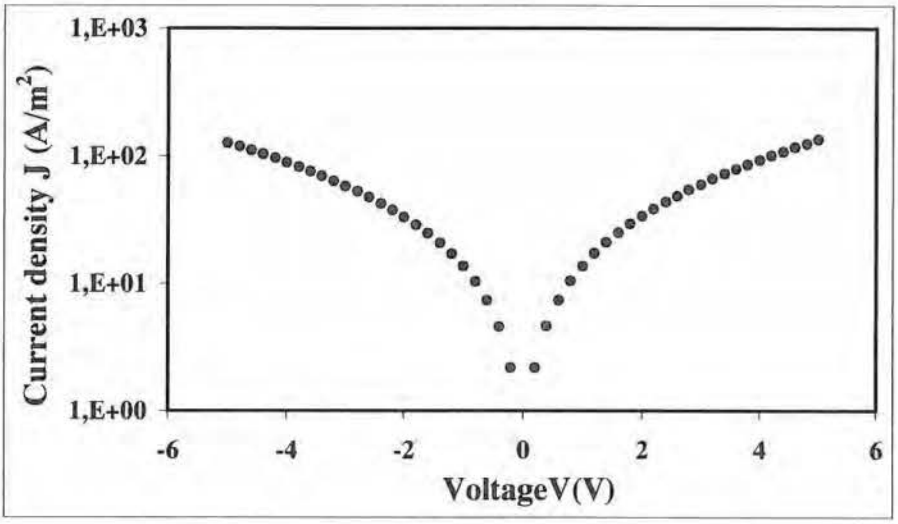

Figure 3.12 Current density J versus voltage V of a PEDOT/Ag device with thickness L = 320 nm, at room temperature.

The temperature dependent J-V curves of the PEDOT/Ag sample are given in [Figure 3.13]. Only a small temperature dependence is observed. The analysis of the PEDOT sample in an Arrhenius manner, yields a small activation energy of Δ=0,04 eV and a C_0= 8x10^{-6} m^2/Vs. These results are comparable as the ones obtained for the PEDOT/PPV/Ag sample (Δ=0,054 eV and C_0= 6x10^{-7} m^2/Vs). This means that the leakage current of PEDOT mainly dominates the temperature dependence of our hole-only device (PEDOT/PPV/Ag). The field dependent behaviour mainly originates from the field dependent mobility of PPV.

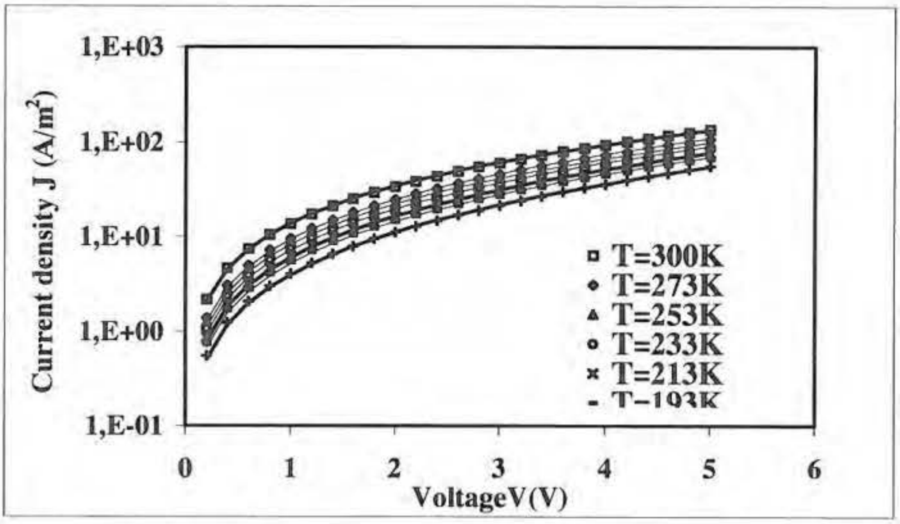

Figure 3.13 Current density J versus voltage V of a PEDOT/Al device with thickness L= 320 nm for various temperatures. The calculated J-V characteristics as predicted by Eq. 3.19.

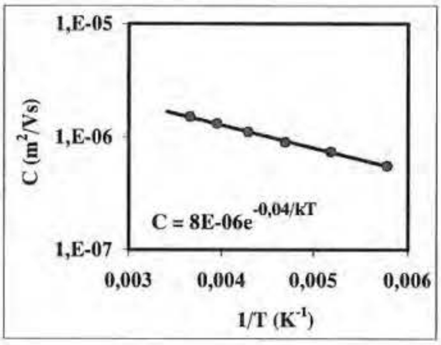

Figure 3.14 The Arrhenius plot of the pre-factor C versus inverse temperature 1/T. The data are obtained using Eq. 3.20, yielding an activation energy Δ*=0,04 eV and a* C_0*=* $8x10^{-6}$ m^2/Vs

One can rescale the PEDOT J-V curve in order to estimate the area of the device that contributes to the leakage current [Figure 315]. The rescaling in the figure shows that according to this hypothesis 0,7 % of the area the Al electrode should be directly contacted to the PEDOT.

If 0,7% of the area of our hole-only device consists of direct contacts of the Ag with the PEDOT electrode, then one expects that there are pinholes in the PPV film.

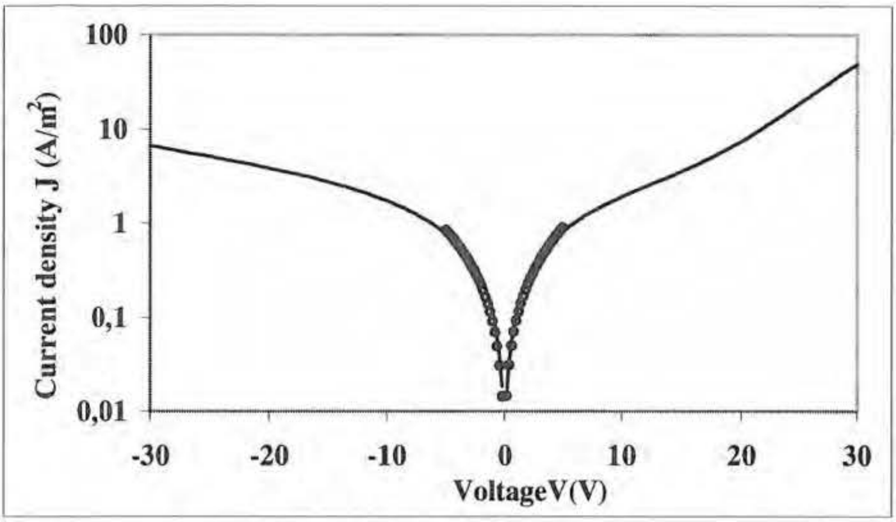

Figure 3.15 Current density J versus voltage V of a PEDOT/PPV/Ag device (—) as in [Figure 3.7] and the J-V curve of a PEDOT/Ag (o) devices as in [Figure 3.12] at room temperature. The PEDOT current is divided by 150.

We have examined a PPV film with a thickness of 150 nm in the atomic force microscope (AFM). The AFM makes it possible to study the roughness and depth profile of an area with a resolution of a few angstroms. [Figure 3.16] shows such a profile of a 12 mm^2 area on a PPV film obtained by our precursor. One can clearly see two crater like holes in the film and some spikes. The depth of these craters is the same as the film thickness; the area of the craters is a few square microns. The presence of the craters implies that upon evaporating the Ag electrode, the craters are filled with Ag. This results in a direct contact of PEDOT with Ag. The spikes are also possible candidates for contacting the top and bottom electrode. When the spikes are particles that are completely pierced through the PPV film, then they will contribute to the leakage current.

The craters are most likely due to explosions during the thermal conversion of the precursor film at 220°C in vacuum. The spikes are impurity particles on the bottom electrode surface or within the PEDOT and PPV film. Changing the temperature profile and atmosphere during conversion may solve the problem of crater formation. An other solution can be given by changing the leaving group and so reduce its volume. The problem of the impurity particles is clearly a cleaning problem. Since these parameters have a large influence on the quality of the polymer film, by improving them, one should be able to reduce the leakage current in the devices.

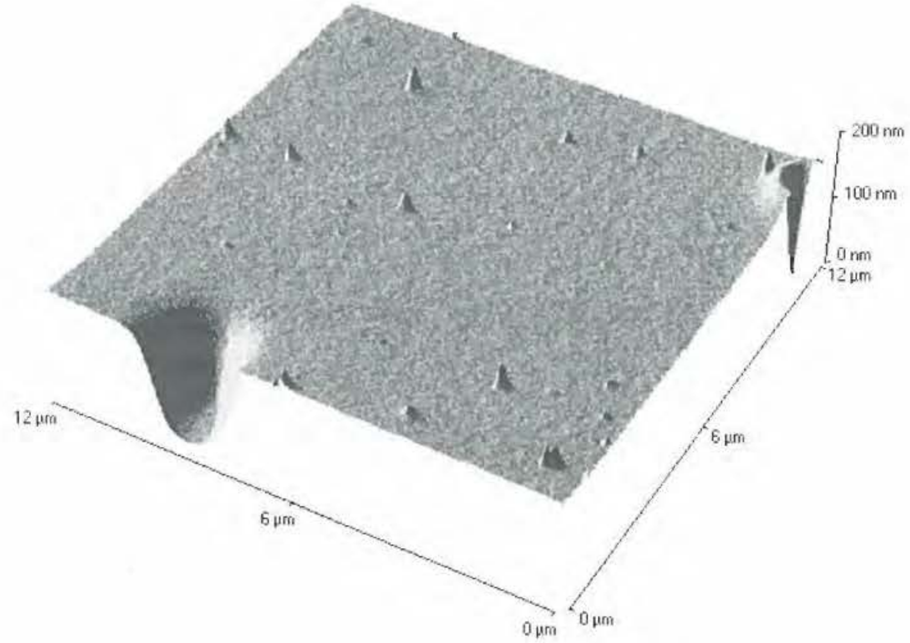

Figure 3.16 An AFM image a of 12 mm^2 area on a PPV film, showing the presence of craters and spikes in the polymer film.

Leakage current is a process that is not an inherent property of the polymer material. It is a side effect that covers up the effects that we want to study. By taking approximately all current away from the active layer it reduces the efficiency of the device to almost zero. This means that if we want to study the properties of devices based on precursor PPV we need to improve the film properties.

3.6.3. OC_1C_{10}: a dialkoxy substituted PPV

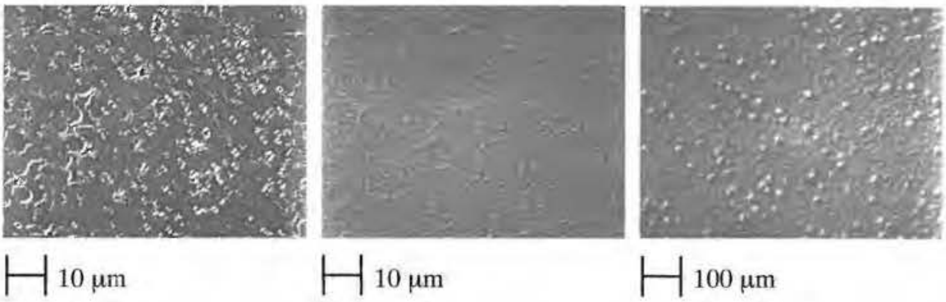

Figure 3.17 ***Left (a)*** *1 cm = 14 μm An OC_1C_{10} spincoated films out of a pure toluene solution (at 50°C) stirred at 50°C over night after filtration.* ***Centre (b)*** *1 cm = 14 μm An OC_1C_{10} films spincoated out of toluene/THF (75/25) at 80°C, stirred at 50°C over night after filtration.* ***Right (c)*** *1 cm = 140 μm An OC_1C_{10} spincoated films spincoated directly after filtration (0,54μm) out of toluene/THF (75/25) at 80°C.*

In a direct and easy approach one can overcome the problem of crater-hole formation in polymer film during thermal conversion on the substrate. This is achieved by using a soluble derivative, which can be spincoated in its conjugated form, so that the thermal treatment of the device becomes unnecessary. In this synthesis approach the precursor polymer is converted in solution. Note the fact that the OC_1C_{10} we use is still prepared by our precursor route. An additional advantage of this approach is the fact that the polymer/anode interface is not heated, as shown above for PPV the process of conversion on the substrate enlarges the possibility for an ohmic contact. A disadvantage is the fact that one loses the insolubility of the polymer. This means that the glass transition temperature (Tg) drops below 100°C, making this material softer and much more vulnerable. The decisive argument to use these kinds of materials is the good film properties: completely amorphous with no pinholes and very little film defects. This implies that the leakage current is reduced by a few orders of magnitude. These good film properties together with the other material properties make that LED's based on OC_1C_{10} have a high efficiency$^{(15)}$.

However there is a crucial point that one has to keep in mind when using soluble polymers: gelation (aggregation). Conjugated molecules have the tendency to aggregate. As a result of the solubility (and since the long tails are not able to prevent it) the polymers will aggregate in solution and during spincoating. This results in bad film properties. However this can be overcome by tuning the solvent mixture, temperature and concentration. Optical microscope images of OC_1C_{10} spicoated films are given in [Figure 3.17 a,b,c]. Films spincoated out of a pure toluene solution (at 50°C) have very bad properties [Figure 3.17 a]. One can clearly see islands, induced by gelation during spin coating. These defects in the film result in symmetrical J-V curves and leakage current [Figure 3.18]. By adding 25% percent of THF to the solution, one obtains a more or less homogeneous film [Figure 3.17 b] (spinning at 80°C, after stirring at 50°C over night); the defects are 10 times smaller. A remarkable observation is the fact that when spincoating this polymer solution (toluene/THF) directly after filtration (0,54μm) one obtains a film with gel particles of ± 30 μm randomly distributed on the substrate [Figure 3.17 c]. This means that by pushing the solution through the filter pores, the polymer chains align and form aggregates, these are much bigger that the pores size of the filter. The devices that are discussed below are prepared by spinning a solution of toluene/THF (75/25) at 80°C, stirred at 50°C over night after filtration.

A J-V characteristics of a PEDOT/OC_1C_{10}/Ag hole only devices spincoated form a pure toluene solution as in [Figure 3.17 a] is plotted in [Figure 3.18]. The curve is almost completely symmetrical, this means that it is dominated by leakage current as discussed above. Therefore not only holes, but also bad film properties in general result in devices dominated with leakage current. For the rest of the OC_1C_{10}-study we use the more or less homogeneous polymer films, as described in [Figure 3.17 b].

[Figure 3.19] shows an J-V curve of such a more or less homogeneous film. At room temperature (293 K) the characteristic is assymetrical, as it should be. The revers current is more than two orders of magnitude less than the forward current. Meaning that leakage current is reduced and the data can be analysed in terms of bulk properties

(SCLC).

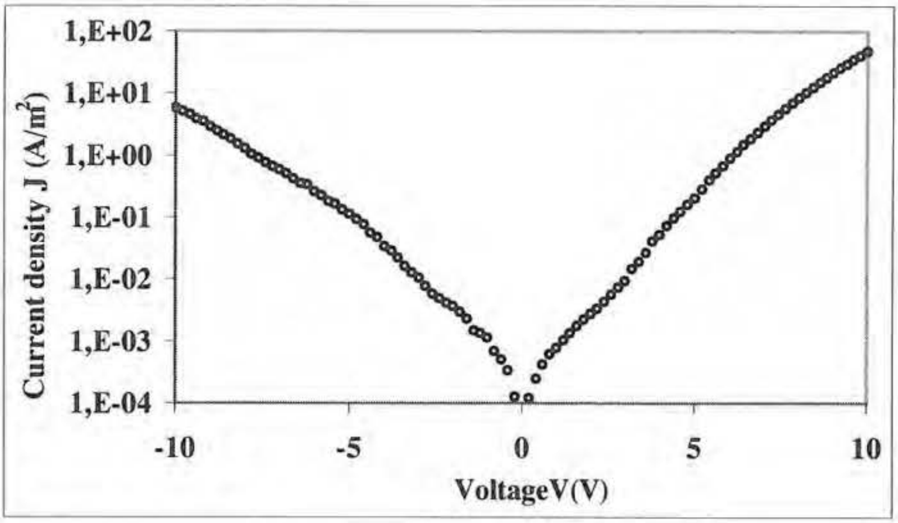

Figure 3.18 Current density J versus voltage V of a PEDOT/OC$_1$C$_{10}$/Al hole only devices with thickness L= 200 nm. At room temperature. The film is obtained out of a pure toluene solution (at 50°C) stirred at 50°C over night after filtration

The current at 173K however is almost symmetrical. This is a result of the fact that the activation energy of the leakage current is one order of magnitude lower than the SCLC. This means that at low temperatures the bulk current will be suppressed by the leakage current, where at higher temperatures leakage current becomes less important. For this reason only the experimental results down to 213K are used for calculation of the field and temperature dependence of the SCLC current.

In [Figure 3.20] the experimental J-V characteristics of a hole only device with L=70 nm are plotted for temperatures between 173K and 293K. The zero field mobility for the L=70nm and L=250nm is shown in [Figure 3.21] in an Arrenius plot. It decreases over more than 3 orders of magnitude while going from 293K to 213K. For the thickest sample (250nm) we observe an activation energy according to Eq. 3.9 of Δ=0,48 eV and a pre-factor $\mu_p(0) = 2{,}6\text{x}10^{-3}$ m^2/Vs. In [Figure 3.21] also γ for these samples is plotted against 1/T. The experimental results show the lineair dependence according to Eq. 3.10, the T_0 =435 K and the $B_\gamma = 3{,}37\text{x}10^{-5}\text{eV}(\text{m/V})^{1/2}$ for the L=250nm sample. Both samples show a similar behaviour, the thinner sample displays a small deviation of the theoretical curves (Eq. 3.9 and 3.10). This is a result of the fact that thinner films are more sensitive to defects and therefore leakage current becomes more dominant. So we use the results of the thicker sample to calculate the parameters.

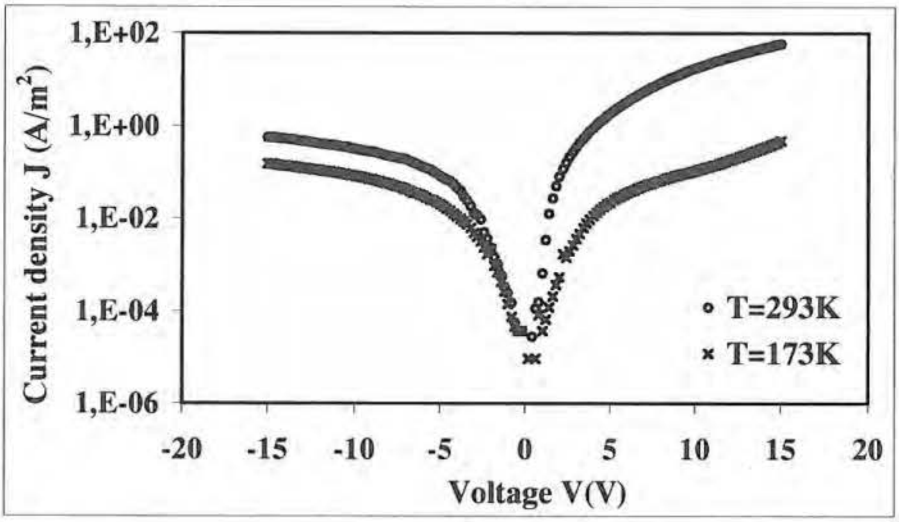

Figure 3.19 Current density J versus voltage V of a PEDOT/OC_1C_{10}/Ag hole only devices with thickness L= 250 nm, at 293K and 173K. The film is obtained out of a toluene/THF (75/25) at 80°C, stirred at 50°C over night after filtration

The current between 0 and 1 V in [Figure 3.20] is completely dominated by leakage current. The deviation of the theoretical curve at around 4V is called anomalous behaviour and is the subject of chapter 5.

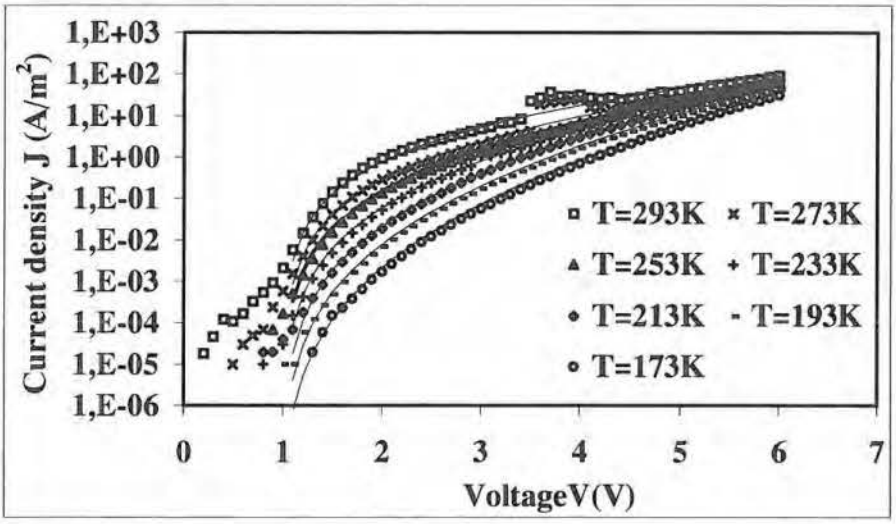

Figure 3.20 Current density J versus voltage V of a PEDOT/OC$_1$C$_{10}$/Ag device with thickness L = 70 nm for various temperatures. The calculated J-V curves as predicted by a SCLC model using a field dependent mobility given by Eq. 3.8-3.10 are plotted as solid lines. The calculated curves are corrected for a built-in voltage V_{bi} of 1V, which originates from the work function difference between PEDOT and Ag.

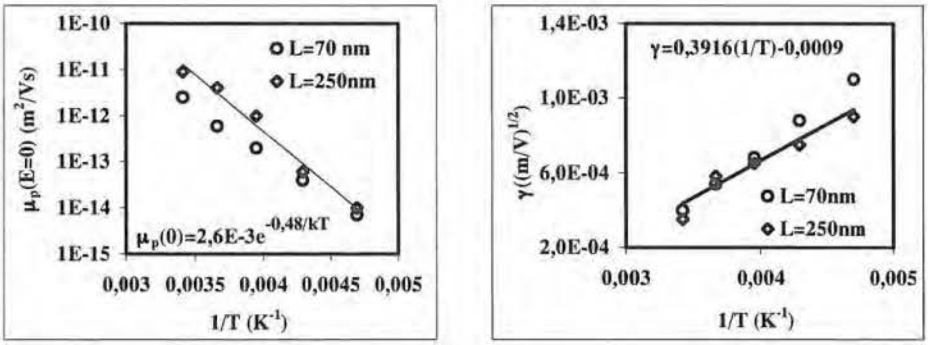

Figure 3.21 ***Left:*** *The Arrhenius plot of the zero field mobility $\mu_p(0)$ versus inverse temperature 1/T. The data are obtained using Eq. 3.20, yielding an activation energy Δ=0,48 eV and a $\mu_p(0)$ = 2,6x10^{-3} m^2/Vs.* ***Right:*** *The coefficient γ (which describes the field dependence of the mobility) as a function of temperature T. Applying Eq. 3.10, gives a T_0 =435 K and a B_γ = 3,37x10^{-5}eV(m/V)$^{1/2}$*

3.6.4. Double carrier devices

In the last part of this chapter we will discuss the actual LED made of PEDOT/OC_1C_{10}/Ca. We compare the J-V characteristic of a PEDOT/ OC_1C_{10}/Ag hole only device with a PEDOT/OC_1C_{10}/Ca double injection device in [Figure 3.22] at room temperature for a thickness of L=200nm. As stated in the theoretical part, the double injection current now only depends on the bimolecular recombination strength. The experimental results in [Figure 3.22] for the double carrier device can be modelled using Eq. 3.18 to Eq. 3.20, assuming that the recombination strength in a PLED is of a Langevin type(15,24) (diffusion controled).

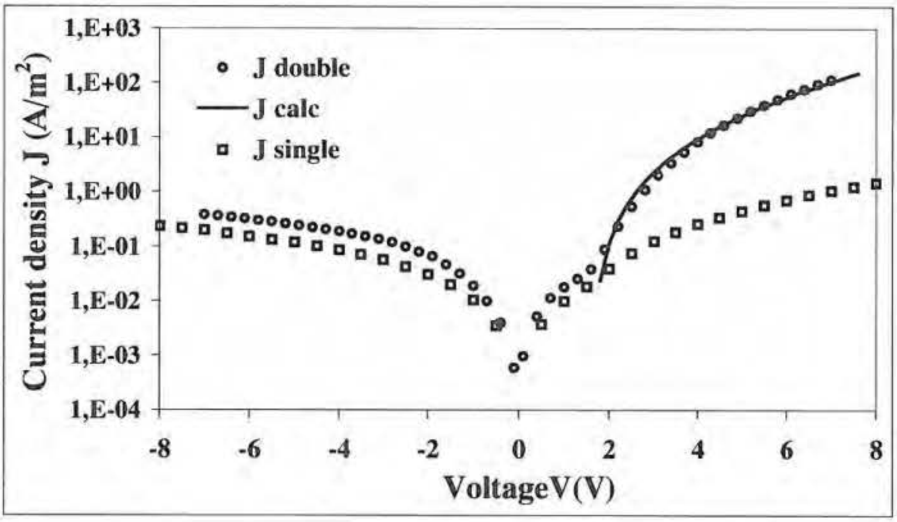

Figure 3.22 Experimental (o) and calculated (—) J-V curves for a double injection device (PEDOT/OC_1C_{20}/Ca) with a thickness of L=200nm. The experimental hole only current for this thickness is given for comparison. The calculated curve is corrected for a build-in voltage V_{bi} = 1,6 V, which originates from the work function difference of PEDOT and Ca.

Besides this we assume that the hole and electron mobility are equal ($\mu_p=\mu_e$). By using the parameters : $\Delta=0,48$ eV and $\mu_p(0) = 2,6x10^{-3}$ m^2/Vs, $T_0 = 435$ K and $B_\gamma = 3,37x10^{-5} eV(m/V)^{1/2}$ (calculated for the hole only device) combined with a Langevin type of recombination, we obtain a good agreement of the simulated data with the experiment, as can be seen in [Figure 3.22].

3.6.5. *Conversion efficiency*

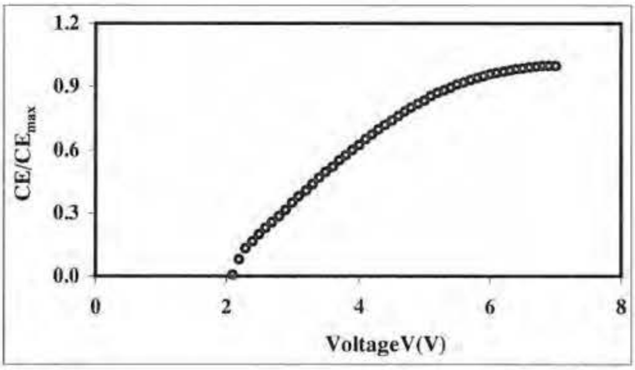

Figure 3.23 Efficiency (photons/carrier) versus voltage for a PEDOT/OC$_1$C$_{10}$/Ca double injection device with a thickness of L=200nm.

An other aspect in an PLED is conversion efficiency (CE), defined as photon per charge carrier. The normalised efficiency CE/CE_{max} is shown in [Figure 3.23], CE_{max} is around 1%. It is observed that CE is dependent on the applied voltage, which is a fundamental difference between PLED's and the conventional inorganic LED's. The CE gradualy increases and saturates at around 5V. Blom et al.$^{(18)}$ suggested that the reduced efficiency at low voltages is due to nonradiative recombination losses at the interface. Therefore a quenching region with a width of $L_q=10$ nm is introduced in the calculations.

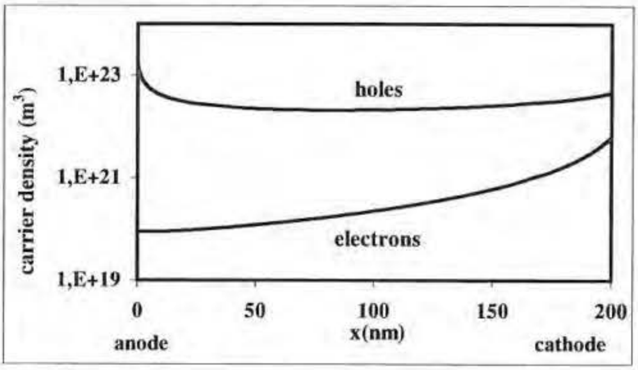

Figure 3.24 Calculated charge distribution as function of distance at 2.8 V (x=L).

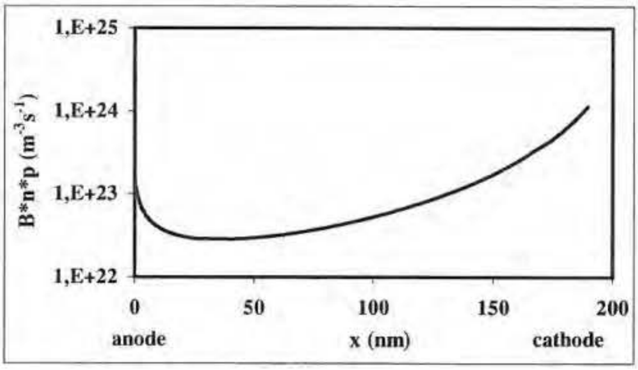

Figure 3.25 Calculated distribution of light generated in a PLED as Bn(x)p(x). With B the Langevin recombination constant $[B=e/\varepsilon_0\varepsilon_r(\mu_n+\mu_p)]$ *and n(x), p(x) the density of mobile electrons and holes.*

We also calculated the charge carrier distribution of holes and electrons at 2.8V [Figure 3.24]. The free electron density (responsible for the light output) decreases with increasing distance from the cathode. Almost no positional variation of holes throughout the sample is observed. In [Figure 3.25] it can be seen that the generation of light changes with a factor of 20, by going from the anode to the cathode, in a PLED.

These results show clearly that holes are the dominant charge carriers in a device with a conducting polymer as active layer. The hole density is 1 to 2 orders of magnitude higher that the electron density.

These simulated results, with the assumption of a quenching region, are in good agrement with the experiment as shown in [Figure 3.26]. We have used a L_q=10 nm, as proposed by Blom, to make a comparison of their OC_1C_{10} with our OC_1C_{10}. The only difference between the materials used is their synthesis.

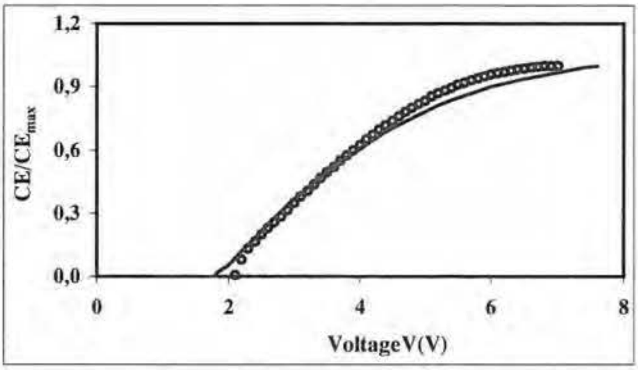

Figure 3.23 Efficiency (photons/carrier) versus voltage for a PEDOT/OC_1C_{10}/Ca double injection device with a thickness of L=200nm, Experimental (o) and calculated (—). The modelled data are obtained by taking into account quenching of excitons at the cathode in a region with a length Lq=10nm.

3.7. Conclusion

The SCLC-model proposed by Blom, not only works fore the PLED's fabricated by the Philips process, but it can also be used to evaluate PLED's prepared by the non-ion precursor route of the Vanderzande group. Of importance is, that one makes sure that the bulk properties of the active layer are measured and not some defect in the device.

	Temperature dependent Parameters			**Field dependend Parameters**	
	Δ eV	**$\mu_p(0)$ m^2/Vs**	**C(0) m^2/Vs**	**T_0 K**	**B_γ $eV(m/V)^{1/2}$**
Native PPV low field part	0,054				
PEDOT	0,04				
Native PPV high field part	0,17	$4{,}0x10^{-10}$		828	$2{,}14x10^{-5}$
OC1C10 LUC-precursor	0,48	$2{,}6x10^{-3}$		435	$3{,}37x10^{-5}$
OCIC10 Philips(11)	0,48	$3{,}5x10^{-3}$		600	$2{,}9x10^{-5}$

Table 3.1 The parameters describing the experimental J-V curves of hole only devices, as function of temperature.

As conclusion we will comment on the experimental parameters obtained for the PPV precursor materials. The parameters describing the experimental J-V curvers are given in [Table 3.1].

The low field part of the native PPV hole only device is dominated by the leakage current of PEDOT. The high field part is dominated by the bulk properties of PPV itself. Since the field dependent parameter γ is determined from the high field part of the experimental J-V curve and the mobility is obtained from the low field part, the field dependent parameters for the native PPV are more reliable. To get more information about the bulk properties of the native PPV we need to improve the film quality. As long as leakage current is the dominating process in these devices the efficiency of double injection devices is practicaly zero and the turn on voltage for light emision is above 10 V.

With regard to OC_1C_{10}, one can see that the parameters describing the J-V curves of the OC_1C_{10} obtained by different synthesis routes are similar. This means that despite of the small structural differences, the bulk properties are similar. The higher gelation temperature of the OC_1C_{10} prepared by our precursor route (most likely the result of the more pure chemical structure), makes that gelation occurs more easily. This results in worse film properties. The film properties can account for the fact that leakage current still conceals in the background at room temperature and becomes dominant at low temperatures. The small leakage current that is still present, causes the apparent efficiency of the precursor OC_1C_{10} to be lower than the Philips OC_1C_{10}. Since the bulk properties are similar, there is no reason why, if the films are optimised, the efficiency of the two OC_1C_{10} materials should not be similar.

Out of the experimental J-V curves one can see that optimalisation of the film properties of the active layer in a PLED is of crucial importance. If there are defects present, regardless of their origin, leakage current takes the charge carriers away from the bulk material and the efficiency of the device drops to almost zero. Therefore one should be careful when interpretating experimental J-V curves, and first make sure, that leakage current do not dominate the characteristics. As the results indicate, temperature dependent measurements are ideal to distinguish between the occurring mechanisms. To draw further conclusions about the double injection devices we need more temperature dependent information of these samples, and therefore first optimise the films.

3.8. References

(72) Sze, S., *Physics of semiconductor devices, 2nd edition*, J Wiley&Sons, NY (1981)

(73) Karg, S., Meier, M. and Riess, W., *J. Appl. Phys*, **82 (4)**, 1951 (1997)

(74) Vaubel, G. and Bässler, H., *Phys. Lett.*, **27A**, 328 (1968)

(75) Fowler, R.H. and Nordheim, L., *Proc. R. Soc. London*, **Ser A119**, 173(1928)

(76) Simmons, J.G., *Phys. Rev. Lett.*, **15 (25)**, 967 (1965)

(77) Bässler, H., *Charge Transport in Random Organic Semiconductors, in Semiconducting polymers*, in print

(78) Arkhipov, V.I., Emelianova, E.V., Tak, Y.H. and Bässler, H., *J. Appl. Phys*, in print

(79) Parker, I.D., *J. Appl. Phys.*, **75**, 1656 (1994)

(80) Davids, P.S., Kogan, S.M., Parker, I.D. and Smth, D.L., *Appl. Phys; Lett.*, **69**, 2270 (1996)

(81) Blom, P.W.M., de Jong, M.J.M., Vleggaar, J.J.M., *Appl. Phys. Lett*, **68**, 3308 (1996)

(82) Blom, P.W.M., de Jong, M.J.M. and Munster, M.G., *Phys. Rev. B*, **55**, R656 (1997)

(83) Blom, P.W.M., de Jong, M.J.M., Liedenbaum, C.T.H.F. and Vleggaar, J.J.M., *Synth. Met.*, **85**, 1287 (1997)

(84) Blom, P.W.M., de Jong, M.J.M. and Breedijk, S., *Appl. Phys. Lett.*, **71**, 930 (1997)

(85) Blom, P.W.M. and Vissenberg, M.C.J.M., *Phys. Rev. Lett.*, **80**, 3819 (1998)

(86) Blom, P.W.M., de Jong, M.J.M, *IEEE Journal of selected topics in quantum electronics*, **4 (1)**, 105 (1998)

(87) Blom, P.W.M., Black, D.W. and Vissenberg, M.C.J.M. *Phys. Rev. Lett.*, submitted

(88) Vissenberg, M.C.J.M. and Matters, M., to be published

(89) Vissenberg, M.C.J.M., submitted

(90) Lampert, M.A. and Mark, P., *Current injection in solids*, Academic, New York (1970)

(91) Simmons, J.G., *J. Phys. Chem. Solids*, **32**, 1987 (1971)

(92) Frenkel, J., *Phys. Rev.*, **45**, 647 (1938)

(93) Davids, P.S., Campbell, I.H. and Smith, D.L., *J. Appl. Phys.*, **82 (12)**, 6319 (1997)

(94) Antoniades, H., Abkowitz, M.A. and Hsieh, B.R., *Appl. Phys. Lett.*, **65**, 2030 (1994)

(95) Langevin, P., *Ann. Chim. Phys.*, **28**, 433 (1903)

Chapter 4

Ageing of polymer light emitting diodes

As far as quantum efficiencies and brightness are regarded, PLED's have reached a level, where technical applications seem to be the next step. A drawback however, are the limitations due to their relatively short lifetimes. Lifetime and stability of PLED's are prerequisites for future applications of these materials. Moreover, stable devices, which allow reproducible measurements form the basis for a detailed understanding of the microscopic processes involved in EL and the underlying physics.

In this chapter we report on detailed investigations on the lifetime, stability and degradation processes of PLED's based on precursor PPV. The ITO/PPV/Al LED's have been examined during continuous electrical stress in an oxygen-rich atmosphere.

In the previous chapter we have studied the general electric characteristics of PLED's made with PPV using a non-ionic precursor route with ITO (coated with PEDOT) as an anode and Al or Ag as cathode. We have pointed out that leakage current plays a dominant role in devices prepared by our precursor route. Despite of the use of PEDOT, which results in a severe suppression of the leakage current compared to pure ITO(1-3), the properties of these devices are still dominated by leakage current. J-V curves can be considered as time zero experiments, meaning that J-V curves present the properties of the device before applying any electrical stress.

4.1. Experimental set-up.

4.1.1. *Electro-optical characterisation.*

A dedicated computer program controls the measurement of both the current and the light output as function of applied voltage. The program controls a Keithley 2400 combined voltage source-electrometer measuring unit to measure the J-V characteristics and a Keithley 487 picoammeter to read out total light output of the device in terms of current generated by the photodiode. Electrical measurements were performed both in constant current and in constant voltage mode. All the measurements were performed under ambient conditions.

The substrates used for this study have four different active areas (ITO-coating). The smaller area (10 mm^2) is used due to the better reproducibility. As evaporated cathode materials Al is used to make measurements in air possible. The thickness of the active polymer layer is varied between 50 nm and 300 nm.

4.1.2. *Analytical characterisation.*

Analytical investigation of the PLED's in the various phases of the ageing has been performed by Scanning Electron Microscopy (SEM) and with Secondary Ion Mass Spectroscopy (SIMS).

SEM experiments were performed using a XL30-FEG (Philips) scanning electron microscope, equiped with a super ultra thin window EDX detector (DX4i / EDAX), which allows the detection of light elements (with mass above B). All electron images shown in the following section are secondary electron (SE) images.

SIMS depth profiles were performed using a Cameca Ims-5f magnetic sector instrument. A primary Cs^+-beam of 5.5 keV was used with an incidence angle of 42° off normal. Since the ionisation probability strongly depends on the chemical environment (matrix effect) of the analysed species, and as a consequence, the relationship between the intensity of a mono atomic ion signal and the concentration of the species in the sample is rather complicated, positive MCs^+ ions were detected to reduce this matrix effects(4,5). A primary beam intensity of 2.5 nA was used with a spot size of about 20 μm. The detection field was 45 μm square in the centre of the 125 μm rastered area. The spectrometer was operated at low mass resolution ($m/\Delta m \sim 500$) to allow the detection of the low intensity HCs^+ and SCs^+ signals in the polymer layer. More details on this technique can be found in the work of Vlekken et al.(5) Although SIMS is a rather commonly used technique, there are only a few reports on SIMS analysis of polymer layer systems(4,6).

4.1.3. Emission microscopy (EMMI).

To study in-situ the effect of ageing on the light output of the PLED's EMMI experiments have been performed. These experiments were performed using a Hypervision Visionary 2000 system equipped with a highly sensitive GENIII-NIR detector. This system allows for continuous two dimensional monitoring of the light emitted by the PPV devices, with a sensitivity much higher than the human eye. By comparing the image of the emitted light with an illuminated image of the device, the location of the emissive regions could be determined. This allowed to pinpoint, in-situ, the degradation sensitive areas.

4.2. Electro-optical monitoring of ageing

In order to obtain an electro-optical monitoring of the ageing of PLED's, measurements have been performed in a measurement room under various electrical conditions and atmospheres.

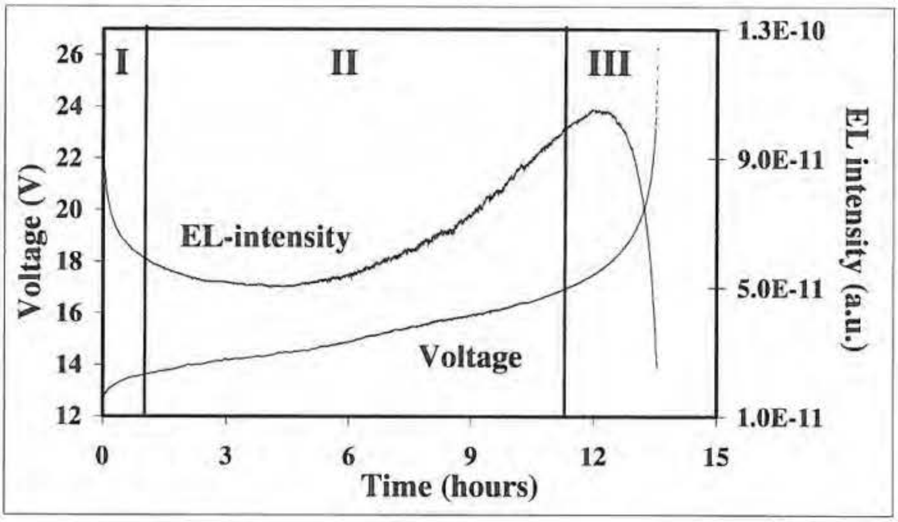

Figure 4.1 PLED (ITO/PPV/Al) ageing at constant current (1mA) in an oxygen-rich atmosphere showing the voltage and luminance. Note the three different regions in the ageing behaviour.

[Figure 4.1] shows the change of both voltage and light output of a device as a function of time under a constant current stress of 1mA. The ageing behaviour of this diode is typical for all the devices tested in an oxygen-rich atmosphere. Three different regions can be distinguished in this ageing behaviour. The first region is characterised by a steep voltage increase at the beginning of the stress period. This is rapidly followed by the second region: a gradual voltage increase. The third region shows a dramatic voltage increase, accompanied by Joule heating, resulting in the total destruction of the device configuration. Within the second region, the occurrence of sudden voltage drops may be observed in some cases, as illustrated in [Figure 4.2]. This latter figure shows a detail of a stress experiment on a similar device, stressed under the same conditions as the one of [Figure 4.1]. The three domains that can be established in the electrical behaviour are also present in the time evolution of the light emission. In the beginning of the constant current stress the light output decreases dramatically, followed by a more steadily decrease starting at the moment when the voltage gradually increases.

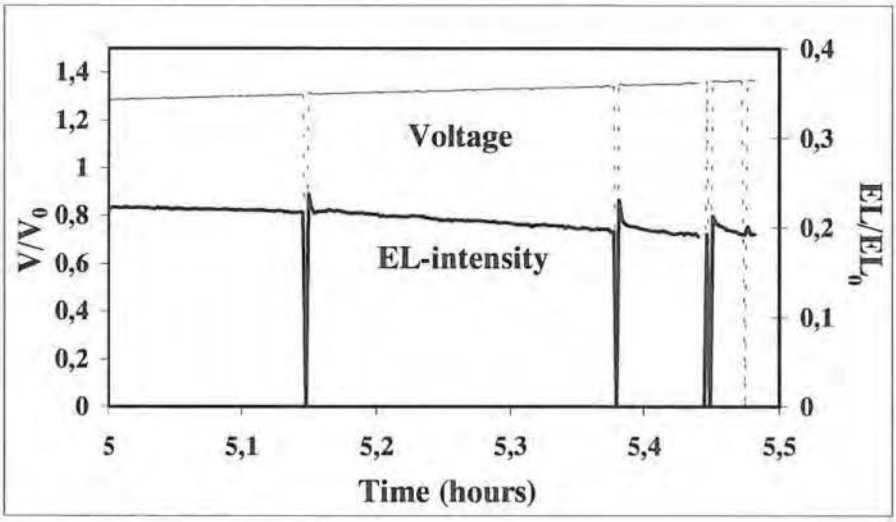

Figure 4.2 The gradual degradation for a PLED driven at a constant current (1mA) in an oxygen-rich atmosphere [showing the voltage (dotted line) and luminance (solid line) each relative to their initial values] is suddenly interrupted by voltage drops corresponding with complete loss in light output.

In order to get a better understanding of the first region of the degradation profile we have set-up an experiment in which the light intensity and voltage is studied under a pulsed current stress. Every ten minutes the current is shut off for one minute. [Figure 4.3] displays the temporal evolution of light and voltage. When the current is turned on again at the same level as before the light emission increases significantly and than start again its continuous decrease. At the same time the voltage almost unaffectedly carries on increasing, with a steep increase the first seconds. This behaviour can be repeated and is similar to the first region in the degradation profile. However we observe that not all of the intensity is recovered and that the decay is sharper when we repeat the switching. The origin of this more or less reversal behaviour is not fully understood. A possible explanation is given by Zou et al.(7) in terms of the formation of an internal field. When the current is applied, ionic impurities diffuse towards the electrodes, cations towards the Al electrode and anions towards the ITO layer. Consequently, an internal electric field in the opposite direction to the external field is formed. This internal field reduces the carrier injection efficiency. Thus at a constant current density the voltage and luminance decrease. Furthermore the internal field can also arise from permanent and induced electrical dipoles. Additionally, these impurities might act as traps and luminance-quenching centres, reducing the light out-put. These processes can lead to thermal heating of the sample and by doing so, damage the sample, resulting in an unrecoverable change, as can be seen in the experiment.

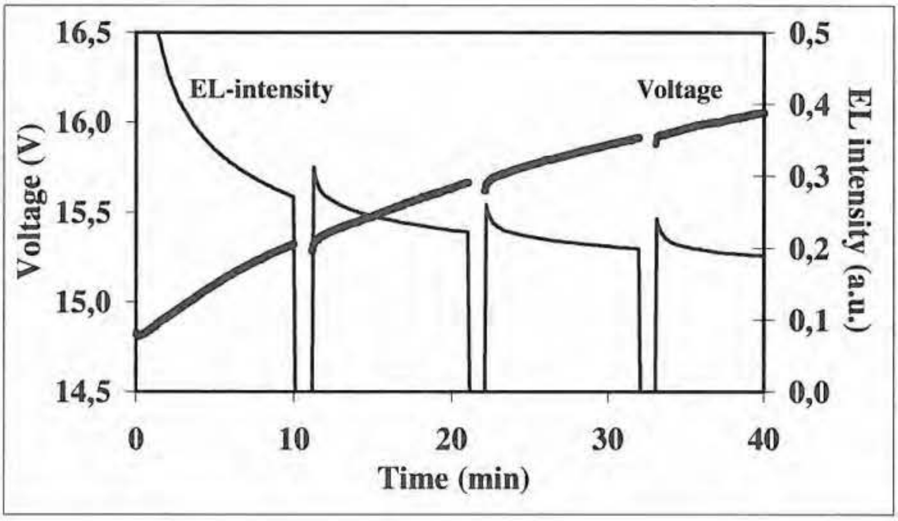

Figure 4.3 Spontaneous recovery phenomena after a short interruption of the device operation

The gradual degradation of the light emission is in some cases [Figure 4.2] suddenly interrupted by a complete loss of light, coinciding with abrupt voltage drops. This gradual degradation has been attributed to phenomena like chemical degradation of the polymer and structural changes in the electrode structure. Chemical degradation reduces the ability to transport charge and can introduce carbonyl sites leading to a quenching of the light emission. For MEH-PPV it has been proposed that electroluminescent operation in an oxygen-rich atmosphere leads to oxidation of the polymer involving the formation of excited-state singlet oxygen which attacks the vinyl double bond. This results in a decreased conjugation length and the formation of carbonyl groups(8). Gill et al.(9) reported the same gradual voltage increase extended over a very long period (life time-a decrease in efficiency to 50%-of 5000 h, at 70°C) in an encapsulated device (without the presence of oxygen). They consider cross-linking of the polymer via the vinylene groups to be the dominating mechanism. It does not matter whether it is cross-linking or oxidation, what is important is that the weak link in the bulk material is the vinyl double bond. As a result of the presence of excited states (by charge injection) in the polymer material, the vinyl double bond becomes reactive and leads to interruption of the conjugated system. This results in a decrease in charge carrier mobility and an increase in quenching sites. This phenomenon has been indicated to cause the gradual voltage increase.

The abrupt voltage and light drops in the second degradation region were established to be caused by the formation of ohmic leakage paths, indicated by dielectric breakdown. In an oxygen-rich atmosphere these leakage paths heal by oxidation, reducing the active area of the device. In contrast to the monotone voltage increase in the second degradation region, the EL intensity starts to increase after some time, until the third region is reached where the voltage increases dramatically. This third region results in a complete loss of emission. The increase in EL intensity at the end of the second region can be explained by the fact that when the active area of the device (m^2) is decreasing (degradation) at a constant current (I(A)) , the current density ($J(A/m^2)$) is increasing, resulting in an increase in EL-intensity. The increase in current density even enhances the degradation.

The onset electrical field of luminescence (1MV/cm) is close to the typical breakdown fields for polymers (2-15 MV/cm)(10) and therefore likely to induce degradation of the device. In some devices [Figure 4.2] a sudden interruption of the gradual degradation by a voltage drop is observed. This voltage drop and complete loss in light output indicates the appearance of ohmic leakage paths. These leakage paths appear as blisters with the dimension of around 100μm; this is more than ten times the dimension of the pineholes induced during fabrication of the devices. Since a very high current density runs through the channels, they heat up and can grow in dimension. In the end one of the channel becomes large enough to support the complete device current. In an oxygen-rich atmosphere however this channel will be completely destroyed and oxidised due to its high temperature. The current is spread out over the remaining area of the device and another channel is able to grow. The loss of active area caused by these oxidative burnouts can clearly be observed in the SE micrograph [Figure 4.4]. A complete description of this phenomenon will be discussed in chapter 5, when we describe the properties of PLEDS in an inert atmosphere.

4.3. IR, SEM and SIMS analysis.

Using infra-red monitoring it was demonstrated that the high local current density through the shorts is accompanied with a considerable heating up to 400°C(10,11).

4.3.1. SEM and EDX-analysis

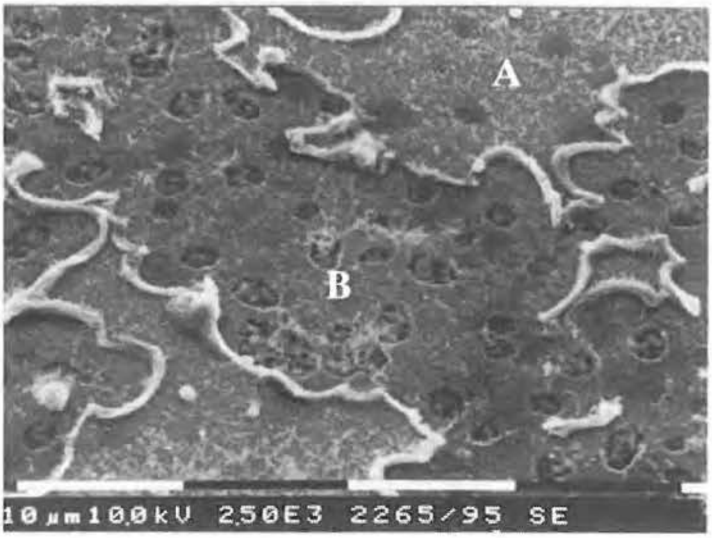

*Figure 4.4 SE Micrograph of a PLED (ITO/PPV/Al) run until complete failure. The loss of active area caused by oxidative burnouts can clearly be seen (Al like zone **A**, damaged parts zone **B**). The craters due to electrical breakdown can be observed.*

The inhibition of the ohmic path formation by oxidation under ambient conditions results in a local delamination of the electrode, shrinking the active area of the device.

The loss of active area caused by oxidative burnouts can clearly be observed in SE micrographs [Figure 4.4] and is consistent with SIMS depth profiling.

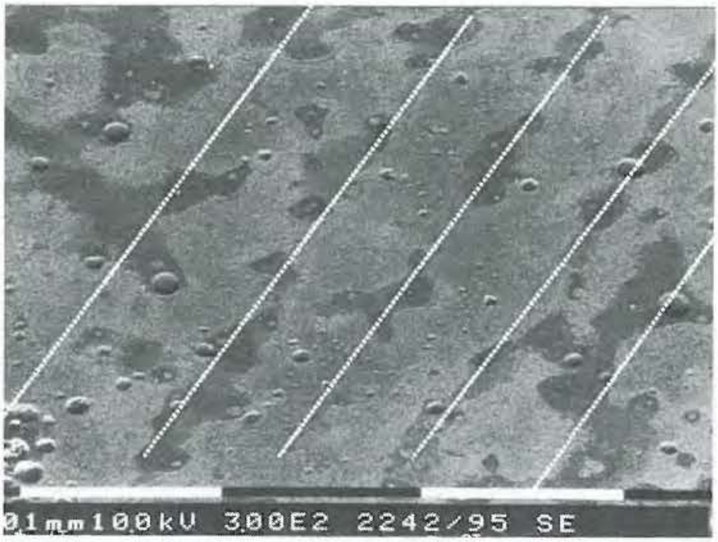

Figure 4.5 SE Micrograph of a device where stress is stopped in the region of gradual voltage rise. The formation of blisters and tight packed bubbles in the Al-electrode can be seen. Also a stripe pattern can be recognised (dotted).

At distinct points in all three regions of the ageing profile [Figure 4.1] the current stress was stopped and the samples were examined using SEM. In the beginning of the experiment no sample damage can be observed, although the emission of the LED has already decreased with a factor of 2. In the region of the gradual voltage rise, increasing blister formation, tightly packed bubbles and a stripe pattern can be seen in the Al-electrode [Figure 4.5]. Here, it is important to note that at the edges of the Al-electrode much more damage can be observed as compared to other parts of the device. Also electrical breakdown induced craters arise earlier at the edges as compared to the rest of the device area. At the moment of the sudden voltage rise, a complete destruction of the device (delamination of the electrode in the form of exploded blisters and craters) can clearly be observed. [Figure 4.6 a, b] shows such a distructed area. EDX measurements indicate that a high concentrations of Al-oxide and free-standing polymer is present in the crater and even parts of the ITO bottom electrode can be observed at the Al-surface of the sample.

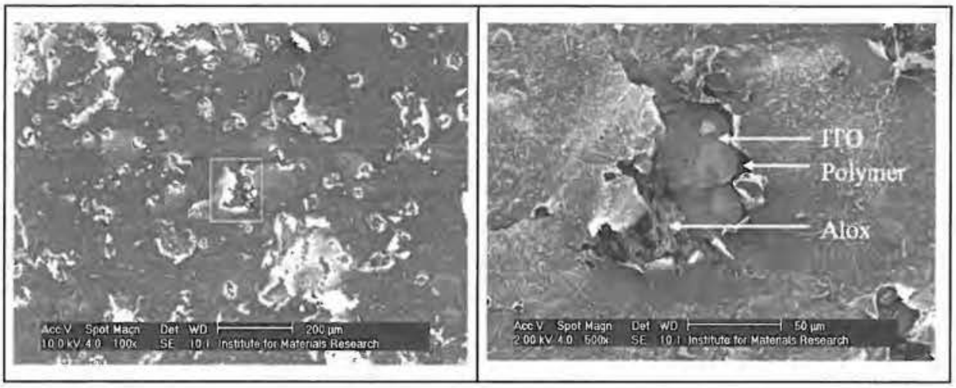

Figure 4.6 Left: SE Micrograph taken at the moment of sudden voltage rise. Exploded blisters and crates can be established. Right: Enlargement of the window (crater site) in figure 7a. EDX analysis indicates the presence of Al-oxide, freestanding polymer and ITO in the crater region.

4.3.2. SIMS-analysis

The results of a semi-quantitative SIMS depth-profiling analysis with a large area (field of view) of a non-stressed device is presented in [Figure 4.7 a]. Besides the high oxygen concentration on top of the Al-electrode, a high oxygen concentration can be located at the Al-polymer interface. This indicates that Al at the surface oxidises due to air contact and that an interfacial Al_xO_y layer is formed as a result of the oxygen absorbed at the polymer surface before Al-evaporation. The broad interface region indicates the initial roughness of the as-produced devices. This is confirmed by roughness measurements. Further roughening of the surface during sputtering, enhances this effect.

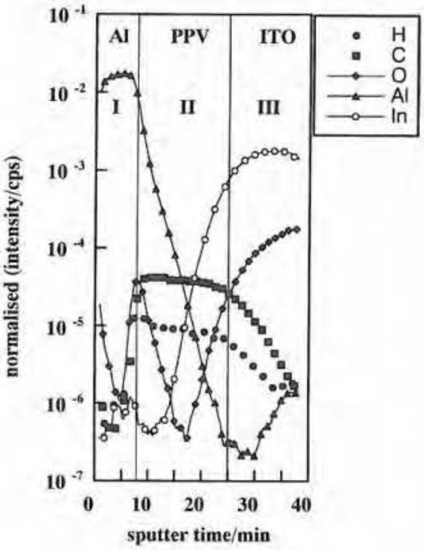

Figure 4.7 SIMS depth profiling of the main elemental constituents of an Al/PPV/ITO device.

SIMS depth profiling of heavily aged devices, stressed until complete failure, reveals an almost homogenous depth distribution of the different elements, indicating the complete absence of any layered structure. Since it is know from SEM-investigation that LED's fail inhomogeneously on a scale of a few tenths of microns, local SIMS analysis was performed on both non affected and affected zones. [Figure 4.8 a] shows the analysis on a non-affected zone, indicated as zone A on the SE-micrograph shown in [Figure 4.4, zone A] of the aged device. The depth profile reveals the same layered structure as the non-aged device confirming the inhomogeneous ageing of the device. Depth profile analysis of the affected zone, as in [Figure 4.4, zone B], indicates that only an Al-penetrated ITO structure remains [Figure 4.8 b].

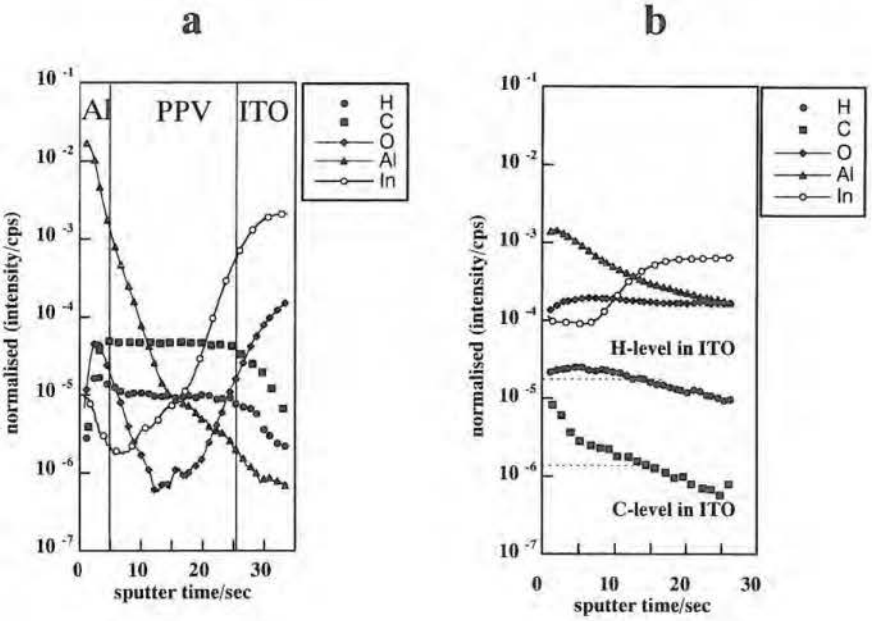

Figure 4.8 SIMS depth profiling of reduced areas on a device destroyed during operation right. left: *The area of an Al like zone has been profiled and demonstrates still the layered structure.* right: *Analysis of the damaged parts shows no layered structure anymore.*

4.4. In-situ optical monitoring.

EMMI was used to monitor in-situ the light emission of the devices. In contrast to a photodiode, EMMI provides a two dimensional image of the light emission. This makes it possible to locate inhomogeneities in the light emission of the device. In a first experiment, the detection sensitivity for light of the EMMI and a photo-diode was compared. Using the photo-diode, light emission was only observed for LED-currents in the mA range, while using the EMMI, emission was already detected at LED-currents of about 1 μA.

In a second experiment, a constant current of 3 mA was supplied to a sample. The shape of the resulting voltage curve in function of time was similar to the one shown in [Figure 4.1]. The value of 3 mA was chosen in order to enhance the degradation time. [Figure 4.9.1, sample] shows a normal illuminated microscope image of a non-stressed device recorded with the EMMI detector. Due to thickness variations of the polymer a stripe pattern can be observed as well as some black spots caused by dust particles and leakage channels. A large dust particle is indicated by the arrow on [Figure 4.9.1, sample]. [Figure 4.9.1, emission] shows the emission image of the light emitted by the device at the beginning of the experiment. A strong light emission can be observed at the edge of the Al electrode and at the large dust particle. In addition, a non-uniform stripe-pattern can be observed over the entire area of the device (± 1 stripe / 100 μm). The emission pattern and the illuminated microscope image of the devices are identical. In the emission image [Figure 4.9.1, emission] also dark spots can be recognised.

[Figure 4.9.2, sample and emission] shows, respectively, the normal illuminated image and the emission image of the device at a further stage of the experiment. It can be seen in [Figure 4.9.2, sample] that damage occurs at the edges, along the stripe pattern and at the dust particle. In contrast to [Figure 4.9.1, emission], no emission can be observed at the dust particle in [Figure 4.9.2, emission]. In addition, at places along the stripe pattern with bright emission in the beginning of the experiments [Figure 4.9.1, emission], emission stopped [Figure 4.9.2, emission].

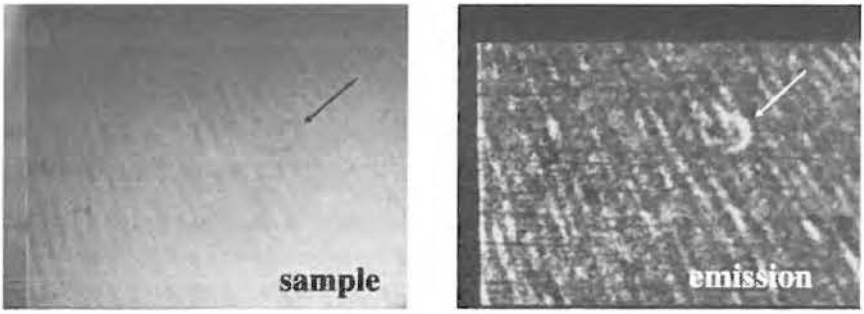

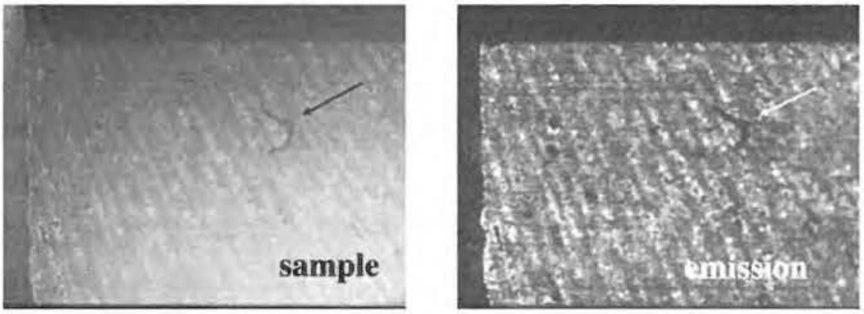

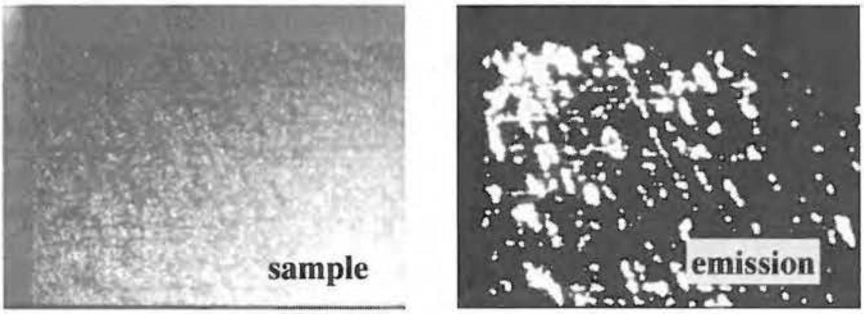

Figure 4.9.1 *[top]* Sample: *the illuminated image of an Al/PPV/ITO device before electrical stress, showing a stripe pattern and some dust particles, notice the large dust particle indicated by the arrow.* Emission: *the emission image at the beginning of the run. The images are 5* mm^2*; this is the same as the device area. To see the edges, the device is slightly shifted.* ***Figure 4.9.2*** *[centre]* Sample and emission: *show, respectively, the normal illuminated image and the emission image in a further stage of the stress period. At this stage damage can be seen at the edges, on the stripe pattern and at the dust particle. No emission is observed anymore at the dust particle.* ***Figure 4.9.3*** *[bottom]* Sample: *The illuminated image of an Al/PPV/ITO device after total breakdown.* Emission: *The emission image shows random flashing light spots, ending in strong emissive spots just before total breakdown.*

4.5. Macroscopic smoothness measurements.

The EMMI results presented above can be interpreted in terms of device preparation. The devices measured in these stress experiments where prepared out of a pure alcohol solution. This results in devices with a polymer thickness variation of about 10%, occurring as radial stripes due to the spincoating process (± 1 stripe / 100 μm) as measured using a mechanical profilometer. This microscopic smoothness (buckling) [Figure 4.10] results in higher local electric fields at the thinner regions, which explains the stripe-patterned light emission. This local thickness variation along stripes, the occasional dust particles, the leakage channels and the edge effect, are the main sources for increased degradation and can be considered as the most important drawbacks present in these devices.

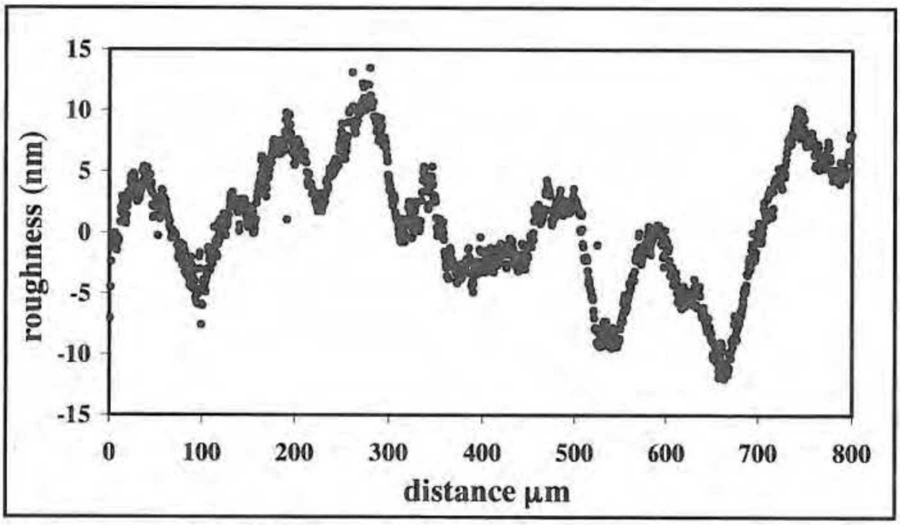

Figure 4.10 Dektak smoothness measurements. The thickness variation in form of a stripe pattern (buckling) can clearly be observed. The dimension is identical as the stripe pattern shown in the EMMI images.

4.6. Calculation of the current density at the electrode edges.

The higher luminescence and hence ageing at the Al electrode edges can be explained by a local high charge build-up. The singular charge density behaviour near straight edges has been described by Meixner(12): the charge density is proportional to $t^{1/\mu}$ with t the distance to the edge and μ a parameter depending on the edge geometry(12). For sharp edges μ becomes small and the singular behaviour is more pronounced. In the case of bended corners (top of the ITO electrode) instead of straight edges (bottom of Al electrode) the singularity disappears and the charge build-up near the corner is less important. This explains the higher light intensity that can be observed on the aluminium strip side as compared to the ITO side. The charge build-up near the aluminium edge has been verified numerically, at IMEC, using a moment method applied to the Poisson integral equation in a layered dielectric medium(13). [Figure 4.11] shows the charge density near the aluminium edge for a potential of 15 V between the Al and the ITO strip. The charge density deviates from the parallel plate value (3.89 $10^{-3}C/m^2$) near the edges following a $t^{-0.23}$ Meixner behaviour with t the distance to the edge.

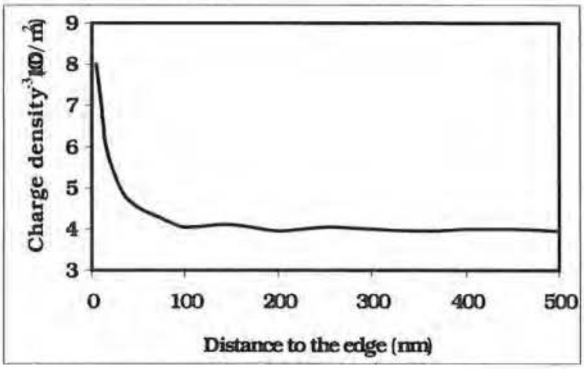

Figure 4.11 The charge density distribution near the Al edge as numerically verified using a moment method on the Poisson integral equation in a layered dielectric medium.

4.7. Conclusions

Three distinct regions in the time evolution of the equivalent electrical resistance and the light output are identified. Various electrical and analytical measurement results are presented to explain the main failure mechanisms. The most severe degradation mode can be identified as dielectric breakdown, resulting in 'hot spots' and ohmic leakage paths. The inhibition of the ohmic path formation by oxidation under ambient conditions results in a local delamination of the electrode, shrinking the active area of the device.

The light emission of PLEDS is influenced by the morphology of the device. Thickness variations of the polymer (buckling), caused by the spinning process, lead to stripe patterned emission. This results in a field induced stripe patterned ageing. A high charge build-up at the edges of the Al electrode results in a higher luminescence, and faster ageing. The combination of electrical measurements, SEM, SIMS and EMMI imaging, showed that when a constant current is forced through the polymer, it will initially flow through a large area of the device, with severe loss of current through leakage paths present in the as-produced sample. Subsequently blister formation and electrode delamination, resulting in a gradual increase of the voltage and a decrease of the luminescence reduce the active area of the device. The increase in EL intensity at the end of the second region can be explained by the fact that when the active area of the device (m^2) is decreasing (degradation) at a constant current (I(A)) , the current density ($J(A/m^2)$) is increasing, resulting in an increase in EL-intensity. The increase in current density even enhances the degradation. When the voltage increased to a certain level, random light flashes start to appear, resulting in an increase of the emission. EMMI showed that this emission originates from random, bright spots, instead of from an uniform luminescence of the device.

EMMI provides evidence for the shorting process, which can be used to explain the electro-optical ageing experiments. It was shown to be a very useful technique for the analysis of polymer light emitting devices. EMMI can locate weak spots a long time before breakdown occurs and can be used to monitor the in-situ degradation of the device.

These experiments(14) suggest that pre-existing particles and pinholes may cause the formation of leakage current. Very high electric fields can be formed locally at these leakage paths, at the edges of the Al and at the thinner parts of the buckled polymer film. This can produce intense local heating that melts the organic layer and establish an electrical short. These phenomena are also observed in vacuum vapour-deposited oligomers based LED's(15). In oxygen however, these shorts are not stable since they can not support the high local current density, and become oxidised. This results in a loss of active area and a lower total intensity. This process eventually leads to a complete destruction of the device. These pre-existing particles and film imperfections are the cause for the formation of a leakage current, meaning that leakage current is the electrical fingerprint of the device imperfections.

4.8. References

(96) Imai, K., Shinkai, M., Wakimoto, T. and Shirota, Y, *US patent 5,256,945, Pioneer Electronic Corp.* (1993)

(97) Berntsen, A., Croonen, Y., Liedenbaum, C.T.H., Schoo, H.F.M., Visser, R.J., Vleggaar, J.J.M. and van de Weijer, P., *Optical Materials,* **9**, 125 (1998)

(98) Liedenbaum, C., Croonen, Y., van de Weijer, P., Vleggaar, J. and Schoo, H., *Synth. Met.*, **91**, 109 (1997)

(99) Bijnens, W., Manca, J., Wu, T.D., D'Olieslaeger, M., Vanderzande, D. , Gelan, J., De Ceuninck, W., De Schepper L. and Stals, L. M., *Synth. Met.,* **83**, 261 (1996)

(100) Vlekken, J., Wu, T.D., D'Olieslaeger, M., Knuyt, G., De Schepper L. and Stals, L.M *International Journal of Mass Spectrometry and Ion Processes*, **156**, 61 (1996)

(101) Sauer, G., Kilo, M., Hund, M., Wokaun, A., Karg, S., Meier, M., Riess, W., Schwoerer, M., Suzuki, H., Simmerer, J., Meyer, H., Haarer, D. *Fresenius Journal Of Analytical Chemistry,* **353**, 642 (1995)

(102) Zou, D., Yahiro, M. and Tsutsui, T., *Synth. Met.*, **91**, 191 (1997)

(103) Cumpston, B.H., Parker, I.D., Jensen, K. F.j *J. Appl. Phys.,***81 (8)**, 3716 (1997)

(104) Gill, R.E., van de Weijer, P., Liedenbaum, C.T.H, Schoo, H.F.M., Berntsen, A., Vleggaar, J.J.M and Visser, R.J., *presented at the E-MRS Spring Meeting,* Strassbourg (1998)

(105) Manca, J., Bijnens, W., Kiebooms, R., D' Haen, J., D'Olieslaeger, M., Wu, T.D., De Ceuninck, W., De Schepper, L., Vanderzande, D., Gelan J. and Stals, L. M.,*Optical Materials*, **9 (1,2)**, 134 (1998)

(106) Bijnens, W., Manca, J.V., Kiebooms, R., De Ceuninck, W., De Schepper, L., Vanderzande, D., Gelan J. and Stals, L. *presented at the ECME*, Cambridge (1997)

(107) Meixner, J., *IEEE Trans. Antennas,Propagat.*, **AP-20**, 442 (1972).

(108) Bernal, J., Medina F. and Horno, M., *IEEE Trans. Microwave Theory Tech.*, **MTT-45 (9)**, 1619 (1997)

(109) Bijnens, W., De Wolf, I., Manca, J.V., D'Hean, J., D'Olieslaeger, M., Beyne, E., Wu, T.D., De Ceuninck, W., De Schepper, L., Vanderzande, D., Gelan J. and Stals, L. M., *Synth. Met.*, **96 (2)**, 87 (1998)

(110) Antoniadis, H., Hueschen, M.R., McElvain, J., Miller, J.N., Moon, R.L., Roitman, D.B. and Sheats, J.R., *polymer preprints*, **38** (1), 383 (1997)

Chapter 5

Anomalous behaviour: negative resistance and switching effects

5.1. Introduction

In this chapter we will discuss the effect of the ambient gas on the electrical properties of a PLED sandwich structures. We have addressed these phenomena as anomalous behaviour [Figure 5.2] and gas sensor properties (switching) [Figure 5.4]⁽¹⁾. These properties appear when one does an experiment under inert atmosphere. When we first spotted these properties and consulted the PLED literature, we only could come up with two papers⁽²,³⁾. These papers only reported on the phenomena and did not discuss nor explain it. It seems that due to problems with the reproducibility and the fact that this is a severe disadvantage for these devices, researchers tried to ignore the problem. The fact that, if one applies a short high voltage pulse to the device the phenomenon disappears, supported this strategy. This trick makes it possible to study the bulk properties without any interference of anomalies. Also the introduction of an extra layer (PEDOT) between the ITO and the active polymer suppresses the anomalies. But nevertheless understanding these phenomena is of great importance at a phase where commercialising of this device is no longer a possibility but a fact.

A sudden change from a high to a low resistive stage when a voltage is applied has been observed in many inorganic materials such as oxides⁽⁴,⁵⁾ and organic polymer films⁽⁶,⁷⁾. This phenomenon is called switching. When a small voltage (2-15 V) is applied to the electrodes of a fresh metal/insulator/metal (MIM) device, a forming process occurs. When this process is complete the electrical conductivity of a sample is raised by a few orders of magnitude and its J-V characteristic shows a maximum in current. This phenomenon is dependent of the temperature and the nature of the gas atmosphere. Theoretical models suggested by various workers consider on the one-hand electrons to penetrate homogeneously through the dielectric of the insulating layer, and on the other hand the passage of current by means of conductive filaments. These concepts are discussed together with our experimental results. In conclusion an attempt to find an explanation is presented.

5.2. Experimental results

5.2.1. Experimental set-up

The electro-optical measurements have been performed using a measurement chamber with a transparent top window and with the possibility to change the ambient gas. A dedicated computer program controls the measurement of both the current and the light output as function of applied voltage. The program controls a Keithley 2400 combined voltage source-electrometer measuring unit to measure the J-V characteristics and a Keithley 487 picoammeter to read out total light output of the device in terms of current generated by the photodiode [Figure 5.1]. Electrical measurements were performed both in constant current and in constant voltage mode.

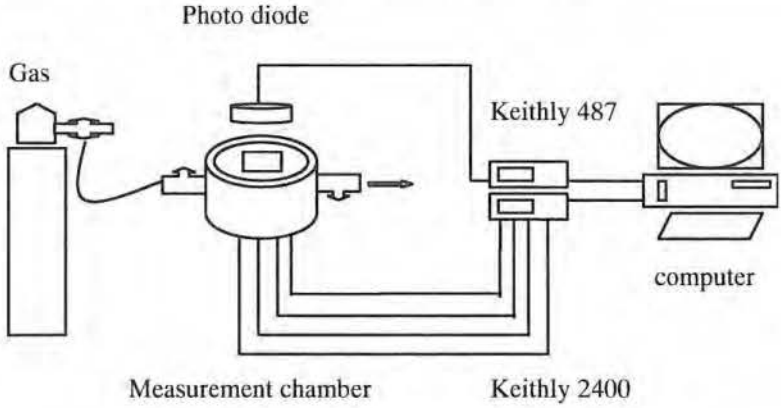

Figure 5.1 experimental setup used to perform electro-optical experiments under different atmospheres.

5.2.2. Anomalous bump: voltage controlled negative resistance (VCNR)

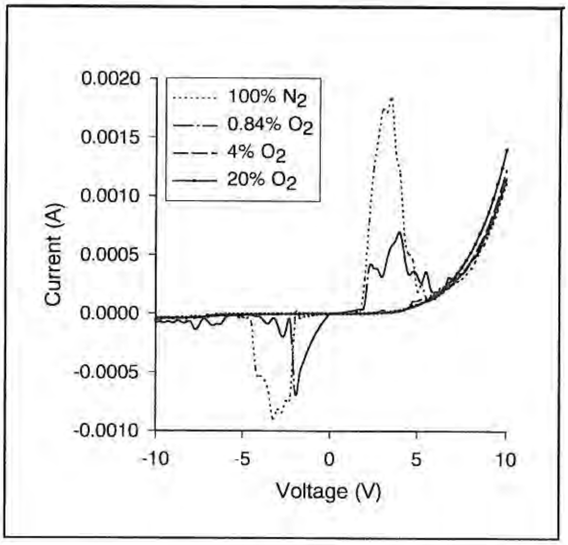

Figure 5.2 Anomalous IV-characteristics of a PLED in various gas atmospheres. Voltage sweep from -10V to 10V.

When J-V measurements on an ITO/PPV/Al device are performed in different gas atmospheres two type of J-V curves are generally observed. In oxygen-rich atmospheres SCLC (chapter 3) can describe the J-V curves. When PEDOT is used SCLC can explain the device characteristics even in an inert atmosphere. When ITO is not coated with PEDOT however, in vacuum, He, Ar and N_2, the J-V curves differ considerably from the SCLC regime. This is illustrated in [Figure 5.2] for gas atmospheres with different oxygen contents. For atmospheres with low oxygen contents (100% N_2= 0% O_2 and 0,84% O_2) the J-V characteristics are SCLC dominated with additional anomalous bumps in both polarities, centred on –3 and +3 V. In [Figure 5.2] it can be seen that the higher the oxygen content, the lower the height of the anomalous bump. For atmospheres with high oxygen contents (4% O_2 and 20% O_2) the results show smooth J-V curves. Simultaneously with the J-V measurements the occurring EL has been monitored. From these coupled electro-optical measurements it has been observed that the homogeneous light emission of a PLED starts at higher voltages than the typical values at which the anomalies occur. Of importance is that when the measurements are performed in an inert atmosphere, microscopic localised light emitting spots are detected. These light emitting spots are randomly distributed over the electrode area. When the J-V measurement is repeated on the same sample, but in an oxygen rich atmosphere, no anomalous bump is observed and no light emitting spots are detected. When the vacuum is re-established the sample reveals the anomalous behaviour again. In this way one can repeatedly switch between a J-V curve with and without an anomaly by changing the atmosphere. The observation of localised light emitting spots is an indication that the anomalous effect may be related with local phenomena in the device.

A few other typical properties of this phenomenon are important to report:

- The slope of the positive resistance part of the bump can be interpreted in terms of ohmic resistance. If one calculates the resistance out of this slope one obtains values around a few 100 Ω. This is a typical value for the ITO electrode. Even sometimes the diode is a perfect resistor up to around 5V and then the current directly drops to the typical J-V behaviour of the bulk polymer [Figure 5.3]. This is a strong indication that some sort of conducting channel shorts the two electrodes. This indication becomes even stronger when we repeat the J-V measurement in vacuum for several times. After a repetition of ± 10 times all devices tested become completely ohmic, even in the high voltage region.

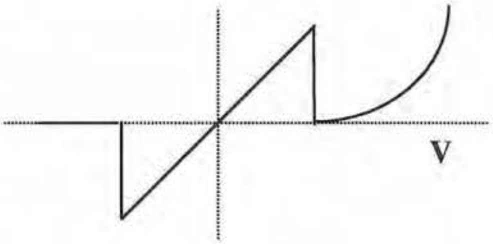

Figure 5.3 Schematic description of an ideal anomaly in the low voltage region.

- In a considerable part of the devices tested in oxygen, the first J-V sweep displays this anomaly and in the following sweeps it completely disappears.

- By applying a short high voltage pulse (± 15 V) on the device, one can obtain even in vacuum J-V curves without anomalies. This is the basic trick to obtain smooth J-V curves.

- Another possibility is to introduce an extra layer in the device between the ITO and active polymer. We have coated ITO with PEDOT to perform the J-V measurements. But even then small anomalies are sometimes observed [Chapter 3, Figure 3.20].

- In this figure one can see that the anomaly disappears at lower temperatures (253K and lower)

- The maximum is always higher for the increasing than for the decreasing voltage (as in [Figure 5.2]). This hysteresis indicates the presence of traps or dopant impurities. This means that the quality of the film plays an important role.

- The degree of anomalous behaviour decreases with increasing thickness.

- The cathode material doesn't seem to play an important role, since the anomalies occur with Al, Ag and Ca.

- Some attempts have been made to reveal the influence of moister on the anomalous properties, but no decisive answer could be given. As well in the presence of moister and in dry nitrogen the anomalies occur.

- No damage could be detected on the electrode surface with the SEM, as long as the behaviour has not become ohmic.

5.2.3. *Gas sensor: switching phenomena, memory behaviour*

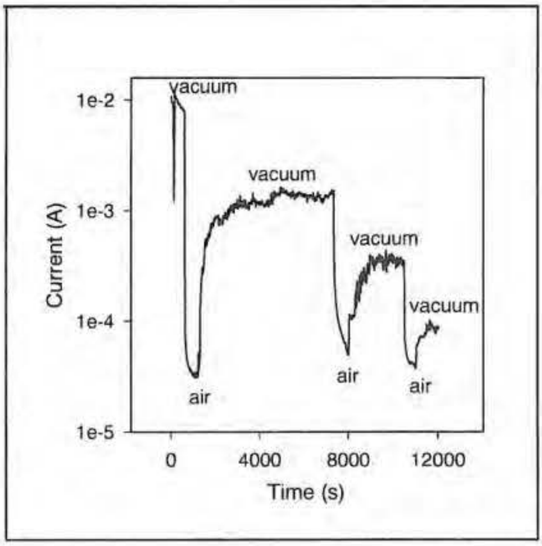

Figure 5.4: PPV-LED's as gas sensor

It has been shown in [Figure 5.2] that the form of the of the J-V curve for PLED's is strongly affected by the presence of oxygen in the surrounding atmosphere. To further investigate the response of the conductivity of the PLED's to a change of the oxygen contents in the atmosphere, a PLED has been submitted to a constant voltage stress and to a cyclic switching of the atmosphere between air and vacuum. The result of this experiment is depicted in [Figure 5.4]. This figure illustrates clearly the gas sensing properties of the PLED's towards the presence of oxygen. In vacuum the current through the device is high (ON state) and in the presence of oxygen the magnitude of the current falls down again (OFF state). One can notice that the response time of the current to a switch of gas atmosphere is dependent of the direction of the switch (air to vacuum, vacuum to air). The formation of a conducting path is much slower than the oxidation of it. The shown response of the current to a change of atmosphere has not only been observed for the voltage values at which the anomalous bumps occur in the J-V curve but also for higher voltages. In contrast to the experiment describing the anomalous bump, a device submitted to a gas sensor experiment shows a defect in the electrode structure in the form of a blister [Figure 5.5]. These results indicate that the phenomenon is the result of a short of leakage channel. Since this shorting phenomenon occurs in an inert atmosphere, ageing tests in this atmosphere with our PLED's (without an extra PEDOT layer) are impossible as long as leakage current is dominant.

Figure 5.5: SEM image of a damaged area in the electrode surface after a gas sensor experiment.

In order to investigate the ohmic leakage paths in more detail, an experiment was performed where the device was kept at a constant voltage of 16 V, and the gas atmosphere was switched between air (I) and vacuum (II). The results are shown in [Figure 5.6]. In an oxygen-rich atmosphere (I), a uniform light emission can be observed. Reduction of the oxygen pressure to 10^{-2}Pa, while maintaining the electrical stress leads to a bright light emission in one single spot while at the same time light emission decreases in the rest of the device area (II). Consequently, the EL intensity in vacuum (II) is mainly determined by the emission from this bright spot, which is larger than the uniform emission observed in air (I). If the pressure is increased again to an oxygen-rich atmosphere these paths are not stable since they can not support the high local current density. The driving current is spread out over the remaining area of the device and the diode emits light again but at a lower total intensity. A repeated switching between vacuum and oxygen-rich atmospheres results in an increased light emission in vacuum (II), mainly originating from the spot, and a decreased emission in air (I). At the moment of breakdown (at a time of about 70 min), the bright spot becomes a conducting path, and the entire current flows through this path. SCLC-current is no longer present and light emission has stopped.

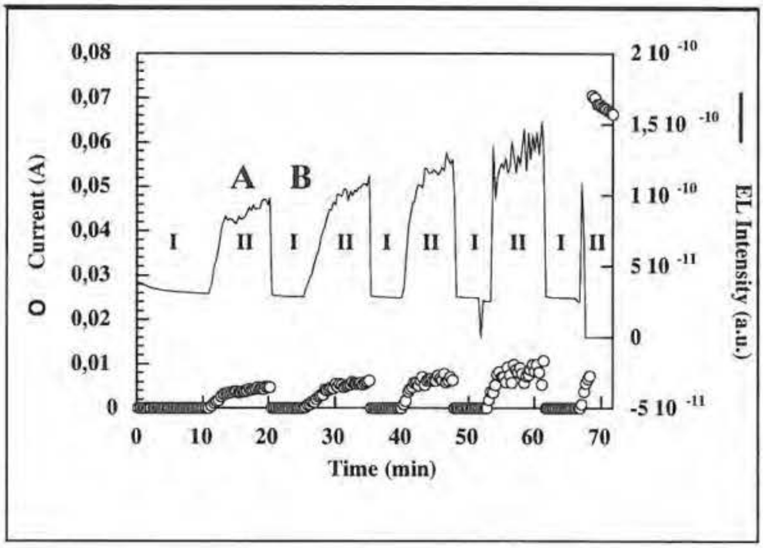

*Figure 5.6 PPV-LED's submitted to a constant voltage stress show changes of current and light output when switching of the gas atmosphere occurs. **I** = air, **II** = vacuum. Switching shows bright light emission in vacuum until breakdown and complete loss in light output. A and B indicate the time position at which the SIMS analyses are performed.*

This experiment shows some similarities with the memory phenomena and anomalous behaviour(3) reported elsewhere. Meaning that the atmosphere dependence of the phenomena is similar, high currents only arise in the absence of oxygen. Notice the fact that anomalies always occur in the low voltage range (2V to 6V) where our switching experiment is performed at 16V, far away from the region where the anomalies occur.

5.2.4. Analysis of damage area in the electrode surface: the blister

In order to get a better understanding of the ohmic channels we have analysed the damaged region on the electrode structure (the blister in [Figure 5.5]) with the SEM and SIMS. For these experiments the SIMS was used in the imaging mode instead of making depth profiles. In this way we obtain cross sections of the device with the two dimensional distribution of the different elements in the defect. By doing so, we obtain a three dimensional idea of the defect structure. We have stopped the experiment in [Figure 5.6] for some devices at position A and for other devices at position B, the sample were then analysed.

5.2.4.1. Sample preparation and SEM analyse

When the electrical stress was stopped in position A, when the device is shorted, of the experiment in [Figure 5.6], the Al-top of the device was covered with one centimetre of epoxy resin. The sample with epoxy resin was than cured for 48 hours at 70°C. The as obtained sample was put in a water solution at 90°C and directly quenched with cold water. Due to the difference in expanding coefficient the different layers are ripped apart. By doing so we obtain two samples: a resin sample and an ITO sample. Both the samples are then studied in the SEM. These photographs are given in [Figure 5.7]. On the left side the image of the resin sample is given. EDX element analysis in a single spot revealed that the structure of this sample is epoxy resin with the Al-electrode and the PPV film. One can see that in the centre of the blister there is a strange particle consisting of Na, Mg, Si, In and Ca. This is most likely an impurity (dust particle) introduced during the fabrication of the devices. Further more there is damage in the Al-electrode layer in the form of cracks. The SEM image on the right side is the ITO substrate. The ITO electrode also exhibits cracks through which one observes the glass bottom substrate. One can see that the left and the right picture are mirror images.

Where on the resin (left) side the Al material is gone, one can find it on the ITO substrate (right). This means that most likely due to joule heating, as a result of the higher field around the impurity particle, the polymer melts and a contact between the Al and the ITO is established. This results in a very high leakage current and eventually in an ohmic contact.

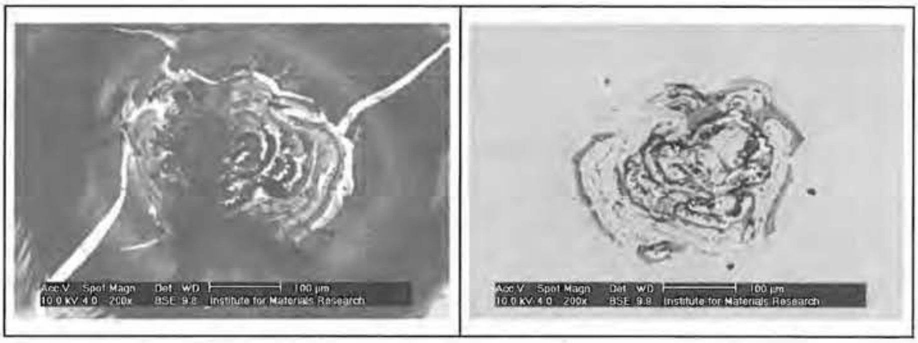

Figure 5.7 SE images of the Al-side of the device (left) and the ITO-side of the device (right) at the blister.

5.2.4.2. SIMS imaging of the element distribution

As discussed before these ohmic leakage paths are not stable in oxygen since they can not support the high local current density. They become oxidised and they burn. For our SIMS analysis we have stopped in position A (when the device is shorted) and B (when the short is oxidised) of the experiment in [Figure 5.6]. By doing so we obtain two samples: a non-oxidised (NO) and an oxidised (O). The samples where directly introduced after electrical stress in the SIMS without extra sample preparation.

It is important to note that, as stated in the previous chapters, the ohmic paths can origin from different type of defects in the sample. This makes a comparison difficult. Here we show two specific measurements, but the discussion gives a global picture of the idea.

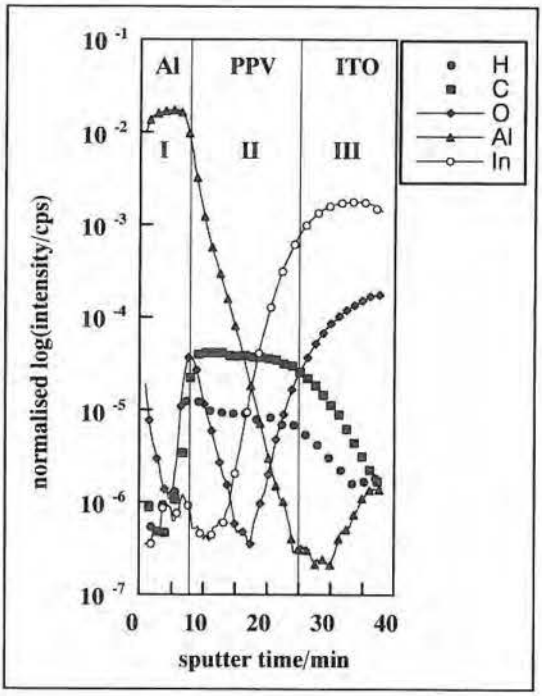

Figure 5.8 normal SIMS depth profiling of the main elemental constituents of an Al/PPV/ITO device. I, II and III indicate the depth location in the device at which the images are taken.

[Figure 5.8] shows a SIMS depth profile of an Al/PPV/ITO device. The picture demonstrates the layered structure. (I) is the electrode structure, (II) the polymer film and (III) the ITO substrate. At each location in the device we have taken SIMS-images, which are discussed below. Only the images taken in the polymer layer are shown, the rest of the images are discussed but not shown.

NO-sample :

- (I) The Al-electrode : the first images were taken directly at the beginning at the top of the Al-electrode. For the NO-sample there is a structure in the Al-image. There is no C signal. The O and In signal has the same structure as the Al-profile. Only where there is no Al there is In and O.
- (II) The polymer film [Figure 5.9]: by going into the polymer film the Al signal becomes weaker and weaker. There is still a clear In signal inside the blister. The structure of the oxygen signal is identical as the In signal, meaning that the structure comes from an ITO particle inside the polymer film. One can see that where we find the In and O signal there is no C signal, this confirms the presence of a particle. The SIMS images in the polymer layer are given in [Figure 5.9].
- (III) The ITO substrate: at the ITO electrode one can see that there is an Al- and C-signal around the particle. From the O- and In-signal one can conclude that the ITO structure is damaged in the centre of the blister. This means that an ITO impurity particle pierce through the polymer layer. Very close to the particle the Al can penetrate to the ITO electrode. In this way an ohmic channel is formed.

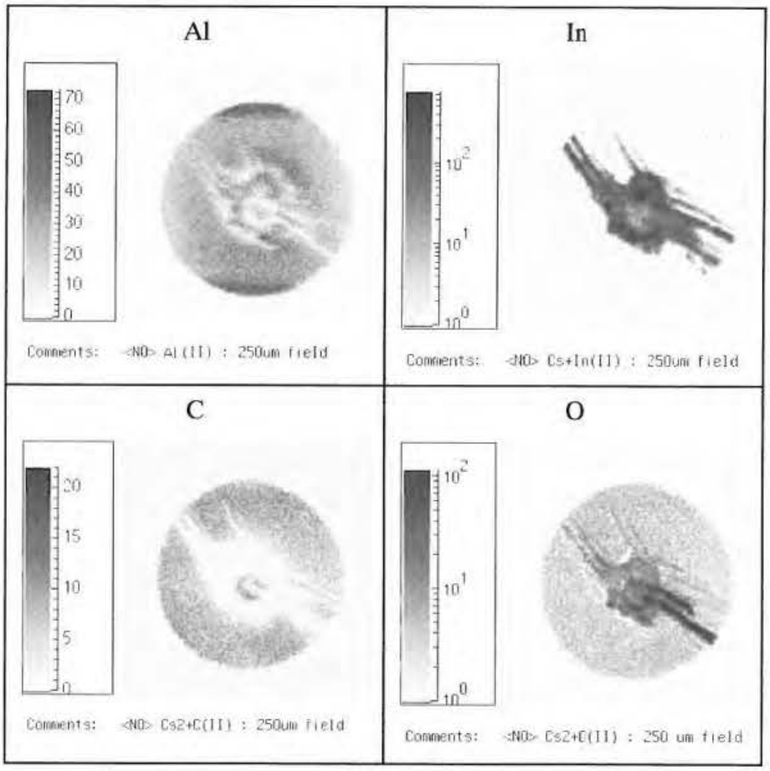

Figure 5.9 A non-oxidised sample: SIMS images of the distribution for the main elements inside the polymer film.

O-sample :

- (I) The Al-electrode : for the oxidised (O) sample the top of the blister consists out of AlOx, no C- and In-signal is found in the beginning of the profile, a cloud-like structure is recognised comparable with the circle-like defect structure in the SEM figures of a blister [Figure 5.7].

- (II) The polymer film [Figure 5.11]: by going into the polymer layer one can see that the polymer is melted away under the blister. The defect (blister) is very good outlined by a higher O- and In-signal at the edges, the centre of the blister is filled with Al [Figure 5.11].
- (III) The ITO substrate: at the ITO surface there is still some C signal, a high Al signal and one can see the cracks in the ITO layer, as in [Figure 5.7]. There is no clear indication for a particle. For the oxidised sample the structure under the blister is more like a complete mixture of all elements. A schematic drawing of the defect after oxidation is given in [Figure 5.10].

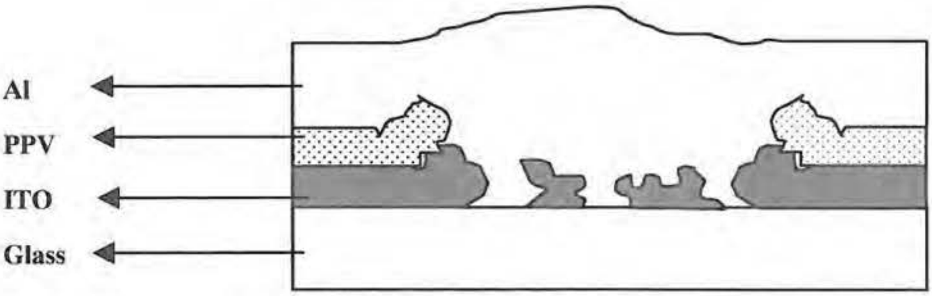

Figure 5.10 schematic reconstruction of a blister-like defect, out of the SIMS images.

Out of these experiments it can be concluded that impurities in the device lead to leakage current and in the end to an ohmic path. By introducing oxygen in the atmosphere this path becomes oxidised and can not support the high current, so the path burns and the driving current is spread out over the remaining area of the device. The path is recognised as a blister like defect on the electrode surface.

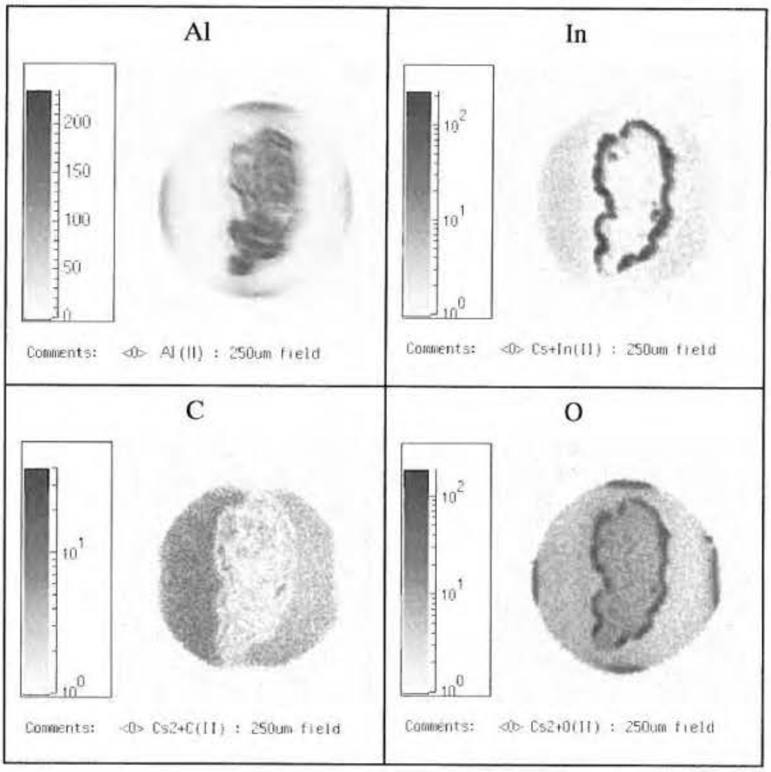

Figure 5.11 An oxidised sample: SIMS images of the distribution for the main elements inside the polymer film.

5.3. Different models describing anomalies in the J-V curves

5.3.1. Filamentary models

Memory states with lifetimes of the order of years are reported in the literature. A variety of models have been proposed concerning the stability of both states, also explaining switching mechanisms in both directions. Typical examples and models are described in two review articles(8,9). In most cases the ON state is imagined to be related to spatially separated current paths of irregular shape, which are called filaments. These filaments can bridge the contact gap between the two electrodes. The OFF state may be described either by the background insulator, or by a low-conducting state of the filaments, either materially or e.g. induced by any field effect. The simplest case is one in which the filament is intact or interrupted like an electrical fuse. An example is metal filament growth through an air gap between two metal tips(10), thus establishing an ON state, and rupturing by melting or explosion. Current paths in sandwiched insulator structures are sometimes explained with metal filaments(11). A lot of authors speculated about the possibility of filament formation(12,13). Dearnaley et al(14) presented a global model of high acceptance, based on few terms, for it yielded good fits to the measurable J-V curves and it frequency dependence. In this model there is thermal rupturing by joule heating and recoverage within a dead time as a re-growth process. The negative differential resistance (NDR) branch originates from rupturing filaments with a distribution of different resistance.

5.3.2. Models based on homogeneous penetration

A completely different approach is based on the insulator band structure and a particular broad impurity band(5,15,16). Sakai et al.(17,18) discussed the nature of these impurities. They observed that if chemical impurities were the cause of these electrical anomalies, a normal J-V behaviour could be established by elimination of the impurities by repeated precipitation. They also suggested that chain ends act as trap site and by doing so account for the anomalies in metal/polymer/metal structures. These models based on impurities in the active layer, incorporate ionisation and neutralisation of the impurities(19) (in the energy picture: the impurity band). The largest part of the applied voltage is probably situated at the negative electrode and the remaining active layer is almost without an electric field. When the voltage increases, free holes are created at the top of the valence band by electrons tunnelling to the acceptor levels. Free holes can than recombine with electrons from the impurity band. By further increasing the voltage the electrons start tunnelling from the acceptor level to the impurity band and the conductivity decreases as a result (VCNR). At the maximum in the J-V curve ionisation and neutralisation in the impurity band are equal.

5.4. Conclusion

By examining the experimental results and discussing the different models one has the tendency to support the filament theory. The gas sensor experiment and switching can adequately be explained by this theory. Also the SEM and SIMS measurements point in the direction of an ohmic path. The explanation that the VCNR-like shape of the J-V curves is caused by superimposed characteristics of individual filaments, having each a certain conduction (which may change during repeated operation) at which they switch OFF, is a little harder to accept.

Defects in the device certainly play a crucial role. These defects are already present in the as-produced sample, e.g. particles impurities, pinholes and crevices in the active layer, interface roughness and structural weakness (edges of the metal electrode). Even chemical defects like interruption of the conjugation of the active polymer by cross-linking or carbonyl chain-ends can play a dominant role, as well as monomer and solvent impurities.

Without any doubt the leakage current resulting from these defects is the main cause for the anomalies in the electrical behaviour of these devices. Leakage current is the concentration of current in a localised area of the device. This localised area can be around a particle, in a crevice of the polymer layer. It can also be located at the edge of the electrodes, or where the polymer film is locally thinner. It could even occur at just a local concentration of chemical defects (trapping sites) in the film through which the charge carriers can hop from one metal to the other.

In this way it does not matter if this leakage channel is interpreted in terms of superimposing individual filaments or an impurity band. One can see the filaments as the physical-picture and the impurity band as the energy-picture of the same phenomenon.

As a result of this leakage current the device heats locally and this higher temperature can account for the emission in local spots. Since most of the current runs through these areas, the heating results in an increase of the charge carrier mobility of the active polymer resulting in a local higher emission (hot spot).

But high temperatures result in local melting of the polymer and in the end this results in the establishing of an ohmic channel. Now the entire current flows through this path. SCLC is now longer dominant and the light emission has stopped. As discussed, the channel can be oxidised and then the current is spread out again over the remaining area of the device and the diode emits light but at a lower intensity.

5.5. References

(111) Manca, J., Bijnens, W., Kiebooms, R., D'Hean, J., D'Olieslaeger,M., Wu, T.D., De Ceuninck, W., De Schepper, L., Vanderzande, D., *Optical Materials,* **9**, 134 (1998)

(112) Bröms, P., Birgersson, N. and Slananeck W.R., *Synth. Met.*, **74**, 179 (1995)

(113) Cimrová, V. and Neher, D., *Synth. Met.*, **76**, 125 (1996)

(114) Verderber, R.R., Simmons, J.G. and Eales, B., **Phil. Mag.**, 1049 (1967)

(115) Simmons,J.G., and Verderber, R.R., *Proc. Roy. Soc*, **A 301**, 77 (1967)

(116) Sakai, K., Matsuda, H., Kawada, H., Eguchi, K. and Nakagiri, T., *Appl. Phys. Lett.*, **53 (14)**, 1274 (1988)

(117) Takimoto, K., Kawade, H., Sakai, K., Yanagisawa, Y., Eguchi, K. and Nakagiri, T., *Thin Solid Films*, **179**, 283 (1989)

(118) Biederman, H., *Vacuum*, **26 (12)**, 513 (1976)

(119) Pagnia, H. and Sotnik, N., *Phys. Stat. Sol.*, **a 108**, 11 (1988)

(120) Chapman, R., Electronics Letters, 5, 246 (1969)

(121) Dearnaley, Thin Solid Films, 3, 161 (1969)

(122) Sutherland, R.R., *J. Phys D*, **4**, 468 (2971)

(123) Miller, L.S., and Kershaw, *Thin Solid Films*, **29**, 165 (1975)

(124) Dearnaley, G. and Stoneham, A.M., *Rep. Progr. Phys.*, **33**, 1129 (1970)

(125) Hickmott, T.W., *J. Appl. Phys.*, **35**, 2679 (1964)

(126) Emmer, I., *Thin Solid Films*, **20**, 43 (1974)

(127) Sakai, Y., Sadaoka, Y. and Okada, G., *Polymer Journal*, **15 (3)**, 195 (1983)

(128) Sakai, Y., Sadaoka, Y. and Okada, G., *Polymer Journal*, **15 (9)**, 663 (1983)

(129) Hickmott, T.W., *J. Appl. Phys.*, **36**, 1885 (1965)

Chapter 6

General summary

This thesis describes the electro-optical properties and ageing behaviour of conjugated polymers LED's, fabricated by a non-ionic precursor route. The understanding of the electro-optical properties is important for the optimisation of device stability.

It has been discussed that in reality conjugated polymers can not be described by the semiconductor band model, although the basic concepts of this model help to clarify the phenomena that take place in PLED's.

Polymer chains are not infinitely long and the conjugation is often broken due to defects. In practice conjugated polymer chains consist of conjugated parts separated by non-conducting links. Since there is a weak coupling between the conjugated parts in these materials the conjugated segments behave as individual molecules. The fact that these segments behave as individual molecules results in a Gaussian distribution of localised states. The charge carriers have a very low mobility, which reflects their localisation on the conjugated segments. Mobility is thus described in terms of hopping transport in disordered semiconductors.

Experiments have indicated similarities in the observed features in disordered molecular solids, despite the wide diversity in chemical and physical structures. The most striking features are:

- A carrier mobility yielding an activation energy of about 0.4 to 0.6 eV independent of chemical constitution and synthesis if analysed in terms of Arrhenius equation.
- A field dependence of mobility resembling the Pool-Frenkel low, $ln\mu \sim SE^{1/2}$, over an extended range of electrical field.

This field and temperature dependence is first incorporated into an empirical relation for hole and electron mobility by Gill. A theory of high-field hopping transport in disordered materials is given by Vissenberg and Blom, starting from the Gill equation. We have used these concepts to study the J-V behaviour of our PLED's.

We can conclude, that models describing the properties of polymer LED's in terms of injection as a dominant process fail to describe the temperature and field dependence of LED's. The model of Blom however adequately describes the experimental results.

The experiments in ITO/PEDOT/PPV/Al PLED's show that the low field part of the native PPV hole only device is dominated by the leakage current of PEDOT. The high field part is dominated by the bulk properties of PPV itself. Since the field dependent parameter γ is determined from the high field part of the experimental J-V curve and the mobilty is obtained from the low field part, the field dependent parameters for the native PPV are more reliable. To get more information about the bulk properties of the native PPV we need to improve the film quality. As long as leakage current is the dominated process in these devices the efficiency of double injection devices is practicaly zero and the turn on voltage for light emision is above 10 V.

With regard to OC_1C_{10}, one can see that the parameters describing the J-V curves of the OC_1C_{10} obtained by different synthesis routes are similar. This means that despite of the small structural differences, the bulk properties are similar. The higher gelation temperature of the OC_1C_{10} prepared by our precursor route (most likely the result of the more pure chemical structure), makes that gelation occurs more easily. This results in worse film properties. The film properties can account for the fact that leakage current still conceals in the background at room temperature and becomes dominant at low temperatures. The small leakage current that is still present, causes the apparent efficiency of the precursor OC_1C_{10} to be lower than the Philips OC_1C_{10}. Since the bulk properties are similar, there is no reason why, if the films are optimised, the efficiency of the two OC_1C_{10} materials should not be similar.

Three distinct regions in the time evolution of the electrical resistance and the light output are identified. Various electrical and analytical measurement results are presented to explain the main failure mechanisms. The most severe degradation mode can be identified as dielectric breakdown, resulting in 'hot spots' and ohmic leakage paths. The inhibition of the ohmic path formation by oxidation under ambient conditions results in a local delamination of the electrode, shrinking the active area of the device.

The light emission of PLEDS is influenced by the morphology of the device. Thickness variations of the polymer (buckling), caused by the spinning process, lead to stripe patterned emission. This results in a field induced stripe patterned ageing. A high charge build-up at the edges of the Al electrode results in a higher luminescence, and faster ageing. The combination of electrical measurements, SEM, SIMS and EMMI imaging, showed that when a constant current is forced through the polymer, it will initially flow through a large area of the device, with severe loss of current through leakage paths present in the as-produced sample. Subsequently blister formation and electrode delamination, resulting in a gradual increase of the voltage and a decrease of the luminescence reduce the active area of the device. When the voltage increased to a certain level, random light flashes start to appear, resulting in an increase of the emission. EMMI showed that this emission originates from random, bright spots, instead of from a uniform luminescence of the device.

All the experiments (J-V curves, reliability studies and the negative resistance) suggest that pre-existing defects cause the formation of **leakage current** :

- Out of the experimental J-V curves one can see that optimalisation of the film properties of the active layer in a PLED is of crucial importance to prevent leakage current. If there are defects present, regardless their origin, leakage current takes the charge carriers away in the bulk material and the efficiency of the device drops to almost zero. Therefore one should be careful when interpretating experimental J-V curves, and first make sure, that leakage current does not dominate the characteristics. As the results indicate, temperature dependent measurements are ideal to distinguish between the occurring mechanisms.
- Very high electric fields can be formed locally at these leakage paths, at the edges of the Al and at the thinner parts of the buckled polymer film. This can produce intense local heating that melts the organic layer and establish an electrical short. In oxygen however, these shorts are not stable since they can not support the high local current density, and become oxidised. This process

eventually leads to a complete destruction of the device.

- Without any doubt the leakage current resulting from these defects is the main cause for the anomalies in the electrical behaviour of these devices. Leakage current is the concentration of current in a localised area of the device. It could even occur at just a local concentration of chemical defects (trapping sites) in the film through which the charge carriers can hop from one metal to the other.

Pre-existing defects and film imperfections are the cause for the formation of leakage current, meaning that leakage current is the electrical fingerprint of the device imperfections. Therefore one should be very careful when interpreting electrical data of LED's. And before any conclusion is drawn it needs to be made very clear that one is measuring the bulk properties of the active layer and not some side effect like leakage current.

Chapter 7

Prospective

As has been discussed in the previous chapters, we have worked on an experimental set-up that enables the study of the bulk properties of the polymer-in terms of mobility- and the ageing behaviour of polymer LED's. The results that have been presented, are only preliminary investigations on a standard conducting polymer.

This work is of a prospective nature in the large domain of conjugated polymers. The choices that have been made are purely based on a personal view of the domain. Other authors also study many of the discussed items but from a different point of view. We have tried to introduce existing analytical techniques in the rather new field of synthetic metals. The strength of this work is situated in the combination of these analytical techniques with in-situ electro-optical techniques.

7.1. Field and temperature dependent carrier-mobility.

As already mentioned, despite the wide diversity in chemical and physical structures of disordered molecular solids, the field and temperature dependence seems to be of an universal nature. The mobility can be described by:

$$\mu = \mu_0 e^{-\beta\Delta + B(\beta - \beta_0)\sqrt{E}}$$

with $\beta = 1/(kT)$ and $\beta_0 = 1/(kT_0)$. Numerous experiments on moleculary doped polymers, pendant group polymers, amorphous molecular glasses and conjugated polymers have revealed a similar behaviour, with typical parameter values of $\Delta \sim 0.5$ eV, $B \sim 3\ 10^{-5}$ eV(m/V)$^{1/2}$ and $T_0 \sim 600$ K.

Temperature dependent J-V measurements on a metal/polymer/metal/ sandwich structure deliver information on the mobility (bulk properties).

So far, no systematic study of the mobility of conjugated polymers has been performed. The more knowledge we obtain about the bulk properties of these materials, the easier it gets to select new materials for applications.

In the laboratory of Dirk Vanderzande there is a large stock of conjugated polymers available. The time is ripe to make an inventory of the bulk properties of these materials. The model of Blom, as discussed in chapter 3, can be used for this study.

This type of experiments can also be used to study the quality of the polymer film in a sandwich-structured device (eg. PLED).

7.2. Ageing of polymer light emitting diodes.

Lifetime predictions can be made by means of constant current measurements. The results discussed in chapter 4 are obtained by measuring bare devices under ambient conditions. In spite the fact that these conditions are far from the ones necessary for application, the ageing curves follow the same behaviour. The only difference is the time to breakdown.

In this work it is shown that the combination of analytical techniques as SIMS, SEM and EMMI makes it possible to screen the device for pre-existing defects, which causes the devices to fail.

For the moment no systematic reliability study of PLED's has been performed. With the large amount of samples, that will be provided by the test factory of Philips, the reliability study presented in this work can be used to perform a systematic statistical analysis on these PLED's. And by doing so, it will be possible to do precise predictions of the lifetime of these devices.

This statistical analysis and the knowledge one obtains is crucial information at a time when commercialisation of the product is in progress. This lack of knowledge is in my opinion the biggest shortcoming in the domain. As a result it is an enormous challenge to continue the ageing study presented in this work.

By doing a statistical reliability study one obtains detailed information about the breakdown modes of PLED's. This study together with the analytical investigations will make it possible to get a physical understanding of what is causing the devices to breakdown. And by doing so, one can predict life time. Only this type of study will give a decisive answer about the question if there is a reliability problem with these PLED's.

One can use the reliability knowledge obtained in the field of silicon-oxide as a guideline. The program FAILURE, developed by IMEC and IMO and commercialised by DESTIN will make it possible to analyse these electrical data.

Hoofdstuk 8

Algemene beschouwing

Dit werk beschrijft de elektro-optische eigenschappen en het verouderingsgedrag van polymere licht emitterende diodes (PLED's), vervaardigd via een niet-ionische precursorroute. De kennis van het elektro-optisch gedrag is van groot belang voor het verbeteren van de devices.

In een eerste deel wijzen we op het feit dat het bandenmodel uit de halfgeleiderfysica problemen geeft bij het beschrijven van deze polymere systemen. Nochtans wordt het model zeer vaak gebruikt en kan het zeker helpen om de fenomenen, die optreden in deze systemen, te begrijpen.

Polymeerketens zijn niet oneindig lang en hun conjugatie is vaak onderbroken door defecten (niet geleidende schakels). De geleidende delen gedragen zich als onafhankelijke moleculen, met een andere omgeving en een verschillende lengtes, met als gevolg verschillende energieën. Dit individueel gedrag resulteert in een Gauss-distributie van gelokaliseerde energieniveaus. De ladingsdragers hebben een zeer lage mobiliteit door hun lokalisatie op deze segmenten. Mobiliteit zal dan ook beschreven worden in termen van een hopping-model en niet door een bandenmodel.

Experimenten hebben aangetoond dat de eigenschappen van wanordelijke moleculaire vaste stoffen een zekere trent vertonen. En dit ongeacht hun chemische en fysische structuur, nl. :

- De Arrhenius activeringsenergie van de mobiele ladingsdragers is rond de 0.4 tot 0.5 eV.
- De veldafhankelijkheid van de mobiliteit volgt de Pool-Frenkel wet, $\ln\mu \sim SE^{1:2}$, over een groot elektrisch-veld-domein.

Deze veld- en temperatuursafhankelijkheid is voor het eerst empirisch beschreven door Gill. Vissenberg en Blom hebben zowel experimenteel als theoretisch aangetoond dat de Gill formule bruikbaar is voor het beschrijven van de eigenschappen van geleidende polymeren in LED's. Hun concept hebben wij gebruikt voor de beschrijving van onze experimentele resultaten.

Enerzijds kunnen we experimenteel besluiten dat de traditionele modellen die de eigenschappen van PLED's beschrijven, door middel van injectiemechanismen, er niet in slagen de veld- en temperatuursafhankelijkheid van de stroom-spanning-(J-V)-karakteristieken te beschrijven. Anderzijds beschrijft het Blom-model onze experimenten op een bevredigende wijze over heel het elektrische veld.

De experimenten op ITO/PEDOT/PPV/Al PLED's tonen aan dat bij laag veld, de J-V curve van een zuiver PPV gaten-enkel device, volledig gedomineerd wordt door de lekstroom van PEDOT. Bij hoog veld daarentegen, is de J-V curve gedomineerd door de bulkeigenschappen van het PPV. Vermits de veldparameter γ berekend wordt bij een hoog veld en de activeringsenergie bij een laag veld, is de veldparameter voor PPV beter betrouwbaar bepaald dan de activeringsenergie. Vooraleer we meer kunnen weten over de bulkeigenschappen van PPV, moeten we de filmkwaliteit verbeteren. Zolang de lekstroom de dominerende factor is in deze devices, zal de efficiëntie van PLED's gebaseerd op zuiver PPV bijna nul zijn. De aanzetspanning voor emissie blijft dan ook boven de 10V.

Wat OC_1C_{10} betreft, kunnen we besluiten dat de parameters die de bulkeigenschappen van het materiaal beschrijven, gelijkaardig zijn voor verschillende syntheserouten. Dit wil zeggen dat ondanks de kleine structurele verschillen, de elektrische bulkeigenschappen ongeveer dezelfde blijven. Het OC_1C_{10}-materiaal, vervaardigd via onze syntheseroute gelleert gemakkelijker vergeleken met het Philips-materiaal. Dit heeft tot gevolg dat onze filmen van een mindere kwaliteit zijn. Deze slechtere filmkwaliteit is de oorzaak van de lekstroom die nog steeds bij kamertemperatuur in de achtergrond aanwezig is en die zelf dominant wordt bij lage temperatuur. Door de aanwezigheid van deze lekstroom is de gemeten efficiëntie van ons materiaal slechter dan dat van Philips. Vermits de elektrische parameters voor de bulk vergelijkbaar zijn voor beide materialen, is er geen enkele reden waarom, beide materialen verschillend zouden presteren, tenminste als we eerst de filmkwaliteit van het precursormateriaal verbeteren.

In de tijdsevolutie van de elektrische weerstand en de lichtevolutie kan men drie regio's onderscheiden. Een groot aanbod van elektrische en analytische metingen wordt in dit werk beschreven om de belangrijkste falingsmechanismen te beschrijven. Het belangrijkste falingsmechanisme is een diëlektrische doorbraak, hetgeen leidt tot 'hot-spots' en ohmse lekpaden. Het verhinderen van deze ohmse paden in de aanwezigheid van zuurstof, leidt tot het vernietigen van de topelektrode en het verkleinen van het actieve oppervlak.

De lichtemissie van een PLED wordt sterk beïnvloed door de morfologie van het device. Diktevariaties, veroorzaakt door het spincoat-proces, leiden tot emissie in een strepenpatroon. Dit resulteert tot een veroudering volgens dit patroon. De hogere ladingsdichtheid aan de randen van de Al-elektrode geeft een hogere emissie, maar ook een snellere veroudering. De experimenten tonen aan dat wanneer er een constante stroom door het device gestuurd wordt er in eerste instantie homogeen licht door heel het device uitgezonden wordt. Een groot gedeelte van de stroom gaat verloren via ohmse paden die reeds aanwezig zijn vanaf de productie van het device. Deze lokaal hoge stroom veroorzaakt blaasvorming en vernietigt het actieve oppervlak van het device. Hierdoor stijgt de spanning over de LED. Vanaf een zeker spanningsniveau beginnen er random lichtflitsen te komen en wordt het device uiteindelijk volledig vernietigd.

Alle experimenten (zowel de J-V curves als de verouderingsstudie en de negatieve weerstand) tonen aan dat defecten, ontstaan bij de productie van de devices, lekstroom veroorzaken.

- De studie van de J-V curves maakt duidelijk dat de verbetering van de filmkwaliteit van PLED's zeer belangrijk is om lekstroom te voorkomen. Als er defecten aanwezig zijn, van welke aard dan ook, worden de ladingsdragers door de lekstroom uit de actieve laag genomen en zal de efficiëntie van de LED zeer laag zijn. Daardoor is het van het grootste belang dat men er zeker van is dat lekstroom niet het dominante mechanisme is. Zoals blijkt uit de experimenten zijn temperatuursafhankelijke metingen uiterst geschikt voor de studie van het stroom-spanningsgedrag van zulke devices.

- In lokale lekpaden, in dunnere delen en aan de randen van het device kunnen er zeer hoge elektrische velden ontstaan. Dit veroorzaakt lokaal zeer hoge temperaturen, zodat de polymeerfilm smelt en er een kortsluiting onstaat. In de aanwezigheid van zuurstof is deze korstsluiting niet stabiel en wordt ze geoxideerd. Hierdoor verliest het device aan actief oppervlakte en lichtintensiteit. Uiteindelijk leidt het proces tot de volledige vernietiging van de LED.

- Zonder enige twijfel wordt het anomaal gedrag in deze devices veroorzaakt door de lekstroom in de aanwezige defecten.

Defecten die in het device geslopen zijn tijdens de fabricatie veroorzaken lekstroom. Dit wil zeggen dat lekstroom de elektrische vingerafdruk is van de defecten. Hierdoor moet men zeer voorzichtig zijn bij het interpreteren van elektrische metingen van PLED's. Men moet er dus eerst voor zorgen dat men zeker is dat men metingen uitvoert op de bulkeigenschappen gemeten worden en niet op de aanwezige defecten, voordat men conclusies gaat trekken.

Chapter 9

Glossary, acronyms and symbols

AFM : Atomic force microscopy

aliphatic tail : chemical group consisting of a carbon-hydrogen backbone.

bulk limited transport (SCLC) : The movement of charge carriers is limited by the properties of bulk (active polymer).

CE : Conversion efficiency

chromophores : Small conjugated organic molecules.

conjugational defect : Interruption of the space in which the electrons are able to freely move (double single bond alternation)

contact limited behaviour : The movement of the charge carriers is limited by the properties of the metal/polymer contact.

dimerisation : The pairing of two successive smallest units (atom, monomer).

DOS : Density of state is the density of energy states in function of energy.

EA : Electron affinity is the change in energy when a molecule gains an electron.

electroluminescence (EL) : The conversion of electrical current into light

elimination : Thermal process by which a chemical removable group is ejected from the polymer backbone. By doing so, the p-conjugated system is formed and the precursor polymer is converted into a conjugated polymer.

EMMI : Emission microscopy

exiton : An electron-hole pair in the excited state (an excess of energy)

FN : Fowler Nordheim tunnelling is a model to describe the tunnelling of charge carriers from a metal through a triangular barrier into polymer bulk material.

forming process : Is a phenomenon that raises the electrical conductivity of a sample by a few orders of magnitude. When this process occurs the J-V characteristic of the sample shows a maximum in current. This phenomenon is also named as switching, anomalous behaviour, NDR and VCNR.

gelation, agregations : Process by which polymer chains are grouped together to form bigger entities (agregates).

GPC : Gel permeation chromatography is an analytical technique to determine the molecular weight

HOMO and LUMO : Highest occupied molecular orbital is the molecular orbital that is occupied last according to the building-up principle.

The lowest unoccupied molecular orbital is the next higher molecular orbital. Jointly, the two are the frontier orbitals of the molecules.

IMO : Institute for material research

IP : ionisation potential is the energy necessary to remove an electron from the solid into the vacuum.

IR : Infra-red monitoring

ITO : Indium-tin-oxide, a transparent anode.

leaving group : Chemical removable group which allows the formation of the conjugated system in a conductive polymer.

MEH-PPV : Soluble derivative of PDMeoPV

monomer : Smallest unit of a polymer.

MSM : Metal-semiconductor-metal sandwich structure

NATLAB : Philips research centre, Eindhoven

NDR : Negative differential resistance, see forming process

1H-NMR and 13C NMR : Nuclear magnetic resonance spectroscopy

OC_1C_{10} : A soluble derivative of PDMeoPV

oligomer : Small organic molecule.

PBPV : poly (4,4'-bisphenylene vinylene), a PPV derivative with an enlarged aromatic system

PDMeoPV : poly (2,5-dimethoxy-1, 4-phenylene vinylene), an electron rich PPV derivative

PDMetPV : poly (2,5-dimethyl-1, 4-phenylene vinylene), an electron rich PPV derivative

PEDOT : Poly ethylene dioxy thiophene, a conductive polymer used as an anode coating.

Peierls distortion : Rudolph Peierls stated that at T=0 K, no one-dimensional solid is a metal. This means that the state of lowest energy is not a solid with a regular lattice spacing. In other words the Peierls distortion leads to the reorganisation of the atoms within the chains, resulting in a lowering of the energy below that of the regular solid. By doing so, the electrons are trapped between the longer-bonded atoms, introducing a band gap in the centre of the original conducting band, in this way the filled orbitals are separated from the empty orbitals.

PL : Photoluminescence, is the emission of light after absorption of light

PLED : Polymer light emitting diode

PNV : poly (2,6-naphtalene vinylene)), a PPV derivative with an enlarged aromatic system

polariser : Chemical group which during polymerisation ensures a head to tail reaction.

polaron : Lowest excited state in a conjugated polymer according to the band model. To stabiles the conjugational defects in a non-degenerated ground state polymer the defects have to create bound double defects. Such a double-defect is called a polaron.

polymerisation : Chemical chain-forming reaction which converts the monomers into polymers.

Pool-Frenkel law : States that the logarithm of the mobility is proportional to the square root of the applied electrical field.

PPV : Poly (p-phenylene vinylene), a conjugated polymer build up by a benzene rings separated by a double bond.

precursor polymer : A pre-polymer, which in the specific case of conjugated polymers, is a processible polymer that facilitate the incorporation of these materials into devices.

The precursor has to be converted into its conjugated (non-soluble) form by thermal conversion.

quenching : Excited states are quenched, when they lose there energy by a non-radiative process.

RS : Richardson Schottky model for injection of charge carrier over an force barrier (metal/polymer interface).

SCLC : Space charge limited current means that the charge transport is limited by the space charge of the bulk polymer.

SE : Secondary electrons

SEM : Scanning electron microscopy

SIMS : Secondary ion mass spectroscopy

soliton : Conjugational defect

SSH : Su-Schieffer-Heeger hamiltonian

sulphoxy-group : Chemical group (>S=O) which is thermally removable.

TFL : Trap filled limited is the strong field dependent mechanism for electron transport in the bulk.

TGA : Thermal gravimetric analysis

THF : Tetra hydro furan, an oxygen containing cyclic organic solvent

VCNR : Voltage controlled negative resistance, see forming process

B : The bimolecular recombination constant

C : Arrhenius temperature dependence

d : The film thickness

e : The elementary charge : 1,602177x10-19 C

E : Applied electrical field

E_c : The energy of the conducting band

h : Planck constant : 6,62608x10^{-34} Js

J : Electrical current

k : Boltzmann constant : 1,38066x10^{-23} JK^{-1}

k T_c : The energy characterising the trap distribution

m* : The affective mass of the charge carrier : 9,10939x10^{-31} Kg

n_c : Reciprocal number of atoms

$n_t(E_t)$: The trap density of states at energy E_t

N_t : The total trap density

p(x) : The charge carrier density.

r : T_c/T, the effective density of states in the conducting band.

t : The distance to the edge.

V : Voltage

x : Position

γ (B_γ, T_0) : The field dependence comparable to the Poole-Frenkel effect.

Δ : Arrhenius activation energy.

$\Delta\Phi$: The barrier height at the metal/polymer interface.

ε_r : The relative dielectric constant.

ε_0 : The permittivity of free space : 8,85419x10^{-12} JC^2m^{-1}.

μ : The charge carrier mobility.

Φ :The work function of a metal is the energy necessary to remove an electron from the metal lattice into the vacuum.

σ_{transp} and σ_{abs} : The width of the Gaussian distribution of states for transport (transp)and optical spectra (abs).

ω : Spinning velocity.